[UCI]I804:48009-200000333270

Doctor of Philosophy

Identification of Potentially Promising Metal Hydrides for Hydrogen Storage Applications

The Graduate School of the University of Ulsan

School of Chemical Engineering

Yuanyuan Li

Identification of Potentially Promising Metal Hydrides for Hydrogen Storage Applications

Supervisor: Professor Jin Suk Chung

A Dissertation

Submitted to
the Graduate School of the University of Ulsan
In partial Fulfillment of the Requirements
for the Degree of

Doctor of Philosophy

by

Yuanyuan Li

School of Chemical Engineering
Ulsan, Korea
June 2020

Identification of Potentially Promising Metal Hydrides for Hydrogen Storage Applications

This certifies that the dissertation of Yuanyuan Li is approved

Committee Chairman Prof. Kang Sung Gu

Committee Member Prof. Chung Jin Suk

Committee Member Prof. Choi Won Mook

Committee Member Prof. Hur Seung Hyun

Committee Member Prof. Lee Jung Kyoo

June 2020

School of Chemical Engineering, University of Ulsan

ACKNOWLEDGEMENTS

Many people have made invaluable contributions, both directly and indirectly to my research. I would like to express my gratitude to all those who have offered me tremendous assistance during the four years in University of Ulsan.

First of all, my heartiest thanks flow to my advisor, Prof. Chung Jin Suk, for his helpful guidance, valuable suggestions, kindly financial support and constant encouragement both in my study and in my life, which will be benefit to my personal and career development. At the same time, I would like to express my sincere gratitude to another advisor, Prof. Kang Sung Gu. He provided me with beneficial help and offered me precious comments during the whole process of my research. His profound insight and accurateness about my work taught me so much that they are engraved on my heart. I feel really lucky to be tutored throughout by them.

I would also like to thank my committee members including Prof. Kang Sung Gu, Prof. Chung Jin Suk, Prof. Choi Won Mook, Prof. Hur Seung Hyun, Prof. Lee Jung Kyoo for taking time out of their busy schedule to serve in my committee, review my dissertation and provide valuable comments and suggestions on the work.

I am also deeply indebted to all the professors who have taught me in this university that greatly broadened my horizon and enriched my knowledge in my study. Their inspirational and conscientious teaching will always be of great value to my future academic research.

Special thanks should go to all my lab members including Aniruddha Molla, Mahima Khandelwal, Kim Byeongsu, Chatchai Rodwihok, Yiming Meng, and Thanh Truong Dang for their support and friendship. We learn from each other and seek common progress, which I will never forget.

Finally, I would like to extend my deep gratefulness to my family and friends, whose endless love and whole-hearted support is indispensable for the successful completion of my research work and my dissertation. My heart swells with gratitude to all the people who helped me.

ABSTRACT

Light metal hydrides are excellent candidates for hydrogen storage. They can store hydrogen effectively, safely and reversibly under moderate conditions. Among them, perovskite hydrides and lithium borohydride ($LiBH_4$) have received special interest due to the low cost, availability, and high gravimetric and volumetric hydrogen density. However, the poor thermodynamic in dehydrogenation process prevents their practical applications. It is important challenge to facilitate hydrogen release in these metal hydrides. In this work, using density functional theory (DFT) calculations, a series of perovskite hydrides with a general formula ABH_3 comprising alkali metals of A, where A is Li, Na, K, Rb, or Cs, and alkaline-earth metals of B, where B is Be, Mg, Ca, Sr, or Ba were screened and the most favorable dehydrogenation pathways were obtained. The thermodynamic properties of these perovskite hydrides, especially for $NaCaH_3$ and $KMgH_3$ for hydrogen storage were mainly investigated. The structural and dehydrogenation properties of lithium borohydride surface were also checked. To tune hydrogen release processes, the destabilization approaches with adaptive dopants have been employed on $NaCaH_3$, $KMgH_3$, and $LiBH_4$. Besides, the effects of pressure/strain on these metal hydrides were examined. Furthermore, the electronic properties such as density of states (DOS) and Bader charge were analyzed to find the reaction mechanism of hydrogen release under these improvements.

Firstly, perovskite hydrides (ABH_3) were studied to screen the highest potential hydrides for hydrogen release. Herein, the ground state structures of all available systems were obtained. We then investigated the most favorable dehydrogenation pathway for each ABH_3 system and found that $NaCaH_3$ was the most attractive ABH_3 system. Analysis was performed to determine the influence of the alkali dopants (at the A-site) and alkaline-earth dopants (at the B-site) on hydrogen release from $NaCaH_3$. For this analysis, we calculated the reaction enthalpies of a $NaCaH_3$ system for hydrogen release with different dopants and pathways. Cs was the best dopant for improving hydrogen release with the lowest reaction enthalpy. However, no clear effect from B-site doping on the dehydrogenation was found.

Mg-Based metal hydrides have attracted considerable attention for hydrogen storage. The perovskite hydride $KMgH_3$ with an ideal cubic structure has been viewed as a promising material to store hydrogen. To make a further study on the improvement of hydrogen release, M-doped $KMgH_3$ (M = Li, Na, Rb, or Cs) were examined for the structural stability and dehydrogenation properties. The reaction enthalpies (ΔH) of the four possible dehydrogenation reaction pathways were calculated using the doped structures with different phases (P$m\bar{3}m$, Pnma, R3c). The most favorable reaction pathway among these four pathways was found. Among the alkali metal dopants M investigated, the most promising dopant for this reaction was Li. In addition, the pressure of 0, 0.5, 1.0, 1.5, and 2 GPa were applied to dopant-free and doped $KMgH_3$. It was found that pressure is useful for tuning the reaction enthalpies of the dehydrogenation reactions.

For most hydrides, the surface property is an important factor responsible for hydrogen release. Lithium borohydride ($LiBH_4$) has excellent properties for hydrogen storage due to its high lightweight (21.78 g/mol) and the gravimetric/volumetric hydrogen densities. For $LiBH_4$(010) surface, the structural and chemical effects on dehydrogenation were considered using the strain (-3% − +3%) and five dopants (M = Na, K, Al, F, or Cl). The hydrogen release energies of a hydrogen molecule decreased with increasing tensile strain on the $LiBH_4$(010) surface. The tensile strain was useful for promoting the dehydrogenation process by weakening the B-H interactions. Among the dopants examined, the most favorable dopant to enhance dehydrogenation was Al. The ranking of dopants for promoting hydrogen release was Al > Cl > F > Na > K. Remarkably, co-doping of Al and Cl was more effective for hydrogen release than the single doping of Al or Cl with the lowest hydrogen desorption energy. These methods that destabilize metal hydrides are practical for tuning the hydrogen release of $LiBH_4$ hydrides.

It is very significant to understand the dehydrogenation mechanism of metal hydrides for hydrogen storage. A first-principle approach is a valuable and powerful tool in the design of alloy systems. Our work shows that both dopant/co-doping and pressure/strain can facilitate the release of hydrogen from $NaCaH_3$, $KMgH_3$, and $LiBH_4$ hydrides by reducing the reaction enthalpies. These results can be utilized as efficient means for the design of highly promising hydride-based hydrogen storage materials.

TABLE OF CONTENTS

LIST OF FIGURES

LIST OF TABLES

LIST OF ABBREVIATIONS

DFT	Density functional theory
DOS	Density of states
MOF	Metal-organic frameworks
CNT	Carbon nanotubes
SWNTs	Single-walled carbon nanotubes
VASP	Vienna ab initio simulation package
GGA	Generalized-gradient approximation
PAW	Projector augmented wave
PBE	Perdew-Burke-Ernzerhof
ZPE	Zero-point energy
DDEC	Density derived electrostatic and chemical

CHAPTER 1. Introduction

1.1. Hydrogen energy

Nowadays, 80% of the energy requirement in the world is supported by fossil fuels, which includes coal, petroleum, and natural gas [1]. Unfortunately, these energy reserves will not persist in abundance forever. In addition, the combustion of fossil fuels also brings a heavy burden to our environment, due to the emission of greenhouse gases like CO_2, sold waste and other pollutions [2]. The energy crisis and environment problems become more and more serious. Thus, exploiting clean and renewable energy is extremely urgency.

Hydrogen has been considered as a promising alternative energy carrier in the 21st century [3]. On the periodic table, hydrogen is found to be the lightest element. It has a density of only 0.0899 kg/m^3 at normal temperature (272.150 K) and pressure (101.325 kPa) [4]. Hydrogen is also the most abundant element in the universe (88.6% by mass). It does not occur naturally in large quantities for pure hydrogen on the earth. Hydrogen is always found in a bonded form, mainly store in water, living organisms and fossil fuels [5]. With current technologies, hydrogen can be produced from methane or by electrolysis of water [6]. The current leading technology for producing hydrogen in large quantities is seam-methane reforming, which is dependent on fossil fuels [7]. In addition, by using thermochemical, photochemical, photoelectrochemical, electrochemical, biochemical, or biophotochemical routes, hydrogen can be generated from water. Among available fuel molecules, hydrogen shows many desirable attributes as a better fuel with good combustion energy. It is not only abundantly available, generates nontoxic emissions, but also high efficiency. The energy density of hydrogen is 143 MJ/Kg. It is approximately 3 times higher than that store by

petroleum-based fuels [8]. A comparison of properties Between hydrogen and the other fuels is listed in Table 1.1 [9]. As an excellent alternative energy carrier, the application of hydrogen becomes one important cyclic part of sustainable global energy system, as shown in Fig. 1.1 [10].

1.2. Hydrogen storage

For the practical utilization of hydrogen energy, hydrogen production is the foundation and the hydrogen storage and transportation are the core processes. To develop the "hydrogen economy", a major obstacle is the problem of hydrogen storage, which is needed to be solved currently. At present, hydrogen can be stored by three different phases: gas, liquid, and solid states [11].

1.2.1. Gaseous hydrogen

Storage of hydrogen as a gas typically requires high-pressure tanks or cylinder (350 - 700 bar tank pressure). The hydrogen gas is kept under pressures to increase the storage density. Hydrogen with a gravimetric capacity of 4.5 wt.% can be stored in the gaseous phase at a pressure of 700 bar [12]. It is low cost and relatively mature for this technology. But there is much lower volumetric hydrogen storage density than hydrocarbon fuels. In addition, the gaseous hydrogen also has safety hazards for leak and explosion [1]. Even though this technique is the most commonly used for vehicle fuel systems until now, it is not the most practical method in the long run.

Table 1.1. Properties of hydrogen and the other fuels [9].

	Hydrogen	Petroleum	Methanol	Methane	Propane	Ammonia
Boiling point [K]	20.3	350-400	337	111.7	230.8	240
Liquid density [kg/m^3] NTP	70.8	702	797	425	507	771
Gas density [kg/m^3] NTP	0.0899	----	----	0.718	2.01	0.77
Heat of vaporization [KJ/kg]	444	302	1168	577	388	1377
Higher heating value [MJ/kg]	41.9	46.7	23.3	55.5	48.9	22.5
Lower heating value [MJ/kg]	120	44.38	20.1	50.0	46.4	18.6
Lower heating value (liquid) [MJ/m^3]	8520	31170	16020	21250	23520	14350
Diffusivity in air [cm^2/s]	0.63	0.08	0.16	0.20	0.10	0.20
Lower flammability limit [vol% (in air)]	4	1	7	5	2	15
Higher flammability limit [vol% (in air)]	75	6	36	15	10	28
Ignition temperature in air [0C]	585	222	385	534	466	651
Ignition energy [MJ]	0.02	0.25	----	0.30	0.25	----
Flame velocity [cm/s]	270	30	----	34	38	----

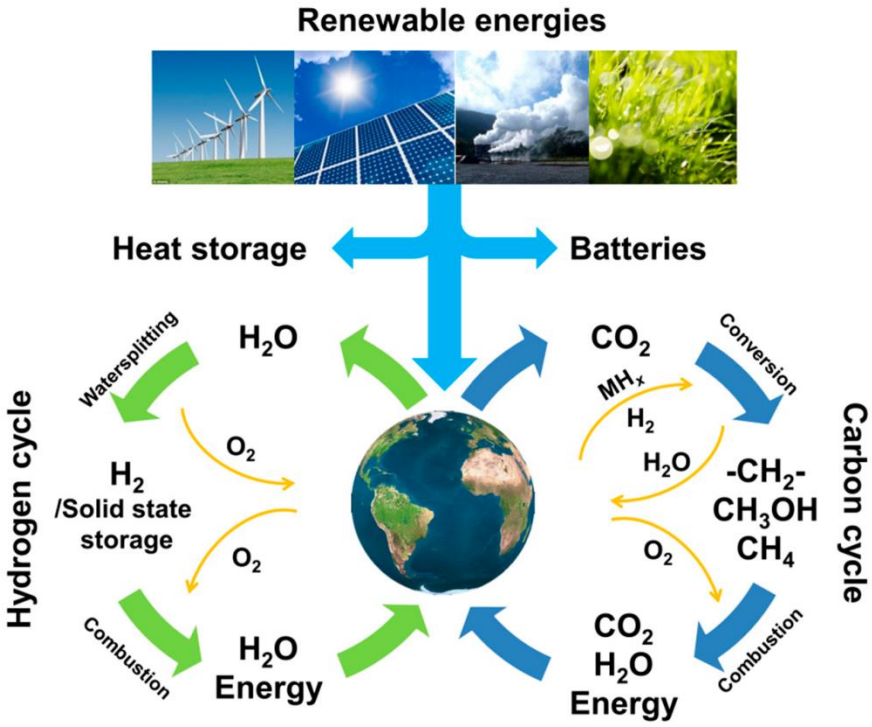

Figure 1.1. A sustainable energy system in global [10].

1.2.2. Liquefied hydrogen

Storage of hydrogen as a liquid requires cryogenic temperatures and high pressure. Because the boiling point of hydrogen at one atmosphere pressure is -252.8℃ [1]. The volumetric hydrogen density in liquid phase is almost 845 times as much as that in gas phase. The transport efficiency of liquid hydrogen is also higher than that of gaseous hydrogen. The application of liquid hydrogen is mostly used in aeronautics and astronautics fields as a liquid fuel [13]. This technique can reduce the requirement of weight and size of cryogenic storage tanks. But the liquefaction process needs high energy consumption and cost. Specialized cryogenic vessels are also necessary to prevent severe boil-off losses.

1.2.3. Solid state for hydrogen storage

Hydrogen can also be stored on the surfaces of solids by physical adsorption, or within solids by chemical reaction [14]. Hydrogen in the solid state can be released by decomposition reactions under the suitable temperature or pressure-based swing techniques. The transport volume of solid state is reduced greatly comparing with gaseous and liquid hydrogen. Moreover, the volumetric hydrogen density in solid state is relatively high. It also has safe and convenient operation to store hydrogen in solid state [15].

1.2.3.1. Hydrogen physisorption

Like other gases, hydrogen molecules can be held to the surface through van der waals interactions. The strength of this physical adsorption for hydrogen is very weak with the enthalpy of adsorption between 4 and 10 KJ/mol. This physisorption process needs low temperatures and high surface area to obtain significant amount of hydrogen gas adsorbed. The

kinetics of hydrogen adsorption and desorption is very fast as no activation energy involved. Porous materials such as metal-organic frameworks (MOF) [16], zeolites [17], carbon nanotubes (CNT) [18], can adsorb a high density of hydrogen molecules by high surface area and pore volume. However, it can achieve the high hydrogen storage capacities only at extremely low temperature about 77 K [19]. In addition, the hydrogen physisorption systems can react with other chemical hydrides. Thus, protective coating should be improved to resist these chemical oxidations [2].

1.2.3.2. Hydrogen chemisorption

The classic materials with chemical bonding for hydrogen storage are metal hydrides. Hydrogen molecules are absorbed on the surface of the metal and dissociate into two hydrogen atoms. These hydrogen atoms diffuse into the metal and form a chemical bond with the metal atoms, which forms the metal hydride [20, 21]. This is the direct dissociative chemisorption to hydrogenate metal. The process of chemisorption is shown in Fig. 1.2 [21]. Generally, the chemical bond between metals and hydrogen is covalent in nature, but some hydrides are formed from ionic bonds. These metal–hydrogen bonds provide a high hydrogen density. Another way to form the metal hydride is electrochemical splitting of water. The two reactions are as follows [4]:

$$\mathrm{M} + \frac{x}{2}\mathrm{H_2} \leftrightarrow \mathrm{MH}_x$$

$$\mathrm{M} + \frac{x}{2}\mathrm{H_2O} + \frac{x}{2}e^- \leftrightarrow \mathrm{MH}_x + \frac{x}{2}\mathrm{OH}^-$$

Where M refers to the metal. Most of the hydrogenation reactions to form hydrides are reversible. The process can be realized safely under moderate temperature and pressure. Thus,

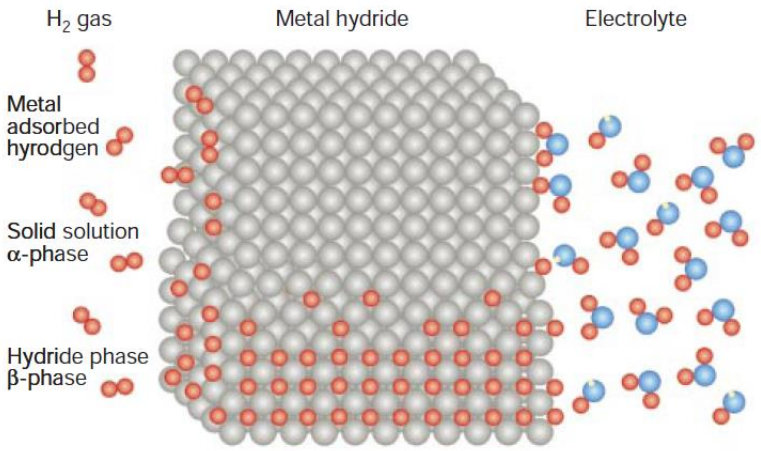

Figure 1.2. Schematic model of hydrogen adsorption process in a metal hydride. The hydrogen atoms in the metal hydride are from hydrogen molecules with physisorption (on the left side) and the dissociation of water molecules (on the right side) [21].

metal hydrides show great advantage to release hydrogen for the practical application. Some metal hydrides like MgH_2 have higher hydrogen-storage density (6.5 H atoms/cm^3) than hydrogen gas (0.99 H atoms/cm^3) or liquid hydrogen (4.2 H atoms/cm^3) [4]. The high stability and safety, the reversibility, limited energy loss, and long cycle life allow the metal hydrides to be promising candidates for on-board vehicle applications. This is one of the important development directions in the future for hydrogen storage.

1.2.4. Liquid Organic Hydrogen Carriers

Another method to store hydrogen at ambient conditions are Liquid Organic Hydrogen Carriers (LOHC) [22]. LOHCs are potentially cheap, safe, and easily manageable. Moreover, they allow for a long-term energy storage without boil-off or other hydrogen losses as well as an uncomplicated transportation. The storage concept of hydrogen within a LOHC is shown in Fig. 1.3 [22]. It is typically based on reversible hydrogenation and dehydrogenation of carbon double bounds. During the hydrogenation process the double bounds are saturated with hydrogen. This process is exothermic and typically takes place at elevated temperatures and pressures. Vice versa the hydrogen can be released again in its pure form based on a catalytic endothermic de-hydrogenation reaction taking place mostly close to atmospheric pressure, although at elevated temperatures. The LOHC-based storage systems include N-ethylcarbazole, dibenzyltoluene, toluene and 1,2-dihydro-1,2-azaborine [22].

1.3. Metal hydrides

For practical applications, an ideal hydrogen storage material should be required to have the main following properties: high energy storage capacity with abundance of hydrogen above 6.5 wt % and no less than 65 g/L of hydrogen from the material [23], low temperature and moderate pressure for hydrogen desorption, reversibility of the thermal absorption/desorption cycle, low heat of formation, limited energy loss, low cost, high stability for long cycle life, fast kinetics, and high safety [1, 2, 24]. It is profitable to store hydrogen in the solid state combining with light elements. Because it may achieve high gravimetric hydrogen densities, as seen in Fig. 1.4 [7]. Unfortunately, there is no material known can satisfy all these requirements for commercial applications until now. Metal hydrides possess wide range of compositions, versatile stable structures, and various excellent properties, has been considered as a class promising material for hydrogen storage. It is significant and challenging to develop and explore promising metal hydrides to store hydrogen. More efforts should be devoted to the advanced metal hydrides as a safe and efficient way for hydrogen storage. The properties of some commonly studied materials are listed in Table 1.2 [23].

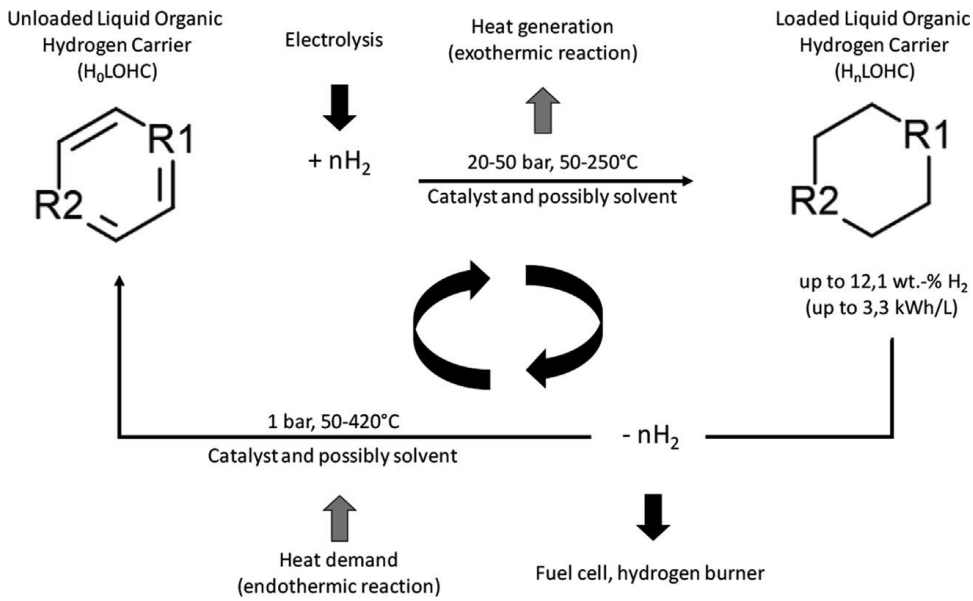

Figure 1.3. Concept of the LOHC storage [22].

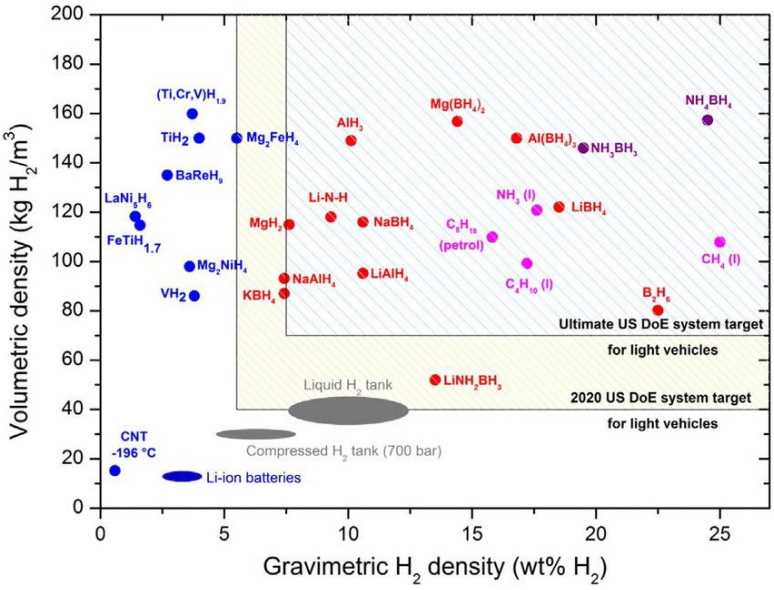

Figure 1.4. Overview of volumetric and gravimetric hydrogen density for part of materials [7].

Table 1.2. Properties of some commonly studied materials [23].

Material	Practical wt % H	Kinetic reversibility	T_{dec}/°C	Notes
$PdH_{0.6}$	0.6	excellent	ambient	$1000/oz.
NaH	4.2	good	425	cheap Na metal
BN (Collapsed nanotubes)	4.2	sufficient	300	expensive
Mg_2NiH_4	3.6	very good	ambient	fails to meet wt% criterion
CaH_2	4.8	good	600	cheap Ca metal
HF(l)	5.0	*c*	boils at +20	highly toxic and corrosive
$NaAlH_4$:TiO_2	5.5	good	125	fails to meet wt% criterion
	6.5			DOE limit
Li_2NH	6.5-7.0	good	285	
MgH_2	7.6	very poor	330	cheap Mg metal
$Li_3Be_2H_7$	8.7	sufficient	300	toxic and expensive
PH_3(l)	8.8	irreverisble	broad range	toxic liquid, low storage temperature, risk of explosion
$LiBH_4$:SiO_2	9.0	so far irreversible	200-400	at present $LiBH_4$ is expensive
$NaBH_4$/H_2O(l)	9.2	irreversible	ambient	expensive Ru-containing catalyst
AlH_3	10.0	irreversible	150	very cheap Al metal
NH_3AlH_3	11.6-12.8	irreversible	broad range	
MeOH(l)	12.5	irreversible	very difficult thermal activation	toxic liquid
SiH_4(l)	12.5	irreversible	broad range	toxic liquid, low storage temperature,
LiH	12.6	poor	720	aggressive Li vapor formed upon decomposition
$NaBH_4$	13.0	irreversible	400	cheap
NH_4F/$LiBH_4$	13.6	irreversible	> ambient	laboratory-scale reaction
petroleum	17.3			
BeH_2	18.2	irreversible	250	extremely toxic and volative powder
NH_3BH_3	18.3	irreversible	melts at +104	multistage decomposition
$LiBH_4$	19.6	irreversible	380	expensive as compared to Na compound
$Be(BH)_2$	20.6	irreversible	sublimes at +40	toxic, flammable, and expensive
B_2H_6(l)	21.7	irreversible	ambient	explosive
NH_4BH_4	24.4	irreversible	-40 to +100	multistage decomposition
CH_4(l)	25.0	irreversible	very difficult thermal activation	gas difficult to liquidify

1.3.1. Intermetallic hydrides

So far, various metal hydrides and their properties for hydrogen storage have been investigated. In early research, intermetallic compounds are attractive for storing hydrogen. They have the ability to absorb large amount of hydrogen. The common intermetallic hydrides studied include $PdH_{0.6}$, $LaNi_5H_6$, $FeTiH_2$, Mg_2NiH_4 [25, 26]. The properties of some common intermetallic metal hydrides are listed in Table 1.3 [2]. In intermetallic compounds, there are interactions between the hydrogen atoms and metal atoms. It can determine the hydrogen storage properties of intermetallic hydrides directly [2, 27]. However, the low gravimetric hydrogen storage capacities and slow kinetics limits their practical application as an energy carrier [28]. To improve the performance of intermetallic hydrides for hydrogen storage, more effort has been put on various aspects of intermetallic hydrides like the composition, the surface, the size of hydrides particles [29].

1.3.2. Complex metal hydride

Recently, the attention has been shifted to the complex metal hydride. Since the composition of most conventional metal hydrides is heavy, formed by the light metals such as lithium (Li), sodium (Na), magnesium (Mg), and aluminum (Al) are especially interesting for hydrogen storage. They have light weight and relatively high volumetric density of hydrogen [30]. In complex hydride, the metal atoms and hydrogen are connected by stable and ionic bonding, whereas covalent bonds are mainly found in the anions. Among the different combining ways, there is a sliding transition for the nature of the quantum chemical binding [31]. In 1996, Bogdanovic and Schwickardi [32] found that the introduction of TiO_2 can decrease the decomposition temperature of $NaAlH_4$. More than that, the reversibility of the

reaction was also discovered for several desorption/absorption cycles. They showed a good example to develop the potential of such hydrides for hydrogen storage. Then, the relevant research is extended to a variety of complex metal hydrides, including alanates ($LiAlH_4$, $Ca(AlH_4)_2$, $KAlH_4$), borohydrides ($LiBH_4$, $NaBH_4$, $Mg(BH_4)_2$), and nitrides (Li_2NH) [2, 10, 33, 34].

Although the complex metal hydrides have advantages to store hydrogen, they are unsuitable for vehicle applications due to the poor thermodynamic and kinetic properties. The hydrogen release and uptake of these hydrides need high temperature and pressure. In addition, the decomposition process may produce highly stable structures and it is also hard to handle safely [35]. It also remains not fully understood for the complicated hydrogen release pathway from complex hydrides. Thus, it is a challenge to apply the complex metal hydrides as an efficient energy carrier.

1.4. Strategies to modify the metal hydrides

Many strategies have been proved to effectively improve the hydrogen storage performance of metal hydrides by numerous experiments and theoretical research. The first method is introducing the appropriate dopants or catalysts. It was discovered that the reaction kinetics of $NaAlH_4$ can be improved drastically after adding a small amount of transition metals Ti or Zr [36]. The temperatures and pressures for cycling are also close to optimal. Using a mechanical ball-milling technique, Zhang et. al [37] reported that the dehydrogenation properties of MgH_2 were remarkably enhanced by doping Ni and graphene. The dehydrogenation temperature is 339.5°C in Ni and graphene doped MgH_2 system. It is approximately 90°C lower than that in pure MgH_2 system. Besides, by introducing Ti based

Table 1.3. Properties of some common intermetallic metal hydrides [2].

Intermetallic compound	Intermetallic hydride	Hydrogen storage capacity (wt%)	Temperature at 1 bar (K)
$LaNi_5$	$LaNi_5H_6$	1.37	295
FeTi	$FeTiH_2$	1.89	185
Mg_2Ni	Mg_2NiH_4	3.59	255
$ZrMn_2$	$ZrMn_2H_2$	1.77	440

additives $TiCl_3$, the initial dehydrogenation temperature of $Mg(BH_4)_2$ was significantly reduced from 535 to 361 K due to the lower stability [38]. It is an efficient strategy to enhance the hydrogen storage properties especially for the dehydrogenation thermodynamics by introducing the dopants or catalysts. Combing appropriate reactant as a destabilization is the second approach. A high hydrogen storage capacity of 6.5 wt.% can be found in Li_2NH which formed by the reversible reaction of $LiNH_2$ and LiH [39, 40]. LiH played an important role in reducing the decomposition temperature by destabilizing $LiNH_2$. Patelli et. al [41] incorporated TiH_2 into MgH_2, and the temperature of reversible hydrogen desorption for MgH_2 was reduced to the range of 340 to 425 K. Furthermore, the nanoscaffolding incorporation can also improve the hydrogenation and dehydrogenation properties [42]. Using DFT method, the dehydrogenation performance of MXH_4 (M = Na, Li and X = Al, B) nanoclusters confined in carbon nanotubes was investigated by Meenakshi et. al [43]. With respect to pure system, the hydrogen release energies of modified nanoclusters were decreased sharply by up to 68.3% [43]. By adding 10 wt.% purified single-walled carbon nanotubes (SWNTs), the composite with $LiBH_4$ and MgH_2 can decompose around 10 wt.% hydrogen at the temperature 450°C within 20 min [44]. The micro-confinement effect of SWNTs is an important contributing factor on this reaction [45]. In spite of this, the hydrogen storage properties especially for hydrogen release need to be further improved. To gain the excellent hydrogen storage materials, more efforts should be devoted to the development of the light metal hydrides.

In recent years, the first-principle calculation is increasingly prevailing. It is a method to calculate basic physical properties directly such as mass, charges, and Coulomb force of an electron based on the quantum mechanical modelling [46]. It is a powerful tool to find agreement between theoretical calculations and experimental results by deducing physical and

chemical properties directly from the basic principle. With the development of the computer performance, it has become possible to calculate various systems including many-body systems with high speed and very low cost. This method is indispensable as a valuable tool in predicting new materials and understanding characterizations of existing materials. Thus, it is significant to design advanced metal hydrides for hydrogen storage using first-principle calculations.

Reference

[1] P.R. Prabhukhot, M.M. Wagh, A.C. Gangal, A review on solid state hydrogen storage material. Adv. Energy Power 2016, 4, 11-22.

[2] N.A.A. Rusman, M. Dahari, A review on the current progress of metal hydrides material for solid-state hydrogen storage applications. Int. J. Hydrogen Energ. 2016, 4, 12108-12126.

[3] C. Winter, Hydrogen energy - Abundant, efficient, clean, A debate over the energy-system-of-change, Int. J. Hydrogen Energ. 2009, 34, S1-S52.

[4] R. Prabhukhot Prachi, M. Wagh Mahesh, C. Gangal Aneesh, A review on solid state hydrogen storage material. Adv. Energy Power 2016, 4, 11.

[5] A. Züttel, Materials for hydrogen storage. Mater. Today 2003, 6, 24-33.

[6] J. C. Jones, Energy-return-on-energy-invested for hydrogen fuel from the steam reforming of natural gas. Fuel 2015, 143, 631.

[7] K.T. Møller, T.R. Jensen, E. Akiba, H.W. Li, Hydrogen-A sustainable energy carrier. Prog. Nat. Sci. 2017, 27, 34-40.

[8] L.Z. Ouyang, J.M. Huang, H. Wang, Excellent hydrolysis performances of Mg3RE hydrides. Int. J. Hydrogen Energ. 2013, 38, 2973-2978.

[9] B. Vishwanathan, M.A. Scibioh, Handbook of Fuel cells, Principle and Applications. Hyderabad, Univerisity Press, 2006.

[10] K.T. Møller, D. Sheppard, D.B. Ravnsbæk, C.E. Buckley, E. Akiba, H.W. Li, T.R. Jensen, Complex metal hydrides for hydrogen, thermal and electrochemical energy storage. Energies 2017, 10, 1645.

[11] K.C. Kim, A review on design strategies for metal hydrides with enhanced reaction thermodynamics for hydrogen storage applications. Int. J. Energy Res. 2018, 42, 1455-1468.

[12] U. Eberle, B. Müller, R. Von Helmolt, Fuel cell electric vehicles and hydrogen infrastructure, status 2012. Energy Environ. Sci. 2012, 5, 8780-8798.

[13] M.S. Sadaghiani, M. Mehrpooya, Introducing and energy analysis of a novel cryogenic hydrogen liquefaction process configuration. Int. J. Hydrogen Energ. 2017, 42, 6033-6050.

[14] J. Ren, N.M. Musyoka, H.W. Langmi, M. Mathe, S. Liao, Current research trends and perspectives on materials-based hydrogen storage solutions, a critical review. Int. J. Hydrogen Energ. 2017, 42, 289-311.

[15] K.L. Lim, H. Kazemian, Z. Yaakob, W.R.W. Daud, Solid-state materials and methods for hydrogen storage, a critical review. Chem. Eng. Technol. 2010, 33, 213-226.

[16] M.P. Suh, H.J. Park, T.K. Prasad, D.W. Lim, Hydrogen storage in metal-organic frameworks. Chem. Rev. 2012, 112, 782-835.

[17] J. Weitkamp, M. Fritz, S. Ernst, Zeolites as media for hydrogen storage. Int. J. Hydrogen Energ. 1995, 20, 967-970.

[18] F.L. Darkrim, P. Malbrunot, G.P. Tartaglia, Review of hydrogen storage by adsorption in carbon nanotubes. Int. J. Hydrogen Energ. 2002, 27,193-202.

[19] L.J. Murray, M. Dincă, J.R. Long, Hydrogen storage in metalorganic frameworks. Chem. Soc. Rev. 2009, 38, 1294-1314.

[20] B. Sakintuna, F. Lamari-Darkrim, M. Hirscher, Metal hydride materials for solid hydrogen storage, a review. Int. J. Hydrogen Energ. 2007, 32, 1121-1140.

[21] L. Schlapbach, A. Züttel, Hydrogen-storage materials for mobile applications. In Materials for sustainable energy, a collection of peer-reviewed research and review articles from nature publishing group 2011, 265-270.

[22] M. Niermann, A. Beckendorff, M. Kaltschmitt, K. Bonhoff, Liquid Organic Hydrogen Carrier (LOHC)–Assessment based on chemical and economic properties. Int. J. Hydrogen Energ. 2019, 44, 6631-6654.

[23] W. Grochala, P.P. Edwards, Thermal decomposition of the non-interstitial hydrides for the storage and production of hydrogen. Chem. Rev. 2004, 104, 1283-1316.

[24] https,//www.energy.gov/eere/office-energy-efficiency-renewable-energy

[25] G. Sandrock, G. Thomas, The IEA/DOC/SNL on-line hydride databases. Appl. Phys. A 2001, 72, 153-155.

[26] A. Szajek, M. Jurczyk, I. Okonska, K. Smardz, E. Jankowska, L. Smardz, Electrochemical and electronic properties of nanocrystalline Mg-based hydrogen storage materials. J. Alloy Compd. 2007, 436, 345-50.

[27] A. Gasiorowski, W. Iwasieczko, D. Skoryna, H. Drulis, M. Jurczyk, Hydriding properties of nanocrystalline $Mg_{2-x}M_xNi$ alloys synthesized by mechanical alloying (M = Mn, Al). J. Alloy Compd. 2004, 364, 283-8.

[28] H. Leng, T. Ichikawa, H. Fujii, Hydrogen storage properties of Li-Mg-N-H systems with different ratios of $LiH/Mg(NH_2)_2$. J. Phys. Chem. B 2006, 110, 12964-8.

[29] L. Wang, K. Young, J. Nei, D. Pawlik, K.Y.S. Ng, Hydrogenation of AB_5 and AB_2 metal hydride alloys studied by in situ X-ray diffraction. J. Alloy Compd. 2014, 616, 300-5.

[30] I.P. Jain, P. Jain, A. Jain, Novel hydrogen storage materials, A review of lightweight complex hydrides. J. Alloy Compd. 2010, 503, 303-339.

[31] G. Stan, M.W. Cole, Hydrogen adsorption in nanotubes. J. Low Temp. Phys. 1998, 110, 539-544.

[32] B. Bogdanovic, M. Schwickardi, Ti-doped alkali metal aluminium hydrides as potential novel reversible hydrogen storage materials. J. Alloy Compd. 1997, 253, 1-9.

[33] J.-P. Soulié, G. Renaudin, R. Cerný, K. Yvon, Lithiumboro-hydride $LiBH_4$, I. Crystal structure. J. Alloys Compd. 2002, 346, 200-205.

[34] A. Züttel, P. Wenger, S. Rentsch, P. Sudan, P. Mauron, C. Emmenegger, $LiBH_4$ a new hydrogen storage material. J. Power Sources 2003, 118, 1-7.

[35] M.B. Ley, L.H. Jepsen, Y.-S. Lee, Y.W. Cho, J.M. Bellosta von Colbe, M. Dornheim, Complex hydrides for hydrogen storage-new perspectives. Mater. Today 2014, 17, 122-8.

[36] C. Weidenthaler, A. Pommerin, M. Felderhoff, B. Bogdanović, F. Schüth, On the state of the titanium and zirconium in Ti- or Zr-doped $NaAlH_4$ hydrogen storage material. Phys. Chem. Chem. Phys. 2003, 5, 5149-5153.

[37] J. Zhang, H. Qu, G. Wu, L.B. Song, X.F. Yu, D.W. Zhou Remarkably enhanced dehydrogenation properties and mechanisms of MgH_2 by sequential - doping of nickel and graphene. Int. J. Hydrogen Energ. 2016, 41, 17433-17441.

[38] H.W. Li, K. Kikuchi, Y. Nakamori, K. Miwa, S. Towata, S. Orimo, Effects of ball milling and additives on dehydriding behaviors of well-crystallized $Mg(BH_4)_2$. Scr. Mater. 2007, 57, 679-682.

[39] P. Chen, Z. Xiong, J. Luo, J. Lin, K.L. Tan, Interaction between lithium amide and lithium hydride. J. Phys. Chem. B 2003, 107, 10967-10970.

[40] P. Chen, Z. Xiong, J. Luo, J. Lin, K.L. Tan, Interaction of hydrogen with metal nitrides and imides. Nature 2002, 420, 302-304.

[41] N. Patelli, M. Calizzi, A. Migliori, V. Morandi, L. Pasquini, Hydrogen desorption below 150 degrees C in MgH_2-TiH_2 composite nanoparticles, equilibrium and kinetic properties. J. Phys. Chem. C 2017, 121, 11166-11177.

[42] A.F. Gross, J.J. Vajo, S.L.V. Atta, G.L. Olson, Enhanced hydrogen storage kinetics of $LiBH_4$ in nanoporous carbon scaffolds. J. Phys. Chem. C 2008, 112, 5651-7

[43] R.K. Bhakta, S. Maharrey, V. Stavila, Thermodynamics and kinetics of $NaAlH_4$ nanocluster decomposition. Phys. Chem. Chem. Phys. 2012, 14, 8160-8169.

[44] P.J. Wang, Z.Z. Fang, X.D. Kang, P. Wang, Effect of SWNTs on the reversible hydrogen storage properties of $LiBH_4$-MgH_2 composite. Int. J. Hydrogen Energ. 2008, 33, 5611-6.

[45] P.J. Wang, Z.Z. Fang, L.P. Ma, X.D. Kang, P. Wang, Effect of carbon addition on hydrogen storage behaviors of Li-Mg-B-H system. Int. J. Hydrogen Energ. 2010, 35, 3072-5.

[46] C. Wolverton, V. Ozoliņš, First-principles aluminum database, Energetics of binary Al alloys and compounds. Phys. Rev. B 2006, 73, 144104.

CHAPTER 2. Perovskite hydride and lithium borohydride

2.1. Perovskite hydride

As promising candidates for hydrogen storage, perovskite-type hydrides comprising of light metals have light weight, high hydrogen capacities, and flexible structures [1, 2]. These hydrides have a general chemical formula ABH_3, where A is alkali metals (Li, Na, K, Rb, or Cs), and B is alkaline-earth metals (Be, Mg, Ca, Sr, or Ba). To make a comprehensive understanding of the hydrogenation/dehydrogenation properties of the light perovskite-type hydrides, all the possibilities including the experimentally available structures and theoretically designed structures should be considered. Moreover, like most metal hydrides, the high stable thermodynamics and slow kinetics properties limits the practical application of these hydrides. Among them, the mechanism of hydrogen release on the thermodynamic aspects is particularly important. It will provide great help to explore advanced materials for hydrogen storage. Thus, it is a key to find effective ways to promote the hydrogen release of the perovskite-type hydrides.

2.1.1. $ABeH_3$ and $AMgH_3$ perovskite-type hydrides

2.1.1.1. $LiBeH_3$ and $NaBeH_3$

The perovskite-type hydride $LiBeH_3$ is an orthorhombic structure (space group P*nma*, No. 62) with 15.93 wt. % of hydrogen [3]. The $LiBeH_3$ structure is composed of corner-sharing BeH_6 octahedra and the there are eight H atoms around each Li atom. A cubic phase can be found in $NaBeH_3$ and the lattice constant is 3.35 Å using DFT calculations with PBE-GGA method [4]. The crystal structure of $LiBeH_3$ and $NaBeH_3$ is shown as Fig. 2.1. These two

materials display excellent performance to improve the photocatalytic H_2 production systems [6, 7]. The good oxidation ability and high photocatalytic activity can be obtained in $LiBeH_3$ and $NaBeH_3$ due to their indirect band gaps and a strong optical absorption coefficient [5]. Thus, they are also considered as promising materials for light-driven photocatalysts.

2.1.1.2. $KBeH_3$, $RbBeH_3$, and $CsBeH_3$

The ground states of $KBeH_3$ and $RbBeH_3$ have been proved to be at $CaCO_3$(II)-type structural arrangement with $P2_1/c$ space group [8]. The crystal structures of $KBeH_3$ and $RbBeH_3$ are composed by almost-planar BeH_3 molecules around the K and Rb matrix, respectively. For $CsBeH_3$, the structure with $P2_1/m1$ space group have the lowest total energy [8]. The atomic arrangements of these three structures are similar, as shown in Fig. 2.2 [8]. Their structures consist of alkali atoms and almost separated BeH_3 planar molecules. It is rigorous to obtain the experimental data available due to the special precautions for the toxic element Be [8, 9]. These hydrides have high gravimetric densities to store hydrogen. Thus, theoretical studies on these hydrides is safe and efficient way. It is better to explore more fully properties of structures and feasibility as the promising hydrogen storage materials.

2.1.1.3. $LiMgH_3$ and $NaMgH_3$

In recent years, Mg-based hydrides as the typical hydrogen storage materials have been attracted much attention. To develop the new functional materials, more efforts have been made to investigate specific materials properties. No experimentally structural data of $LiMgH_3$ can be acquired hitherto. Theoretical studies have shown that the ground state phase of $LiMgH_3$ is $LiTaO_3$-type [10]. The crystal structure of $LiMgH_3$ is composed by corner sharing MgH_6 octahedra, as shown in Fig. 2.3 (a). This octahedra has been proved to be distorted

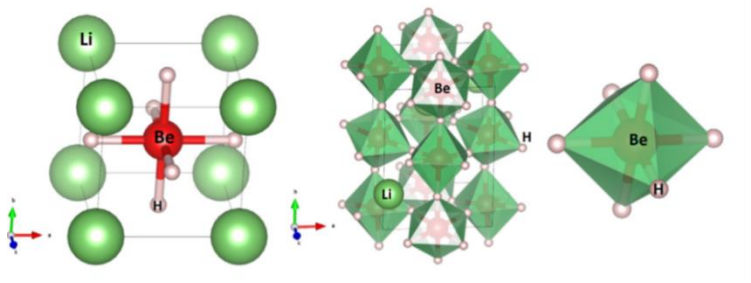

(a)

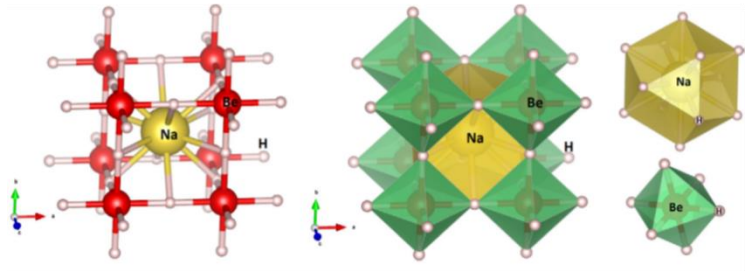

(b)

Figure 2.1. Crystal structure of the perovskite-type hydrides: (a) $LiBeH_3$, (b) $NaBeH_3$.

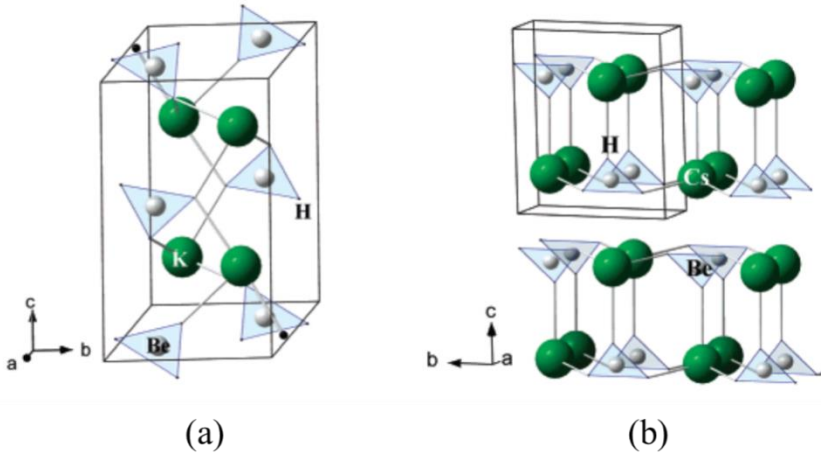

Figure 2.2. Predicted crystal structure of the perovskite-type hydrides: (a) $KBeH_3$ ($RbBeH_3$) (b) $CsBeH_3$ [8].

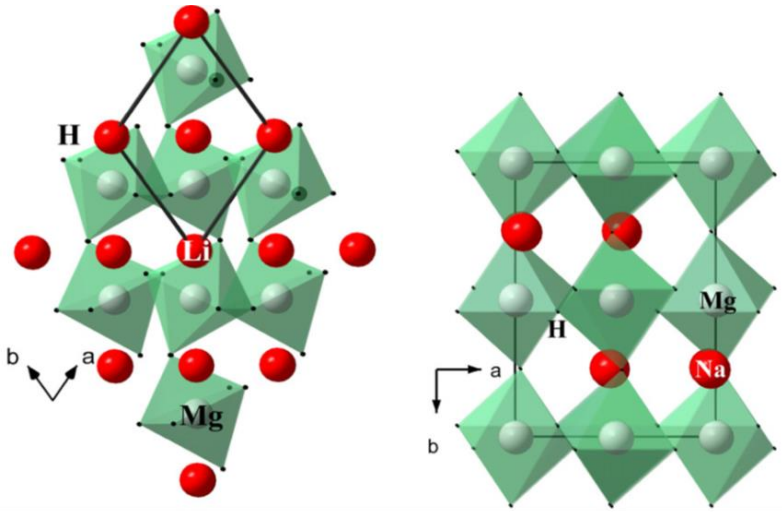

(a) (b)

Figure 2.3. Optimized crystal structure of: (a) $LiMgH_3$, (b) $NaMgH_3$ [10].

highly and each Li is surrounded by 6 H atoms. By the analysis of electronic structure, the $LiMgH_3$ has insulating characteristic [11]. Perovskite-type hydride $NaMgH_3$ can be synthesized using ball-milling method [12]. The crystal structure of $NaMgH_3$ is orthorhombic with P*nma* space group, as shown in Fig. 2.3 (b). It also consists MgH_6 octahedra somewhat distorted [10]. Besides, each Na and Mg cation is surrounded by 12 and 6 H anions, respectively.

$NaMgH_3$ is an insulator because of the direct large band gap and the hydrogen atoms make main contribution on the valence band [10]. The strong ionic character can be found in the mixed bonding between Mg and H atoms [13]. $NaMgH_3$ has been investigated to be as one of the suitable hydrogen storage materials due to the high gravimetric and volumetric H densities (6 wt. % and 88 kg/m^3) and the reversibility [14]. The dehydrogenation properties of $NaMgH_3$ can be improved by introducing the dopant K [15]. The calculated formation enthalpies of different crystal structures of K-doped $NaMgH_3$ are shown as Fig. 2.4 [15]. The destabilized structure of $NaMgH_3$ by 10 at.% of K reveals good hydrogen storage performance. The onset desorption temperature was decreased dramatically from 581 to 430 K.

2.1.1.4. $KMgH_3$, $RbMgH_3$, and $CsMgH_3$

The structure of $KMgH_3$ is an ideal perovskite-type atomic arrangement with P$m\overline{3}m$ space group [10]. The lattice parameter is 4.023 Å by experimentally measurement. Each K and Mg atom in $KMgH_3$ is surrounded by 12 and 6 H atoms, respectively. The unit cell of $KMgH_3$ crystal structure is shown as Fig. 2.5. Like $NaMgH_3$, $KMgH_3$ is also an insulator due to the wide band gap. The main contribution at Fermi level comes from hydrogen atoms. $KMgH_3$ can be synthesized by mechanical ball-milling method [16]. The single-step reaction has been

found in $KMgH_3$ decomposition. Using DFT calculations, the thermodynamic properties of $KMgH_3$ have been investigated [17]. In addition, it reported that the hydrogen positions determine the stability of $KMgH_3$ by first-principles studies [18]. However, little research focus on the hydrogen storage performance of $KMgH_3$ especially for the hydrogen release properties. Thus, it is necessary to make further investigation on the mechanism of hydrogenation/dehydrogenation performance of $KMgH_3$. Under high-pressure and moderate temperature conditions, the $Na_{1-x}Li_xMgH_3$ can be synthesized in one single step and a very short reaction time [19]. The hydrogen desorption temperature is decreased as the lower structural stability after adding Li dopant. Moreover, the decomposition of metal hydrides can be induced by pressure [20]. From these studies, the hydrogen storage properties of $KMgH_3$ may be improved by introducing dopants and pressure.

$RbMgH_3$ is the hexagonal perovskite-type hydride (6H-$BaTiO_3$-type) with $P6_3/mmc$ space group at the temperature of 5-300 K [10]. It contains the corner- and some face-sharing MgH_6 octahedra in the crystal structure of $RbMgH_3$ [21]. The 12-fold coordination of Rb ions with different coordination polyhedral can be found. H anion polarization mainly determines the stability of the 90° Mg-H-Mg bonds. The experiment has been proved that the dehydrogenation of $RbMgH_3$ can happen at low temperature (below 400 °C) and re-hydrogenation under moderate pressure and temperatures [21]. This perovskite hydride has the potential to be as a candidate for hydrogen storage. $CsMgH_3$ can be synthesized experimentally by mixing the binary hydrides [22]. There are two different modifications of $CsMgH_3$ from the available finding. One is β-$CsMgH_3$ with trigonal phase formed at high pressure. Another one is α-$CsMgH_3$ with orthorhombic phase formed at intermediate pressure [22, 23]. The α-$CsMgH_3$ with P*mmn* space group can be synthesized at much lower energy than β-$CsMgH_3$.

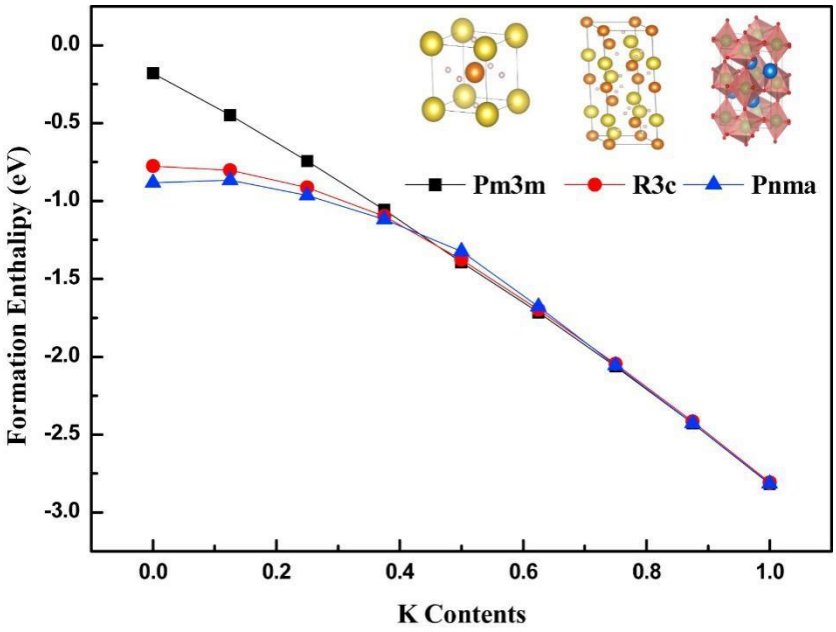

Figure 2.4. Calculated formation enthalpies of different crystal structures of $Na_{1-x}K_xMgH_3$ hydride [15].

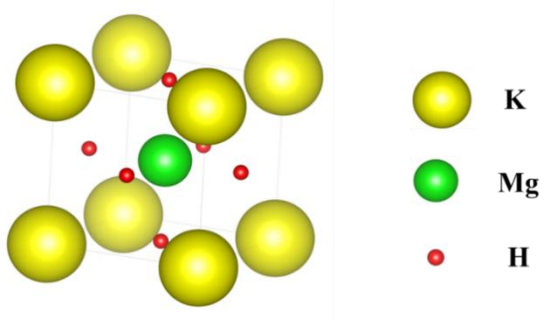

Figure 2.5. Unit cell of $KMgH_3$ crystal structure with $Pm\bar{3}m$ space group.

This structure consists of highly distorted MgH_6 octahedra and the atomic arrangement is superior than other Mg-based structures [8, 24]. Hence, it is interesting to investigate α-$CsMgH_3$ as one of the suitable and potential materials for hydrogen storage at moderate pressures and temperatures. The predicted crystal structures of $RbMgH_3$ and $CsMgH_3$ are shown in Fig. 2.6 [10].

2.1.2. $ACaH_3$, $ASrH_3$, and $ABaH_3$ perovskite-type hydrides

2.1.2.1. $LiCaH_3$, $NaCaH_3$, and $KCaH_3$

The hexagonal structure of $LiCaH_3$ with *R*3*c* space group has been predicted by theoretical calculations [25]. The slightly distorted LiH_6 octahedra in $LiCaH_3$ crystal structure is linked at the corner. Each Ca atoms is surrounded by 9 H atoms and the distances between them vary from 2.32 to 2.57 Å. In the same work, the ground state structure of $NaCaH_3$ is the low symmetry triclinic phase with $P\bar{1}$ space group. Every Na is surrounded by 5 H atoms and 7 H atoms surround one Ca atom. The bond length of Ca–H and Na–H are 2.33 and 2.30 Å, respectively [25]. For $KCaH_3$, the lowest total energy can be obtained in the $GdFeO_3$-type structure. The space group is P*nma*. The crystal structure of $KCaH_3$ consists of the corner-sharing octahedra CaH_6. In these slightly distorted octahedra, the bond length of Ca–H is 2.26 Å. The angles of H–Ca–H vary from 89° to 91°. There are 8 H atoms surrounding at one K atom. The structural features of $LiCaH_3$, $NaCaH_3$, and $KCaH_3$ can be obtained only from the theoretical simulation [25].

2.1.2.2. $RbCaH_3$ and $CsCaH_3$

$RbCaH_3$ and $CsCaH_3$ can be synthesized by experimental means and their crystal structures have almost same atomic arrangement [21, 25-27]. They are cubic structures with $Pm\overline{3}m$ space group. The $RbCaH_3$ structure consists of corner-sharing CaH_6 octahedra. Each Rb is surrounded by 12 H atoms and the distance between Rb and H is 3.21 Å [25]. There are 6 H atoms surrounding one Ca atom and the distance of Ca-H is 2.27 Å in the structure of $RbCaH_3$ [25]. For $CsCaH_3$, similar coordination can be found in. The distances of Cs-H and Ca-H are 3.27 and 2.31 Å in $CsCaH_3$, respectively [25]. The predicted crystal structures of $ACaH_3$ (A = Li, Na, K, Rb, or Cs) are shown in Fig. 2.7 [25]. For the theoretical calculations, the formation enthalpies can be calculated according to the following equations [25]:

$$MH + CaH_2 \rightarrow MCaH_3 \quad (1)$$

$$M + CaH_2 + \tfrac{1}{2}H_2 \rightarrow MCaH_3 \quad (2)$$

$$M + B + \tfrac{3}{2}H_2 \rightarrow MCaH_3 \quad (3)$$

$$MH + B + H_2 \rightarrow MCaH_3 \quad (4)$$

Here, M represents the alkali metals Li, Na, K, Rb, or Cs. The structural properties of these hydrides have been studied experimentally or theoretically, but the extended properties for practical application have not been researched thoroughly. Therefore, it is significance to explore the hydrogen storage performance from these hydrides.

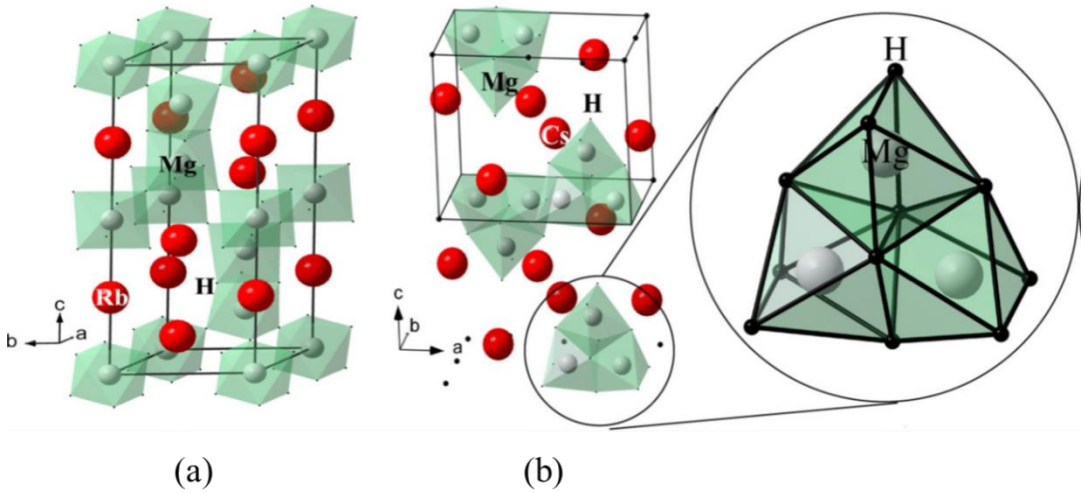

Figure 2.6. Ground state structures for (a) $RbMgH_3$, (b) $CsMgH_3$ [10].

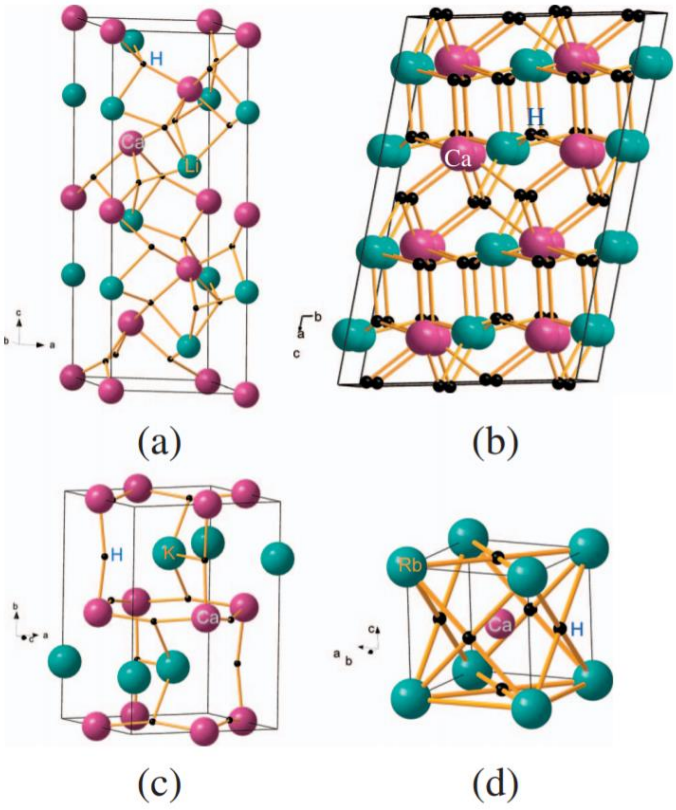

Figure 2.7. Predicted crystal structures of (a) $LiCaH_3$, (b) $NaCaH_3$, (c) $KCaH_3$, (d) $RbCaH_3$ and $CsCaH_3$ by theoretical calculations [25].

2.1.2.3. $ASrH_3$ and $ABaH_3$

For $ASrH_3$ and $ABaH_3$ perovskite-type hydrides (A = Li, Na, K, Rb, or Cs), there is no more data available from experimental or theoretical studies except $LiSrH_3$ and $LiBaH_3$ [28]. The crystal structure of $LiSrH_3$ is composed by cubo-octahedral surrounding with Sr and H atoms [29]. The space group type is P$m\overline{3}m$, as shown in Fig. 2.8 [28]. $LiBaH_3$ has the similar structure with $LiSrH_3$. In addition, the properties of persistent luminescence and thermoluminescence in $LiMH_3$ (M = Sr, Ba) with Eu^{2+} doping are investigated by both experiment and theoretical calculations [30]. There is still a considerable research space for the fundamental properties of these hydrides. First-principles studies are powerful and efficient to predict the properties of structure and thermodynamics of hydrides. Thus, it shows great advantage to screen advanced hydrogen storage materials from these light perovskite-type hydrides using the first-principles approach.

2.2. lithium borohydride

2.2.1. Structure of $LiBH_4$

$LiBH_4$ is an attractive candidate for hydrogen storage due to its lightweight (21.78g/mol) and high gravimetric/volumetric hydrogen densities of 18.5 wt.% and 121 kg H_2/m^3, respectively [1, 31-33]. At room temperature, the crystal structure of $LiBH_4$ is an orthorhombic symmetry group of P*nma* [34]. In this structure, $[BH_4]^-$ ions are almost ideal tetrahedral surrounded by Li^+ cations by the ratio of 1:4 and every Li^+ is surrounded by four $[BH_4]^-$ anions [35]. They form two different types of tetrahedral configurations. Under the different temperature or pressure, $LiBH_4$ may undergo a structural transition. A hexagonal

phase of $LiBH_4$ with the space group $P6_3mc$ can be found at approximately 408 K [36]. Moreover, at room temperature, $LiBH_4$ transforms into a new phase with pseudo-tetragonal A*ma2* space group by tuning the pressure from 1.2 - 10 GPa [37]. A cubic phase of $LiBH_4$ with $Fm\bar{3}m$ structure is formed above 10 GPa. There are octahedrally coordination between Li^+ cations and $[BH_4]^-$ groups [37]. The different crystal structures of $LiBH_4$ are shown in Fig. 2.9 [31].

2.2.2. Surface property of $LiBH_4$

It is very significant to investigate the surface properties of metal hydrides. For most metal hydrides, the dehydrogenation processes can be controlled by altering the surface such as the strain applying. Understanding this microscopic factor is helpful to determining the reactivity and then improving the activity of catalysts in metal hydrides [38, 39]. As one of the promising hydrogen storage material, the surface research of $LiBH_4$ is necessary to gain better performance.

The low-index surfaces of $LiBH_4$ with an orthorhombic structure have been studied by previous DFT calculations [40]. Among all surfaces studied, the (001) surface is more unstable than (010), (100), and (101) surfaces. The (010) surface of $LiBH_4$ with the ~0.12 J/m^2 surface energy was found to be the most stable one. These conclusions are in agreement with experimental results by the synchrotron X-ray diffraction [34, 36]. Thus, the further investigation for the hydrogen release property of $LiBH_4$ surface can be made based on this study.

2.2.3. Hydrogen release of $LiBH_4$(010) surface

The hydrogenation and dehydrogenation process of $LiBH_4$ is reversible. This reaction can produce LiH and boron absorb hydrogen. It is helpful for hydrogen storage. However, the hydrogen desorption of $LiBH_4$ occurs at 600 ℃ and 35 MPa and it requires a long time (>12 h) for the absorption reaction [41]. These conditions are rather harsh for the practical application of hydrogen energy. In the orthorhombic structure of $LiBH_4$, both ionic and covalent bonding exist. To reduce the thermodynamic stability of $LiBH_4$, the key idea is to weaken the bond strength between boron and hydrogen. Previous studies have confirmed that the many physical and chemical methods can overcome the stable thermodynamics of metal hydrides.

The hydrogen release property of $LiBH_4$ substituted with Al are investigated using first principles calculations [42]. The dehydrogenation energy of $LiBH_4$ is found to be reduced after doping Al due to the low structural stability. The energy cost to introduce the Al should be reduced for practical application. The dopant Mg is also useful to destabilize the structure of $LiBH_4$ and reduce the H desorption energy [43]. The bonding strength between Li and B/H was decreased by the Mg substitution. It means that Mg modification can effectively improve the hydrogen release performance of $LiBH_4$. Moreover, for the dehydrogenation reaction of $LiBH_4$(010) surface, Nb has great effect on lowering the average hydrogen desorption energy [44]. The bond strength of B-H in $LiBH_4$(010) surface is reduced due to the import of Nb. It is a great progress to improve the hydrogen storage of $LiBH_4$ by doping method. The synergistic effects of Ti-doping and Li-vacancy on the dehydrogenation properties of $LiBH_4$(010) surface are studied by DFT calculations [45]. The composite modified material exhibits better thermodynamic destabilization than that with single modification with Ti-doping or Li-

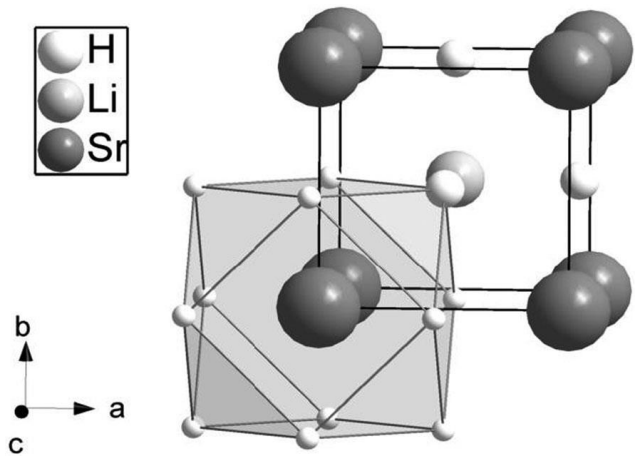

Figure 2.8. Optimized crystal structure of $LiSrH_3$ with P$m\overline{3}m$ phase [28].

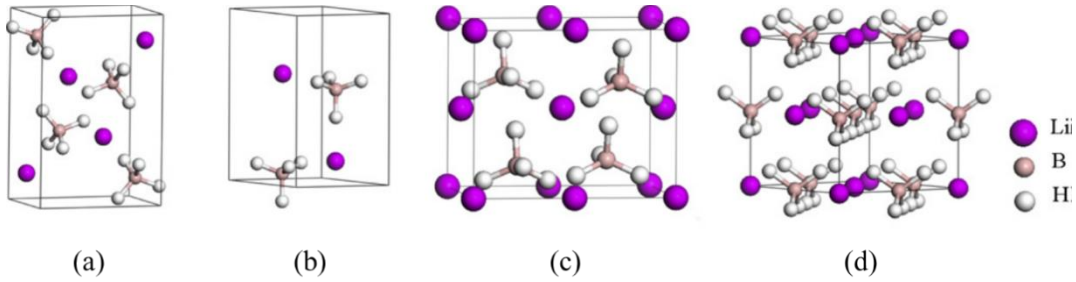

Figure 2.9. The crystal structure of $LiBH_4$ with different phases: (a) P*nma*, (b) P6_3*mc*, (c) A*ma2*, and (d) Fm$\bar{3}$m [31].

vacancy. The weakened B-H bond is the main factor to facilitate the hydrogen desorption of $LiBH_4$ [45]. Experimentally, aluminium hydride and $LiBH_4$ formed the composite using ball milling method [46]. Based on the hydrogen desorption measurements, the hydrogen capacity of this composite is 11.2 wt% and the dehydrogenation temperature is reduced by more than 30 ℃ [46].The typical destabilization example of $LiBH_4$ is using MgH_2 as a destabilizing agent [47-49]. The hydrogenation/dehydrogenation reaction is reversibility. The reaction enthalpy of $LiBH_4$ is reduced by 25 KJ/ (mol of H_2) due to the formation of MgB_2 [50]. This destabilizing process can be described as following [31]:

$$2LiBH_4 + MgH_2 \leftrightarrow 2LiH_2 + MgB_2 + 4H_2$$

The addition of MgH_2 plays an important role in decreasing the dehydrogenation enthalpy of $LiBH_4$. Without the formation of MgB_2, the decomposition of MgH_2 maybe the intermediate step for the dehydrogenation of $LiBH_4$. The reaction enthalpy of $LiBH_4$ with MgH_2 in destabilization process is shown in Fig. 2.10 [49].

More than that, interfacial elastic constraint or elastic clamping [51] was reported to be a possible way to tune the thermodynamics of Mg-based hydrides. The performance of hydrides will be altered along with the change of the structure by extra strain energy. Thus, the effect of strain on hydrides for hydrogen storage has been investigated. The structural deformation can be observed in MgH_2 under the biaxial tensile or compressive strain [52]. The reaction enthalpies and temperature of dehydrogenation are decreased by applying strain on MgH_2 hydride. The biaxial tensile strain has more contribution on the thermodynamic improvement of hydrogen release than that of compressive one in MgH_2. It means that the application of strain is beneficial to enhance the dehydrogenation property of MgH_2. In addition, the

dehydrogenation enthalpy of MgH_2 could be reduced by introducing the misfit strain on MgH_2/Mg films with TiH_2(111) substrate [53]. These studies show that the strain plays an important role in tuning the dehydrogenation properties of metal hydrides.

From the various studies, both doping and strain methods are responsible for the destabilization of metal hydrides. Therefore, these methods can be used in $LiBH_4$(010) surface to improve the hydrogen storage properties. To control the hydrogen release properties of $LiBH_4$(010) surface, suitable dopants such as Na, K, Al, F, or Cl and strain can be applied to reduce the structural stability. This process is shown as Fig. 2.11.

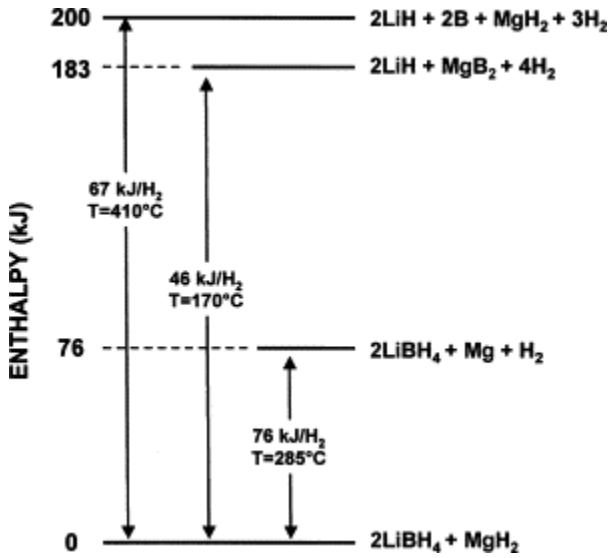

Figure 2.10. Reaction enthalpy of $LiBH_4$ with MgH_2 in destabilization process [49].

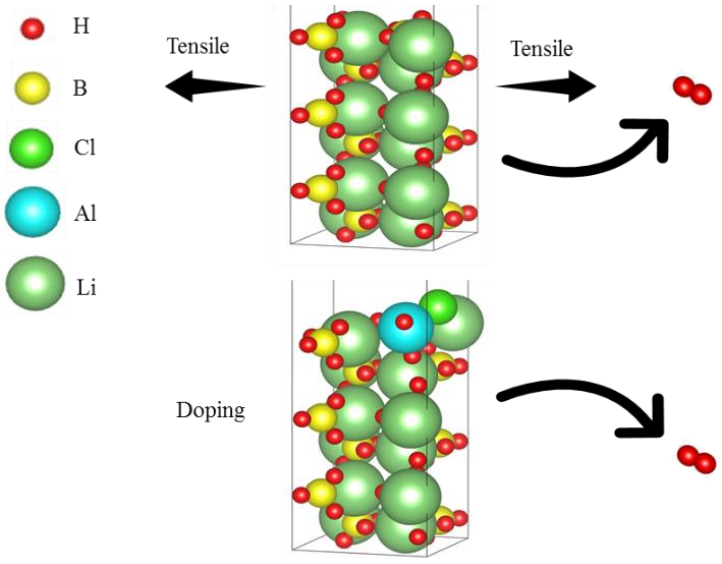

Figure 2.11. Hydrogen desorption of $LiBH_4$(010) surface can be facilitated by tensile strain or doping.

2.3. Research objectives

Light metal hydrides have attracted a lot of interests as energy carrier due to the high hydrogen capacities, light weight and safety. Exploring the structural and thermodynamic performance of promising hydrides including perovskite-type hydrides ABH_3 (A = Li, Na, K, Rb, or Cs, B = Be, Mg, Ca, Sr, or Ba) and lithium borohydride $LiBH_4$ is meaningful to develop the advanced hydrogen storage materials. However, the practical application of these hydrides has been limited because of the high thermodynamic properties. Thus, how to reduce their thermodynamic stability to enhance the dehydrogenation of the metal hydrides is a key problem. To make a comprehensive understanding of the structural and thermodynamic properties and find effective ways to promote the hydrogen release of light metal hydrides, the objectives of this study are as follows:

(1) To obtain all ground state structures of light perovskite-type hydrides ABH_3 and lithium borohydride $LiBH_4$.

(2) To calculate formation and reaction enthalpies of all optimized systems.

(3) To find the most possible reaction pathway to release hydrogen.

(4) To investigate the dopants (Li, K, Rb, Cs, Be, Mg, Ca, Sr, or Ba) effects on hydrogen release of the screened potential hydride $NaCaH_3$.

(5) To identify the most promising dopant for hydrogen release of $KMgH_3$ among dopants Li, Na, K, Rb, and Cs.

(6) To investigate the pressure effects (0~2 GPa) on hydrogen release in the bulk system of $KMgH_3$.

(7) To examine the dopants (Na, K, Al, F, or Cl) effects on the hydrogen desorption of $LiBH_4$(010) surface.

(8) To investigate the strain effects (-3% – 3%) on hydrogen release in $LiBH_4$(010) surface.

Reference

[1] S.-i. Orimo, Y. Nakamori, J.R. Eliseo, A. Züttel, C.M. Jensen, Complex hydrides for hydrogen storage. Chem. Rev. 2007, 107, 4111-4132.

[2] A.H. Reshak, $NaMgH_3$ a perovskite-type hydride as advanced hydrogen storage systems: electronic structure features. Int. J. Hydrogen Energ. 2015, 40, 16383-90.

[3] E. Mamontov, A. I. Kolesnikov, S. Sampath, J.L. Yarger, Hydrogen mobility in the lightest reversible metal hydride, $LiBeH_3$. Sci. Rep. 2017, 7, 1-7.

[4] X.J. San, Z. He, Y.M. Ma, T. Cui, B.B. Liu, G.T. Zou, Electronic structure and optical properties of $LiXH_3$ and $XLiH_3$ (X = Be, B or C). Chin. Phys. B 2008, 17, 2222.

[5] A. H. Reshak, Photocatalytic water splitting solar-to-hydrogen energy conversion, Perovskite-type hydride $XBeH_3$ (X = Li or Na) as active photocatalysts. J. Catal. 2017, 351, 119-129.

[6] S.W. Liu, J.G. Yu, M. Jaroniec, Tunable photocatalytic selectivity of hollow TiO_2 microspheres composed of anatase polyhedra with exposed {001} facets. J. Am. Chem. Soc. 2010,132, 11914-11916.

[7] J.R. Ran, J.G. Yu, M. Jaroniec, $Ni(OH)_2$ modified CdS nanorods for highly efficient visible-light-driven photocatalytic H_2 generation. Green Chem. 2011, 13, 2708-2713.

[8] P. Vajeeston, P. Ravindran, H. Fjellvåg, Structural phase stability studies on $MBeH_3$ (M = Li, Na, K, Rb, Cs) from density functional calculations. Inorg. Chem. 2008, 47, 508-514.

[9] B. Rehmat, M. A. Rafiq, Y. Javed, Z. Irshad, N. Ahmed, S. M. Mirza, Elastic properties of perovskite-type hydrides $LiBeH_3$ and $NaBeH_3$ for hydrogen storage. Int. J. Hydrogen Energ. 2017, 42, 10038-10046.

[10] P. Vajeeston, P. Ravindran, A. Kjekshus, H. Fjellvåg, First-principles investigations of the $MMgH_3$ (M = Li, Na, K, Rb, Cs) series. J. Alloy Compd. 2008, 450, 327-337.

[11] Y. Li, B. K. Rao, T. McMullen, P. Jena, P. K. Khowash, Electronic structure of the $LiMgH_3$ class of compounds, cluster calculations. Phys. Rev. B 1991, 44, 6030-6036.

[12] A. Bouamrane, J. P. Laval, J-P. Soulie, J. P. Bastide, Structural charactrization of $NaMgH_2F$ and $NaMgH_3$. Mater. Res. Bull. 2000, 35, 545-549.

[13] Y. Bouhadda, Y. Boudouma, N.E. Fennineche, A. Bentabet, Ab initio calculations study of the electronic, optical and thermodynamic properties of $NaMgH_3$, for hydrogen storage. J. Phys. Chem. Solids 2010, 71, 1264-1268.

[14] Y. Bouhadda, N. Fenineche, Y. Boudouma, Hydrogen storage, Lattice dynamics of orthorhombic $NaMgH_3$. Physica B Condens. Matter 2011, 406, 1000-1003.

[15] S. Tao, Z. M. Wang, Z. Z. Wan, J. Q. Deng, H. Zhou, Q. Yao, Enhancing the dehydriding properties of perovskite-type $NaMgH_3$ by introducing potassium as dopant. Int. J. Hydrogen Energ. 2017, 42, 3716-3722.

[16] K. Komiya, N. Morisaku, R. Rong, Y. Takahashi, Y. Shinzato, H. Yukawa, M. Morinaga, Synthesis and decomposition of perovskite-type hydrides, $MMgH_3$ (M = Na, K, Rb). J. Alloy Compd. 2008, 453, 157-160.

[17] Y. Bouhadda, N. Kheloufi, A. Bentabet, Y. Boudouma, N. Fenineche, K. Benyalloul, Thermodynamic functions from lattice dynamic of $KMgH_3$ for hydrogen storage applications. J. Alloy Compd. 2011, 509, 8994-8998.

[18] A.H. Reshak, M.Y. Shalaginov, Y. Saeed, I.V. Kityk, S. Auluck, First-Principles Calculations of Structural, Elastic, Electronic, and Optical Properties of Perovskite-type $KMgH_3$ Crystals, Novel Hydrogen Storage Material. J. Phys. Chem. B 2011, 115, 2836-2841.

[19] R. Martínez-Coronado, J. Sánchez-Benítez, M. Retuerto, M.T. Fernández-Díaz, J.A. Alonso, High-pressure synthesis of $Na_{1-x}Li_xMgH_3$ perovskite hydrides. J. Alloy Compd. 2012, 522, 101-105.

[20] D. Duan, X. Huang, F. Tian, D. Li, H. Yu, Y. Liu, Y. Ma, B. Liu, T. Cui, Pressure-induced decomposition of solid hydrogen sulfide. Phys. Rev. B 2015, 91, 180502(R).

[21] H. Wu, W. Zhou, T. J. Udovic, J. J. Rush, T. Yildirim, Crystal chemistry and dehydrogenation/rehydrogenation properties of perovskite hydrides $RbMgH_3$ and $RbCaH_3$. J. Phys. Chem. C 2009, 113, 15091-15098.

[22] B. Bertheville, P. Fischer, K. Yvon, High-pressure synthesis and crystal structures of new ternary caesium magnesium hydrides, $CsMgH_3$, $Cs_4Mg_3H_{10}$ and Cs_2MgH_4. J. Alloy Compd. 2002, 330, 152-156.

[23] G. Renaudin, B. Bertheville, K. Yvon, Synthesis and structure of an orthorhombic low-pressure polymorph of caesium magnesium hydride, $CsMgH_3$. J. Alloy Compd. 2003, 353, 175-179.

[24] A. H. Reshak, DFT calculations for the electronic structure of alpha phase of $CsMgH_3$ as advanced hydrogen storage materials. Int. J. Hydrogen Energ. 2016, 41, 2762-2770.

[25] P. Vajeeston, P. Ravindran, H. Fjellvåg, Structural investigation and thermodynamical properties of alkali calcium trihydrides. J. Chem. Phys. 2010, 132, 114504.

[26] S. Lamichhane, B. Aryal, G.C. Kaphle, N.P. Adhikari, Structural and electronic properties of perovskite hydrides $ACaH_3$ (A = Cs and Rb). BIBECHANA, 2016, 13, 94-99.

[27] F. Gingla, T. Vogt, E. Akiba, K. Yvon, Cubic $CsCaH_3$ and hexagonal $RbMgH_3$, new examples of fluoride-related perovskite-type hydrides. J. Alloy Compd. 1999, 282, 125-129.

[28] N. Kunkel, A. Meijerink, H. Kohlmann, Bright yellow and green Eu (II) luminescence and vibronic fine structures in $LiSrH_3$, $LiBaH_3$ and their corresponding deuterides. Phys. Chem. Chem. Phys. 2014, 16, 4807-4813.

[29] K. Ikeda, T. Sato, S.I. Orimo, Perovskite-type hydrides-synthesis, structures and properties. Int. J. Mater. Res. 2008, 99, 471-479.

[30] N. Kunkel, A.D. Sontakke, S. Kohaut, B. Viana, P. Dorenbos, Thermally stimulated luminescence and first-principle study of defect configurations in the perovskite-type hydrides $LiMH_3$, Eu^{2+} (M = Sr, Ba) and the corresponding deuterides. J. Phys. Chem. C 2016, 120, 29414-29422.

[31] C. Li, P. Peng, D. Zhou, L. Wan, Research progress in $LiBH_4$ for hydrogen storage, a review. Int. J. Hydrogen Energ. 2011, 36, 14512-14526.

[32] L. George, S.K. Saxena, Structural stability of metal hydrides, alanates and borohydrides of alkali and alkali-earth elements, a review. Int. J. Hydrogen Energ. 2010, 35, 5454-70.

[33] I.P. Jain, P. Jain, A. Jain, Novel hydrogen storage materials, a review of lightweight complex hydrides. J. Alloy. Comp. 2010, 503, 303-39.

[34] A. Züttel, S. Rentsch, P. Fischer, P. Wenger, P. Sudan, P. Mauron, C. Emmenegger, Hydrogen storage properties of $LiBH_4$. J. Alloy Compd. 2003, 356, 515-520.

[35] M.R. Hartman, J.J. Rush, T.J. Udovic Jr, R.C. Bowman, S-J. Hwang, Structure and vibrational dynamics of isotopically labeled lithium borohydride using neutron diffraction and spectroscopy. J. Solid State Chem. 2007, 180, 1298-305.

[36] J.-P. Soulié, G. Renaudin, R. ˇCerný, K. Yvon, Lithiumboro-hydride $LiBH_4$, I. Crystal structure. J. Alloys Compd. 2002, 346, 200-205.

[37] Y. Filinchuk, D. Chernyshov, A. Nevidomskyy, V. Dmitriev. High-pressure polymorphism as a step towards destabilization of $LiBH_4$. Angew. Chem. Int. Ed. 2008, 47, 529-32.

[38] C. Stampfl, M.V. Ganduglia-Pirovano, K. Reuter, M. Scheffler, Catalysis and corrosion, the theoretical surface-science context. Surf. Sci. 2002, 500, 368-394.

[39] S. Sakong, A. Groß, Dissociative adsorption of hydrogen on strained Cu surfaces. Surf. Sci. 2003, 525, 107-118.

[40] Q. Ge, Structure and energetics of $LiBH_4$ and its surfaces, A first-principles study. J. Phys. Chem. A 2004, 108, 8682-8690.

[41] S.I. Orimo, Y. Nakamori, G. Kitahara, K. Miwa, N. Ohba, S. Towata, Dehydriding and rehydriding reactions of $LiBH_4$. J. Alloy Compd. 2005, 404-406, 427-30.

[42] J. Weiqing, C. Shilong, Effect of Al on the dehydrogenation of $LiBH_4$ from first-principles calculations. Int. J. Hydrogen Energ. 2017, 42, 6181-6188.

[43] X. Mo, W. Jiang, Dehydrogenation properties of $LiBH_4$ modified by Mg from first-principles calculations. J. Alloy Compd. 2018, 735, 668-676.

[44] S. Yu, X. Ju, C. Wan, S. Li, Nb-doped $LiBH_4$(010) surface for hydrogen desorption, First-principles calculations. Int. J. Hydrogen Energ. 2015, 40, 6365-6372.

[45] H.-C. Wang, X.-J. Yao, Y. Yang, B.-Y. Tang, Synergic effects of V_{Li} and Ti doping on hydrogen desorption on $LiBH_4$(010) surface, A first-principles investigation. Int. J. Hydrogen Energ. 2017, 42, 18442-18451.

[46] H. Liu, X. Wang, H. Zhou, S. Gao, H. Ge, S. Li, M. Yan, Improved hydrogen desorption properties of $LiBH_4$ by AlH_3 addition. Int. J. Hydrogen Energ. 2016, 41, 22118-22127.

[47] D.J. Siegel, C. Wolverton, V. Ozolin, Thermodynamic guidelines for the prediction of hydrogen storage reactions and their application to destabilized hydride mixtures. Phys. Rev. B 2007, 76, 134102.

[48] J. Yang, A. Sudik, C. Wolverton, Destabilizing $LiBH_4$ with a metal (M = Mg, Al, Ti, V, Cr, or Sc) or metal hydride (MH_2 = MgH_2, TiH_2, or CaH_2). J. Phys. Chem. C 2007, 111, 19134-40.

[49] J.J. Vajo, T.T. Salguero, A.F. Gross, S.L. Skeith, G.L. Olson, Thermodynamic destabilization and reaction kinetics in light metal hydride systems. J. Alloy Comp. 2007, 446-447, 409-14.

[50] J.J. Vajo, S.L. Skeith, F. Mertens, Reversible storage of hydrogen in destabilized $LiBH_4$. J. Phys. Chem. B 2005, 109, 3719-22.

[51] A. Baldi, M.G. Silveira, V. Palmisano, B. Dam, R. Griessen, Destabilization of the Mg-H system through elastic constraints. Phys. Rev. Lett. 2009, 102, 226102-5.

[52] J. Zhang, Y. Zhou, Z. Ma, L. Sun, P. Peng, Strain effect on structural and dehydrogenation properties of MgH_2 hydride from first-principles calculations. Int. J. Hydrogen Energ. 2013, 38, 3661-3669.

[53] S.Q. Hao, D.S. Sholl. Effect of TiH_2-induced strain on thermodynamics of hydrogen release from MgH_2. J. Phys. Chem. C 2012, 116, 2045-50.

CHAPTER 3. Screening of perovskite hydrides for hydrogen storage

3.1. Introduction

Exploitation of renewable energy resources has become important owing to the increasing energy crisis [1, 2]. Although hydrogen is currently abundant, characterized by the highest energy per mass [1], its storage limits its application [1, 2]. Light metal hydrides for hydrogen storage has received considerable attention owing to their safe operation and high efficiency [3-5]. Alkali metals/ alkaline-earth metals based on perovskite hydrides with a general formula of ABH_3 possess flexible structures, low cost, lightweight, and high hydrogen capacities [6, 7]. Several perovskite hydrides for hydrogen storage have been experimentally and theoretically studied. For instance, $NaMgH_3$ shows good structural and thermodynamic properties required for hydrogen storage systems [8]. In addition, $RbMgH_3$ and $RbCaH_3$ can be decomposed into metals and hydrogen at a moderate pressure and temperature < 400°C [9]. Rehmat et al. reported that $MBeH_3$ (M = Li and Na) was a stable hydride in their computational studies [10]. The stability of α-$CsMgH_3$ has been explored by theoretical calculations [11]. Several light perovskite hydrides, such as $LiBeH_3$ [12], $NaMgH_3$ [13-15], $KMgH_3$ [16, 17], $RbMgH_3$ [9, 18], $CsMgH_3$ [19, 20], $RbCaH_3$ [9], $CsCaH_3$ [18], $LiSrH_3$ [21], and $LiBaH_3$ [21] have been experimentally explored. Hypothetical perovskite-type hydrides have been investigated using various theoretical methods [22-25]. Vajeeston et al. [26, 27] investigated the structural stabilities and electronic structures of $LiBeH_3$, $NaBeH_3$, $KBeH_3$, $RbBeH_3$, $CsBeH_3$, $LiMgH_3$, $NaMgH_3$, $KMgH_3$, $RbMgH_3$, and $CsMgH_3$ using first-principles methods.

Relatively high thermodynamic stability limits the practical application of most metal hydrides [28]. A high temperature is required for releasing molecular hydrogen from light

perovskite-type hydrides [14]. Komiya et al. [29] synthesized $NaMgH_3$, $KMgH_3$, and $RbMgH_3$ hydrides *via* ball-milling method and found that different hydrides have different decomposition pathways at the temperatures ranging between 673 K and 723 K. Doping suitable elements has been found to be effective in facilitating the dehydrogenation process for most hydrides, making hydrides unstable [30-33]. In comparison with $NaMgH_3$ [34], $Na_{0.9}K_{0.1}MgH_3$ experimentally exhibited the enhanced dehydrogenation performance owing to its reduced structural stability. The temperature for releasing hydrogen from $NaMgH_3$ system was reduced from 580 to 328 K after introducing K_2TiF_6 [35]. He et al. [36] discovered that phosphorus was a useful dopant for hydrogen release from MgH_2, which reduced the energy required for a dehydrogenation process. Furthermore, it was found that introducing appropriate dopants to the hydride systems is a great approach for promoting hydrogen release [34-36].

Although we solely focus on the thermodynamics in this work, both aspects of thermodynamics and kinetics have to be considered in selecting hydrides for hydrogen storage applications. Several methods (i.e., particle size control and catalyst) can be applied for enhancing the kinetics of hydrides [37-41]. First-principles studies show obvious advantages in predicting the structural and thermodynamic performance of hydrides [8, 42, 43]. Using the consistent level theory, all the DFT calculations were done to examine the dehydrogenation performance of light ABH_3-type hydrides (A = Li, Na, K, Rb, or Cs; B = Be, Mg, Ca, Sr, or Ba).

3.2. Computational methods

Periodic calculations were done by employing the Vienna Ab initio Simulation Package (VASP) [44, 45] along with the generalized-gradient approximation of Perdew–Burke–Ernzerhof [46, 47]. We set the energy cutoff to 550 eV. The convergence criterion for each calculation was 10^{-6} eV. The convergence processes continued until the force was < 10^{-2} eVÅ^{-1}. Grimme's dispersion corrections [48] were included. Both cell volume and shape were fully relaxed for each system. Table 3.1 lists the Monkhorst–Pack *k*-points used for different systems [49]. A 2 × 2 × 1 supercell was used in a doped $NaCaH_3$ system. The enthalpy change (ΔH) at 0 K was determined by the following equation [50]:

$$\Delta H = \sum E_{(products)} - \sum E_{(reactants)} \quad (1)$$

where $E_{(products)}$ ($E_{(reactants)}$) was the calculated total energy of the products (reactants).

3.3. Results and discussion

3.3.1. Ground state structures of ABH_3

The light perovskite hydrides ABH_3 (A = Li, Na, K, Rb, or Cs and B = Be, Mg, Ca, Sr, or Ba) including experimentally available structures (i.e., $LiBeH_3$, $NaMgH_3$, $KMgH_3$, $RbMgH_3$, $CsMgH_3$, $RbCaH_3$, $CsCaH_3$, $LiSrH_3$, and $LiBaH_3$) and hypothetically designed structures (i.e., $NaBeH_3$, $KBeH_3$, $RbBeH_3$, $CsBeH_3$, $LiMgH_3$, $LiCaH_3$, $NaCaH_3$, $KCaH_3$, $NaSrH_3$, $KSrH_3$, $RbSrH_3$, $CsSrH_3$, $NaBaH_3$, $KBaH_3$, $RbBaH_3$, and $CsBaH_3$) were optimized by DFT calculations. Among these systems, nine out of 25 perovskite-types are available from experimental studies [18, 20, 21, 51-55]. The optimized lattice parameters of ground state structures based on the DFT calculations are tabulated in Table 3.2. Our calculations are in

agreement with those reported experimentally [18, 20, 21, 51-55] and found theoretically [7, 10, 11, 24, 26, 27, 56, 57]. For an optimized $NaMgH_3$ structure, the range of bond length (d (Mg-H)) and angle ∠H–Mg–H is 1.966–1.967 Å and 88.58°–91.42°, respectively. Similar experimental results (d (Mg–H): 1.961–1.964 Å and ∠H–Mg–H: 88.83°–91.17°) were observed in $NaMgH_3$ structure [58]. The range of Rb–H and Mg–H bonding distances are 2.964–3.049 Å and 2.012–2.056 Å in an optimized structure of $RbMgH_3$, respectively. These are consistent with the experimental results (d (Rb–H): 2.96–3.03 Å and d (Mg–H): 2.01–2.04 Å) [12]. These examples illustrate that our calculations predict the experimental structures. For hypothetical structures of ABH_3, we optimized various crystal structures [10, 22, 23, 26, 27, 56] to determine the most stable phase. For $KCaH_3$, the optimized structure with a *Pnma* phase shows the highest stability. The Ca (K) atom is surrounded by 6 (8) numbers of hydrogen atoms. The average distance ($\overline{d}$) of Ca–H is 2.263 Å. The ∠H–Ca–H range is from 88.88° to 91.13°. The range of K–H bond length is 2.827–3.135 Å. These results agree with other results ($\overline{d}$ (Ca–H): 2.26 Å, ∠H–Ca–H: 89–91°, d (K–H): 2.83–3.15 Å) [24].

Formation enthalpy provides an insight on the stability of compounds [34, 50, 56]. Under appropriate conditions, most hydrides are prepared through the solid-phase reactions of hydride powders [8, 59-61]. Herein, four possible synthesis methods were considered to explore the formation of optimized structures, which are as follows:

$$A + B + \tfrac{3}{2}H_2 \rightarrow ABH_3 \tag{2}$$

$$A + BH_2 + \tfrac{1}{2}H_2 \rightarrow ABH_3 \tag{3}$$

$$AH + B + H_2 \rightarrow ABH_3 \tag{4}$$

$$AH + BH_2 \rightarrow ABH_3 \tag{5}$$

Among these pathways, (2) and (5) are found in the experiments [21, 59-62]. The formation enthalpies (ΔH_f) were calculated using the equation (1). Results show that pathways for the hydrides formation (2)–(5) are either exothermic or endothermic reactions for different systems. Interestingly, pathway (2) is the most favorable for all systems. That is, all hydrides

Table 3.1. *k*-points employed for all perovskite hydrides.

Material	*k*-points	Material	*k*-points
$LiBeH_3$ (*Pnma*)	8 × 6 × 8	$KCaH_3$ (*Pnma*)	8 × 6 × 8
$NaBeH_3$ ($Pm\overline{3}m$)	11 × 11 × 11	$RbCaH_3$ ($Pm\overline{3}m$)	8 × 8 × 8
$KBeH_3$ ($P2_1/c$)	6 × 8 × 6	$CsCaH_3$ ($Pm\overline{3}m$)	8 × 8 × 8
$RbBeH_3$ ($P2_1/c$)	6 × 8 × 6	$LiSrH_3$ ($Pm\overline{3}m$)	10 × 10 × 10
$CsBeH_3$ ($P2_1/m1$)	8 × 8 × 6	$NaSrH_3$ ($P2_1/c$)	6 × 8 × 6
$LiMgH_3$ (*R3c*)	8 × 8 × 4	$KSrH_3$ (*Pnma*)	8 × 6 × 8
$NaMgH_3$ (*Pnma*)	8 × 6 × 8	$RbSrH_3$ (*Pnma*)	8 × 6 × 8
$KMgH_3$ ($Pm\overline{3}m$)	9 × 9 × 9	$CsSrH_3$ ($Pm\overline{3}m$)	10 × 10 × 10
$RbMgH_3$ ($P6_3/mmc$)	8 ×8 × 4	$LiBaH_3$ ($Pm\overline{3}m$)	10 × 10 × 10
$CsMgH_3$ (*Pmmn*)	4 × 8 × 6	$NaBaH_3$ (*R3c*)	8 × 8 × 4
$LiCaH_3$ (*R3c*)	8 × 8 × 4	$KBaH_3$ (*R3c*)	8 × 8 × 4
$NaCaH_3$ ($P2_1/c$)	6 × 8 × 6	$RbBaH_3$ (*R3c*)	8 × 8 × 4
$NaCaH_3$ ($P2_1/c$, 2 × 2 × 1)	4 × 4 × 6	$CsBaH_3$ (*Pnma*)	8 × 6 × 8

Table 3.2. Lattice parameters of optimized ground state phases of perovskite-type hydrides (ABH_3).

Material	Space group	Lattice parameter (Å)				Reference
		a	b	c	β (deg.)	
$LiBeH_3$	*Pnma* (No. 62)	4.517	6.273	4.387		This work
		4.424(2)	6.217(2)	4.639(2)		Expt.[1]
		4.526	6.293	4.404		Calc.[2]
		4.536(1)	6.299(2)	4.410(4)		Calc.[3]
$NaBeH_3$	$Pm\bar{3}m$ (No. 221)	3.346				This work
		3.350				Calc.[2]
		3.352				Calc.[4]
$KBeH_3$	$P2_1/c$ (No. 14)	7.052	5.459	8.692	108.31	This work
		7.085	5.562(1)	8.948(3)	107.45	Calc.[3]
		7.362	5.779	9.297	106.70	Calc.[5]
$RbBeH_3$	$P2_1/c$ (No. 14)	7.502	5.685	9.175	109.43	This work
		7.439	5.789(9)	9.457(9)	108.05	Calc.[3]
		7.150	5.613	9.030	107.40	Calc.[5]
$CsBeH_3$	$P2_1/m1$ (No. 11)	5.098	5.937	7.463	108.01	This work
		5.096(9)	5.935(9)	7.845(1)	107.97	Calc.[3]
$LiMgH_3$	*R3c* (No. 161)	4.945		13.293		This work
		4.958		13.337		Calc.[6]
		4.9226		13.210(6)		Calc.[7]
$NaMgH_3$	*Pnma* (No. 62)	5.446	7.643	5.365		This work
		5.463(4)	7.703	5.410(8)		Expt.[8]
		5.456(8)	7.696(8)	5.377(9)		Calc.[9]
		5.452(5)	7.695(2)	5.368(3)		Calc.[6]
$KMgH_3$	$Pm\bar{3}m$ (No. 221)	4.018				This work
		4.023				Expt.[10]
		4.029(5)				Calc.[6]
		4.010				Calc.[11]
$RbMgH_3$	$P6_3/mmc$ (No. 194)	5.932		14.377		This work
		5.903		14.315(8)		Expt.[12]

Material	Space group	Lattice parameter (Å)				Reference
		a	b	c	β (deg.)	
		5.906(8)		14.326(1)		Calc.[6]
$CsMgH_3$	*Pmmn* (No. 59)	9.994	6.148	8.584		This work
		9.995(8)	6.132(7)	8.573(6)		Expt.[13]
		9.997(6)	6.133(1)	8.574(1)		Calc.[14]
		9.992(2)	6.140(5)	8.576(8)		Calc.[6]
$LiCaH_3$	*R3c* (No. 161)	5.218		12.461		This work
$NaCaH_3$	$P2_1/c$ (No. 14)	6.805		7.191	90.136	This work
$KCaH_3$	*Pnma* (No. 62)	6.325	8.929	6.299		This work
$RbCaH_3$	$Pm\bar{3}m$ (No. 221)	4.547				This work
		4.547				Expt.[15]
		4.542(7)				Calc.[16]
$CsCaH_3$	$Pm\bar{3}m$ (No. 221)	4.631				This work
		4.6170(2)				Expt.[12]
		4.629(7)				Calc.[16]
$LiSrH_3$	$Pm\bar{3}m$ (No. 221)	4.644				This work
		3.835(7)				Expt.[17]
		3.833				Expt.[18]
$NaSrH_3$	$P2_1/c$ (No. 14)	6.853	6.151	7.739	90.716	This work
$KSrH_3$	*Pnma* (No. 62)	6.744	9.394	6.588		This work
$RbSrH_3$	*Pnma* (No. 62)	6.833	9.607	6.785		This work
$CsSrH_3$	$Pm\bar{3}m$ (No. 221)	4.888				This work
$LiBaH_3$	$Pm\bar{3}m$ (No. 221)	4.020				This work
		4.023(9)				Expt.[17]
		4.023				Expt.[18]
$NaBaH_3$	*R3c* (No. 161)	6.207		14.600		This work
$KBaH_3$	*R3c* (No. 161)	6.937		17.459		This work
$RbBaH_3$	*R3c* (No. 161)	7.158		17.856		This work
$CsBaH_3$	*Pnma* (No. 62)	7.390	10.329	7.275		This work

are preferred to be formed through the pathway (2). Table 3.3 lists the results of the enthalpy formation with a pathway (2). Thus, the route (2) is the most favorable pathway to synthesize the hydrides. However, further studies are needed in this direction. The formation enthalpies of all the optimized structures with other different formation pathways are tabulated in Table 3.3.

3.3.2. Hydrogen release of ABH_3-type hydrides

To explore the dehydrogenation performance of ABH_3-type hydrides, three pathways to release H_2 molecules were considered, which are as follows [8]:

$$ABH_3 \rightarrow A + B + \tfrac{3}{2}H_2 \quad (6)$$

$$ABH_3 \rightarrow A + BH_2 + \tfrac{1}{2}H_2 \quad (7)$$

$$ABH_3 \rightarrow AH + B + H_2 \quad (8)$$

The entropy change in decomposition reactions is mainly due to the entropy change of gaseous H_2 [50, 63]. Therefore, reaction enthalpies (ΔH_r) can be used as an efficient indicator to screen the most useful hydride [50, 63]. The reaction enthalpies (ΔH_r) of a dehydrogenation process were calculated based on the pathways of (6)–(8). Table 3.4 lists the reaction enthalpies of all ABH_3 systems investigated herein, showing that all the calculated reaction enthalpies of the pathway (8) (as the boldface shown) are lower than those of pathways (6) and (7) for $ABeH_3$ (A = Li, Na, K, Rb, or Cs) and $LiMgH_3$ systems. This exhibits that the pathway (8) is more favorable for releasing molecular hydrogen than the pathways (6) and (7). For the rest of hydrides (i.e., $AMgH_3$ (except $LiMgH_3$), $ACaH_3$, $ASrH_3$, and $ABaH_3$), the pathway (7) shows the lowest reaction enthalpy, signifying that these hydrides release molecular hydrogen through the pathway (7). The negative reaction enthalpies were found in $LiBeH_3$, $NaBeH_3$,

$LiSrH_3$, $KBaH_3$, $RbBaH_3$, and $CsBaH_3$ structures, indicating that it was exothermic to release hydrogen molecules from these systems.

To screen the best material, both formation and reaction enthalpies were considered. Fig. 3.1 displays the formation (ΔH_f) and reaction enthalpies (ΔH_r) for all light perovskite-type hydrides (ABH_3). Among these systems, $NaCaH_3$ system was found to be one of the most attractive materials with reasonable reaction and formation enthalpies. On the other hand, $LiBaH_3$ ($LiSrH_3$) shows the highest (lowest) reaction enthalpy and the lowest (highest) formation enthalpy. Fig. 3.2 (a) shows the optimized structure of $NaCaH_3$. A total of 4 (6) Na–H (Ca–H) bonds are in the ground state structure (i.e., $P2_1/c$ phase) of $NaCaH_3$. The average Na–H distance and the range of Ca–H distance are 2.242 Å and 2.259–2.395 Å, respectively.

Table 3.3. Formation enthalpies (ΔH_f (eV)) of all hydrides with pathways of (2)–(5).

Material	Eq. (2)	Eq. (3)	Eq. (4)	Eq. (5)
$LiBeH_3$ (*Pnma*)	**−0.630**	−0.475	0.208	0.363
$NaBeH_3$ ($Pm\bar{3}m$)	**−0.258**	−0.103	0.120	0.275
$KBeH_3$ ($P2_1/c$)	**−0.531**	−0.376	−0.131	0.024
$RbBeH_3$ ($P2_1/c$)	**−0.505**	−0.350	−0.196	−0.041
$CsBeH_3$ ($P2_1/m1$)	**−0.583**	−0.429	−0.261	−0.106
$LiMgH_3$ (*R3c*)	**−1.339**	−0.822	−0.501	0.017
$NaMgH_3$ (*Pnma*)	**−1.043**	−0.526	−0.665	−0.148
$KMgH_3$ ($Pm\bar{3}m$)	**−1.292**	−0.775	−0.892	−0.375
$RbMgH_3$ ($P6_3/mmc$)	**−1.142**	−0.625	−0.833	−0.316
$CsMgH_3$ (*Pmmn*)	**−1.194**	−0.676	−0.871	−0.354
$LiCaH_3$ (*R3c*)	**−2.424**	−0.740	−1.585	0.099
$NaCaH_3$ ($P2_1/c$)	**−1.755**	−0.071	−1.377	0.307
$KCaH_3$ (*Pnma*)	**−1.902**	−0.217	−1.502	0.182
$RbCaH_3$ ($Pm\bar{3}m$)	**−1.900**	−0.216	−1.591	0.093
$CsCaH_3$ ($Pm\bar{3}m$)	**−1.961**	−0.277	−1.638	0.046
$LiSrH_3$ ($Pm\bar{3}m$)	**−0.163**	1.455	0.676	2.294
$NaSrH_3$ ($P2_1/c$)	**−1.719**	−0.101	−1.341	0.277
$KSrH_3$ (*Pnma*)	**−1.691**	−0.073	−1.291	0.327
$RbSrH_3$ (*Pnma*)	**−1.676**	−0.058	−1.367	0.251
$CsSrH_3$ ($Pm\bar{3}m$)	**−1.809**	−0.191	−1.487	0.131
$LiBaH_3$ ($Pm\bar{3}m$)	**−2.554**	−1.082	−1.716	−0.243
$NaBaH_3$ (*R3c*)	**−1.723**	−0.251	−1.346	0.127
$KBaH_3$ (*R3c*)	**−1.449**	0.023	−1.049	0.423
$RbBaH_3$ (*R3c*)	**−1.371**	0.102	−1.062	0.410
$CsBaH_3$ (*Pnma*)	**−1.461**	0.011	−1.139	0.334

Table 3.4. Reaction enthalpies (eV) of hydrogen release by pathways of (6)–(8) for $LiBeH_3$, $NaBeH_3$, $KBeH_3$, $RbBeH_3$, $CsBeH_3$, $LiMgH_3$, $NaMgH_3$, $KMgH_3$, $RbMgH_3$, $CsMgH_3$, $LiCaH_3$, $NaCaH_3$, $KCaH_3$, $RbCaH_3$, $CsCaH_3$, $LiSrH_3$, $NaSrH_3$, $KSrH_3$, $RbSrH_3$, $CsSrH_3$, $LiBaH_3$, $NaBaH_3$, $KBaH_3$, $RbBaH_3$, and $CsBaH_3$.

Material	Eq. (6)	Eq. (7)	Eq. (8)
$LiBeH_3$ (*Pnma*)	0.630	0.475	**−0.208**
$NaBeH_3$ ($Pm\bar{3}m$)	0.258	0.103	**−0.120**
$KBeH_3$ ($P2_1/c$)	0.531	0.376	**0.131**
$RbBeH_3$ ($P2_1/c$)	0.505	0.350	**0.196**
$CsBeH_3$ ($P2_1/m1$)	0.583	0.429	**0.261**
$LiMgH_3$ (*R3c*)	1.339	0.822	**0.501**
$NaMgH_3$ (*Pnma*)	1.043	**0.526**	0.665
$KMgH_3$ ($Pm\bar{3}m$)	1.292	**0.775**	0.892
$RbMgH_3$ ($P6_3/mmc$)	1.142	**0.625**	0.833
$CsMgH_3$ (*Pmmn*)	1.194	**0.676**	0.871
$LiCaH_3$ (*R3c*)	2.424	**0.740**	1.585
$NaCaH_3$ ($P2_1/c$)	1.755	**0.071**	1.377
$KCaH_3$ (*Pnma*)	1.902	**0.217**	1.502
$RbCaH_3$ ($Pm\bar{3}m$)	1.900	**0.216**	1.591
$CsCaH_3$ ($Pm\bar{3}m$)	1.961	**0.277**	1.638
$LiSrH_3$ ($Pm\bar{3}m$)	0.163	**−1.455**	−0.676
$NaSrH_3$ ($P2_1/c$)	1.719	**0.101**	1.341
$KSrH_3$ (*Pnma*)	1.691	**0.073**	1.291
$RbSrH_3$ (*Pnma*)	1.676	**0.058**	1.367
$CsSrH_3$ ($Pm\bar{3}m$)	1.809	**0.191**	1.487
$LiBaH_3$ ($Pm\bar{3}m$)	2.554	**1.082**	1.716
$NaBaH_3$ (*R3c*)	1.723	**0.251**	1.346
$KBaH_3$ (*R3c*)	1.449	**−0.023**	1.049
$RbBaH_3$ (*R3c*)	1.371	**−0.102**	1.062
$CsBaH_3$ (*Pnma*)	1.461	**−0.011**	1.139

3.3.3. Dopants effects on Na Site

Alkali/ alkaline-earth metals are effective in improving hydrogen release in hydrides [34, 64, 65]. To facilitate the dehydrogenation process of $NaCaH_3$, alkali dopants, M = Li, K, Rb, or Cs, and the alkaline-earth dopants, M′ = Be, Mg, Sr, or Ba, were introduced to a $NaCaH_3$ system by replacing the Na and Ca sites, respectively. Various configurations of different dopant positions were considered to discover the most preferable dopant position. Based on the most stable configuration of M-doped $NaCaH_3$ (M = Li, K, Rb, or Cs), the study to determine the pathway for hydrogen release was continued. Five different dehydrogenation pathways of (9)–(13) for each doped system are as follows [66]:

$$Na_{1-x}M_xCaH_3 \rightarrow (1-x)Na + xM + Ca + \tfrac{3}{2}H_2 \quad (9)$$

$$Na_{1-x}M_xCaH_3 \rightarrow (1-x)Na + xM + CaH_2 + \tfrac{1}{2}H_2 \quad (10)$$

$$Na_{1-x}M_xCaH_3 \rightarrow (1-x)NaH + xM + Ca + \tfrac{2+x}{2}H_2 \quad (11)$$

$$Na_{1-x}M_xCaH_3 \rightarrow (1-x)Na + xMH + Ca + \tfrac{3-x}{2}H_2 \quad (12)$$

$$Na_{1-x}M_xCaH_3 \rightarrow (1-x)NaH + xMH + Ca + H_2 \quad (13)$$

The enthalpies of hydrogen release, i.e., reaction enthalpies, for pure and doped $NaCaH_3$ systems were obtained and tabulated in Table 3.5. Using the favorable pathway (7), the reaction enthalpy of $NaCaH_3$ without dopants was employed as a reference, setting its ΔH_r to zero. As observed in Table 3.5, the lowest enthalpies of M-doped $NaCaH_3$ structures are found in the pathway (10) for all systems. This indicates that the reaction pathway (10) is the most useful for releasing molecular hydrogen from M-doped systems. On the contrary, Li-doped $NaCaH_3$ shows a high reaction enthalpy in comparison with a dopant-free $NaCaH_3$ system. This demonstrates that Li is not a useful dopant for the hydrogen release from $NaCaH_3$. K-,

Rb-, and Cs-doped $NaCaH_3$ systems show higher negative reaction enthalpies than a pure $NaCaH_3$ system by 0.017, 0.037, and 0.05 eV, respectively. It is found that the Cs-doped $NaCaH_3$ has the lowest reaction enthalpy, indicating that Cs is the most useful dopant for hydrogen release from a $NaCaH_3$ system. Fig. 3.2 (b) shows the optimized structure of Cs-doped $NaCaH_3$.

3.3.4. Dopants effects on Ca site

The following pathways of (14)–(18) determine the reaction enthalpies of alkaline-earth metal (M′)-doped $NaCaH_3$ (M′ = Be, Mg, Sr, or Ba) systems, as follows:

$$NaCa_{1-x}M'_xH_3 \rightarrow Na + (1-x)Ca + xM' + \tfrac{3}{2}H_2 \quad (14)$$

$$NaCa_{1-x}M'_xH_3 \rightarrow Na + (1-x)CaH_2 + xM' + (x+\tfrac{1}{2})H_2 \quad (15)$$

$$NaCa_{1-x}M'_xH_3 \rightarrow NaH + (1-x)Ca + xM' + H_2 \quad (16)$$

$$NaCa_{1-x}M'_xH_3 \rightarrow Na + (1-x)Ca + xM'H_2 + \tfrac{3-2x}{2}H_2 \quad (17)$$

$$NaCa_{1-x}M'_xH_3 \rightarrow NaH + (1-x)Ca + xM'H_2 + (1-x)H_2 \quad (18)$$

Table 3.6 lists the calculated reaction enthalpies of M′-doped $NaCaH_3$ systems of each pathway. Of all dehydrogenation pathways, the pathway (15) had the lowest reaction enthalpy. That is, the M′-doped $NaCaH_3$ systems release molecular hydrogen through it. However, all these reaction enthalpies are high compared to the dopant-free $NaCaH_3$ system. Therefore, doping an alkaline-earth metal at a Ca site is nonbeneficial for releasing molecular hydrogen from $NaCaH_3$. However, alkali metal doping at the Na site is more effective for the hydrogen release than alkaline-earth metal doping at the Ca site in a $NaCaH_3$ system. In addition, the influence of van der Waals interactions on reaction enthalpies of $NaCaH_3$ and Cs-doped $NaCaH_3$ are not found to be large in our DFT calculations with dispersion corrections [48].

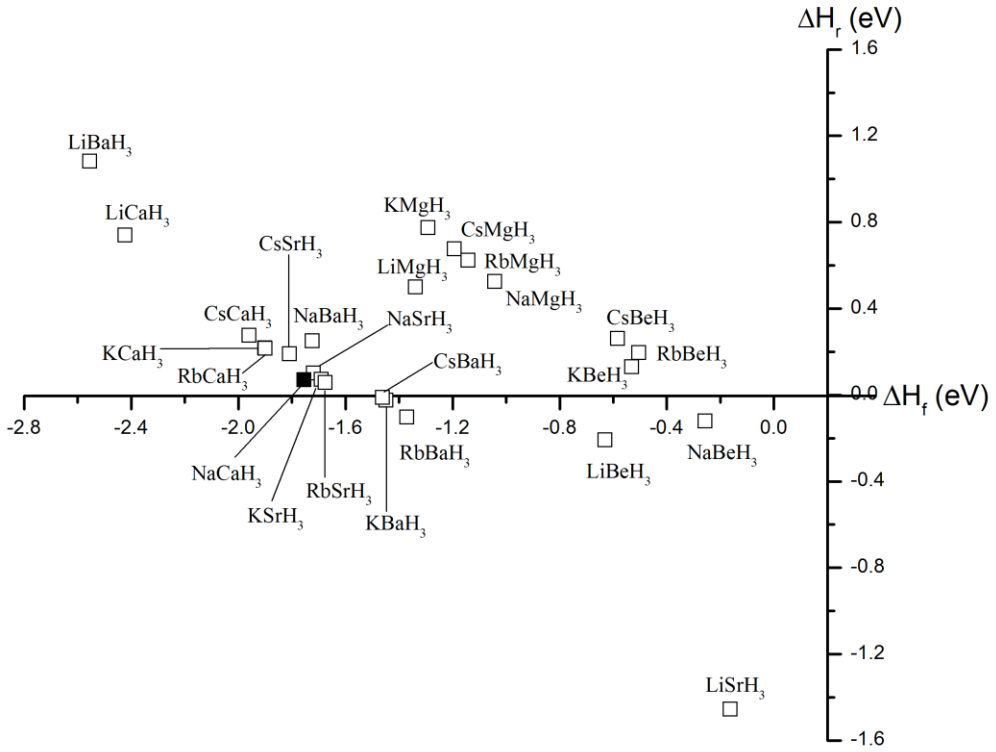

Figure 3.1. Formation (ΔH_f) and reaction enthalpies (ΔH_r) of all light ABH_3-type hydrides.

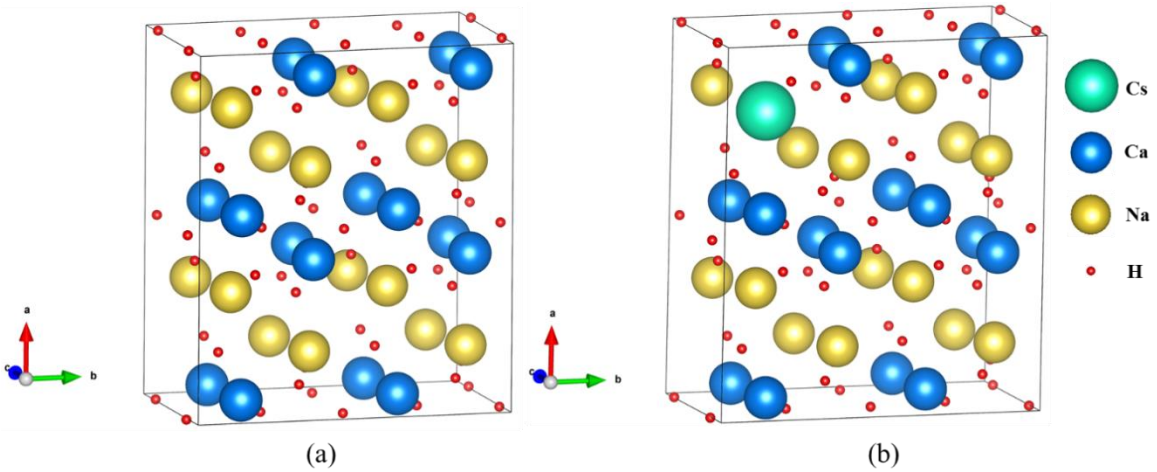

Figure 3.2. Predicted structures of (a) $NaCaH_3$ ($P2_1/c$) and (b) Cs-doped $NaCaH_3$.

Table 3.5. Calculated reaction enthalpies (eV) of M-doped $NaCaH_3$ systems by pathways of (9)–(13) (M = Li, K, Rb, or Cs).

Material	Eq. (9)	Eq. (10)	Eq. (11)	Eq. (12)	Eq. (13)
$NaCaH_3$*	1.684	**0.000**	1.306	-	-
$Na_{0.9375}Li_{0.0625}CaH_3$	1.703	**0.019**	1.349	1.651	1.297
$Na_{0.9375}K_{0.0625}CaH_3$	1.667	**−0.017**	1.313	1.642	1.288
$Na_{0.9375}Rb_{0.0625}CaH_3$	1.647	**−0.037**	1.293	1.628	1.274
$Na_{0.9375}Cs_{0.0625}CaH_3$	1.634	**−0.050**	1.280	1.614	1.260

* Herein, the reaction enthalpies of the pure system were calculated based on Eq. (6)–(8).

The difference of the reaction enthalpy (in the most preferable pathway) of $NaCaH_3$ (Cs-doped $NaCaH_3$) between the calculation with corrections and that without corrections is 0.032 (0.036) eV. Overall, a Cs-doped $NaCaH_3$ system performs the best for dehydrogenation reaction among the other systems investigated by virtue of the lowest reaction enthalpy.

3.3.5. Electronic properties

The atomic charge was calculated via Bader charge methods [67] for exploring the influence of a Cs-doping on the hydrogen release of a $NaCaH_3$ system. Fig. 3.3 (a) and (b) display the Bader atomic charges of dopant-free and Cs-doped $NaCaH_3$ structures, respectively. Using the density derived electrostatic and chemical analysis [68, 69], we determined related bond orders of these two systems listed in Table 3.7. Based on the Bader atomic charges, the sum of atomic charges of total H atoms increased by 0.067*e* after introducing a Cs dopant to a $NaCaH_3$ system, indicating that the amount of electron was reduced after Cs-doping at the Na site of $NaCaH_3$. Specifically, the H atoms around Ca lose electrons by 0.027*e* after Cs-doping. In addition, the average bond order of Ca–H in a Cs-doped $NaCaH_3$ structure is lower than that in the pure $NaCaH_3$ structure, illustrating that Ca–H bond strength becomes weaker after Cs is doped at the Na site of a $NaCaH_3$ system. Similarly, the charge of H atoms around Na decreases by 0.008*e* (on average) after the Cs-doping. The average bond order of Na–H bonds near a Cs atom in a Cs-doped $NaCaH_3$ system is 0.006 lower than that in a dopant-free system. Doping Cs can also weaken the Na–H bond strength in $NaCaH_3$. Then, the reaction enthalpy for hydrogen release can be negatively increased by virtue of the reduced strength of both Na–H and Ca–H bonds in $NaCaH_3$.

Table 3.6. Calculated reaction Enthalpies (eV) of M′-doped $NaCaH_3$ systems by pathways of (14)–(18) (M′ = Be, Mg, Sr, or Ba).

Material	Eq. (14)	Eq. (15)	Eq. (16)	Eq. (17)	Eq. (18)
$NaCaH_3$*	1.684	**0.000**	1.306	-	-
$NaCa_{0.9375}Be_{0.0625}H_3$	1.581	**0.002**	1.203	1.571	1.194
$NaCa_{0.9375}Mg_{0.0625}H_3$	1.618	**0.040**	1.241	1.586	1.208
$NaCa_{0.9375}Sr_{0.0625}H_3$	1.677	**0.098**	1.299	1.576	1.198
$NaCa_{0.9375}Ba_{0.0625}H_3$	1.656	**0.077**	1.279	1.564	1.187

* Herein, the reaction enthalpies of the pure system were calculated based on Eq. (6)–(8).

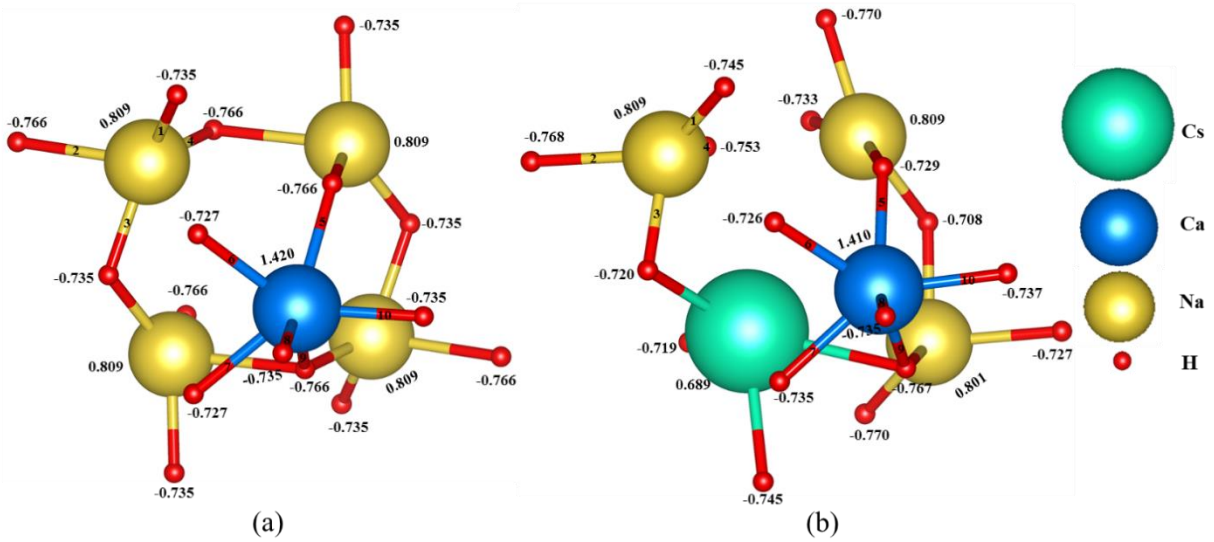

Figure 3.3. Bader atomic charges (*e*) calculated on (a) dopant-free and (b) Cs-doped $NaCaH_3$. Herein, the numbers of 1–10 denote different bonds for bond order analysis (Table 3.7).

Table 3.7. Bond orders of dopant-free and Cs-doped $NaCaH_3$ systems.[a]

System	1	2	3	4	5	6	7	8	9	10
$NaCaH_3$	0.152	0.084	0.151	0.151	0.204	0.198	0.172	0.217	0.234	0.225
Cs-doped $NaCaH_3$	0.130	0.150	0.097	0.136	0.195	0.204	0.181	0.219	0.185	0.219

[a]All bonds of 1–10 are shown in Figure 3.3.

3.4. Conclusions

Herein, we screened a $NaCaH_3$ system from 25 perovskite-type hydrides (ABH_3) comprising A, where A = Li, Na, K, Rb, or Cs and B, where B = Be, Mg, Ca, Sr, or Ba, using DFT modeling. For facilitating the dehydrogenation process of $NaCaH_3$, the alkali dopants, M = Li, K, Rb, or Cs, and alkaline-earth dopants, M′ = Be, Mg, Sr, or Ba, were introduced at the Na and Ca sites in a $NaCaH_3$ system, respectively. Doping alkali metal at the Na site was found to be useful in comparison with doping alkaline-earth metal at the Ca site of $NaCaH_3$. Among all the dopants studied, Cs was found to be the most beneficial dopant for dehydrogenation of $NaCaH_3$ with the lowest reaction enthalpy in a dehydrogenation process. Analyzing atomic charges and bond order was helpful in understanding the effect of a Cs-doping at the Na site on hydrogen release. The bond strength of both Na–H and Ca–H bonds are reduced after Cs-doping. Overall, these studies suggest a valuable system of Cs-doped $NaCaH_3$ as the novel hydrogen storage material.

Reference

[1] A. Züttel, Materials for hydrogen storage. Mater. Today 2003, 6, 24-33.

[2] L. Schlapbach, A. Züttel, Hydrogen-storage materials for mobile applications. In Materials for sustainable energy: a collection of peer-reviewed research and review articles from nature publishing group, World Scientific, 2011, 265-270.

[3] J. Yang, A. Sudik, C. Wolverton, D. J. Siegel, High capacity hydrogen storage materials: attributes for automotive applications and techniques for materials discovery. Chem. Soc. Rev. 2010, 39, 656-675.

[4] M. B. Ley, L. H. Jepsen, Y. S. Lee, Y. W. Cho, J. M. B. Von Colbe, M. Dornheim, M. Rokni, J. O. Jensen, M. Sloth, Y. Filinchuk, J. E. Jørgensen, F. Besenbacher, T. R. Jensen,

Complex hydrides for hydrogen storage -new perspectives. Mater. Today 2014, 17, 122-128.

[5] J. Ren, N. M. Musyoka, H. W. Langmi, M. Mathe, S. Liao, Current research trends and perspectives on materials-based hydrogen storage solutions: A critical review. Int. J. Hydrogen Energ. 2017, 42, 289-311.

[6] K. Ikeda, T. Sato, S. I. Orimo, Perovskite-type hydrides - synthesis, structures and properties. Int. J. Mater. Res. 2008, 99, 471-479.

[7] A. H. Reshak, $NaMgH_3$ a perovskite-type hydride as advanced hydrogen storage systems: Electronic structure features. Int. J. Hydrogen Energ. 2015, 40, 16383-16390.

[8] D. Pottmaier, E. R. Pinatel, J. G. Vitillo, S. Garroni, M. Orlova, M. D. Baró, G. B. Vaughan, M. Fichtner, W. Lohstroh, M. Baricco, Structure and thermodynamic properties of the $NaMgH_3$ perovskite: a comprehensive study. Chem. Mater. 2011, 23, 2317-2326.

[9] H. Wu, W. Zhou, T. J. Udovic, J. J. Rush, T. Yildirim, Crystal chemistry and dehydrogenation/rehydrogenation properties of perovskite hydrides $RbMgH_3$ and $RbCaH_3$. J. Phys. Chem. C 2009, 113, 15091-15098.

[10] B. Rehmat, M. A. Rafiq, Y. Javed, Z. Irshad, N. Ahmed, S. M. Mirza, Elastic properties of perovskite-type hydrides $LiBeH_3$ and $NaBeH_3$ for hydrogen storage. Int. J. Hydrogen Energ. 2017, 42, 10038-10046.

[11] A. H. Reshak, DFT calculations for the electronic structure of alpha phase of $CsMgH_3$ as advanced hydrogen storage materials. Int. J. Hydrogen Energ. 2016, 41, 2762-2770.

[12] A. W. Overhauser, Crystal structure of lithium beryllium hydride. Phys. Rev. B 1987, 35, 411.

[13] E. Rönnebro, D. Noréus, K. Kadir, A. Reiser, B. Bogdanovic, Investigation of the perovskite related structures of $NaMgH_3$, $NaMgF_3$ and Na_3AlH_6. J. Alloy Compd. 2000, 299, 101-106.

[14] Z. M. Wang, J. J. Li, S. Tao, J. Q. Deng, H. Zhou, Q. Yao, Structure, thermal analysis and dehydriding kinetic properties of $Na_{1-x}Li_xMgH_3$ hydrides. J. Alloy Compd. 2016, 660, 402-406.

[15] D. A. Sheppard, M. Paskevicius, C. E. Buckley, Thermodynamics of hydrogen desorption from $NaMgH_3$ and its application as a solar heat storage medium. Chem. Mater. 2011, 23, 4298-4300.

[16] R. Schumacher, A. Weiss, $KMgH_3$ single crystals by synthesis from the elements. J. Less-Common Met. 1990, 163, 179-183.

[17] A. J. Maeland, W. D. Lahar, The hydride-fluoride analogy. Zeitschrift für Physikalische Chemie 1993, 179, 181-185.

[18] F. Gingla, T. Vogt, E. Akiba, K. Yvon, Cubic $CsCaH_3$ and hexagonal $RbMgH_3$: new examples of fluoride-related perovskite-type hydrides. J. Alloy Compd. 1999, 282, 125-129.

[19] B. Bertheville, P. Fischer, K. Yvon, High-pressure synthesis and crystal structures of new ternary caesium magnesium hydrides, $CsMgH_3$, $Cs_4Mg_3H_{10}$ and Cs_2MgH_4. J. Alloy Compd. 2002, 330, 152-156.

[20] G. Renaudin, B. Bertheville, K. Yvon, Synthesis and structure of an orthorhombic low-pressure polymorph of caesium magnesium hydride, $CsMgH_3$. J. Alloy Compd. 2003, 353, 175-179.

[21] C. E. Messer, J. C. Eastman, R. G. Mers, A. J. Maeland, Ternary perovskite phases in systems of lithium hydride with barium, strontium, and calcium hydrides. Inorg. Chem. 1964, 3, 776-778.

[22] A. H. Reshak, Photocatalytic water splitting solar-to-hydrogen energy conversion: Perovskite-type hydride $XBeH_3$ (X = Li or Na) as active photocatalysts. J. Catal. 2017, 351, 119-129.

[23] M. Santhosh, S. Kanagaprabha, R. Rajeswarapalanichamy, K. Iyakutti, First principles study of structural stability, electronic structure and mechanical properties of alkali beryllium hydrides $ABeH_3$ (A = K, Rb, Cs). J. Phys. Chem. Solids 2015, 81, 34-39.

[24] P. Vajeeston, P. Ravindran, H. Fjellvåg, Structural investigation and thermodynamical properties of alkali calcium trihydrides. J. Chem. Phys. 2010, 132, 114504.

[25] Y. Li, B. K. Rao, T. McMullen, P. Jena, P. K. Khowash, Electronic structure of the $LiMgH_3$ class of compounds: cluster calculations. Phys. Rev. B 1991, 44, 6030-6036.

[26] P. Vajeeston, P. Ravindran, H. Fjellvåg, Structural phase stability studies on $MBeH_3$ (M = Li, Na, K, Rb, Cs) from density functional calculations. Inorg. Chem. 2008, 47, 508-514.

[27] P. Vajeeston, P. Ravindran, A. Kjekshus, H. Fjellvåg, First-principles investigations of the $MMgH_3$ (M = Li, Na, K, Rb, Cs) series. J. Alloy Compd. 2008, 450, 327-337.

[28] L. George, S. K. Saxena, Structural stability of metal hydrides, alanates and borohydrides of alkali and alkali-earth elements: a review. Int. J. Hydrogen Energ. 2010, 35, 5454-5470.

[29] K. Komiya, N. Morisaku, R. Rong, Y. Takahashi, Y. Shinzato, H. Yukawa, M. Morinaga, Synthesis and decomposition of perovskite-type hydrides, $MMgH_3$ (M = Na, K, Rb). J. Alloy Compd. 2008, 453, 157-160.

[30] Y. Li, X. Ding, F. Wu, D. Sun, Q. Zhang, F. Fang, Enhancement of hydrogen storage in destabilized $LiNH_2$ with $KMgH_3$ by quick conveyance of N-containing species. J. Phys. Chem. C 2016, 120, 1415-1420.

[31] Y. Li, J. S. Chung, S. G. Kang, First-principles rational design of M-doped $LiBH_4$(010) surface for hydrogen release: Role of strain and dopants (M = Na, K, Al, F, or Cl). Int. J. Hydrogen Energ. 2019, 44, 6065-6073.

[32] A. L. Chaudhary, M. Paskevicius, D. A. Sheppard, C. E. Buckley, Thermodynamic destabilisation of MgH_2 and $NaMgH_3$ using group IV elements Si, Ge or Sn. J. Alloy Compd. 2015, 623, 109-116.

[33] L. F. C. Vasquez, Y. Liu, C. Paterakis, D. Reed, D. Book, Hydrogen sorption properties of $Li_xNa_{1-x}MgH_3$ (x = 0, 0.2, 0.5 & 0.8). Int. J. Hydrogen Energ. 2017, 42, 22589-22597.

[34] S. Tao, Z. M. Wang, Z. Z. Wan, J. Q. Deng, H. Zhou, Q. Yao, Enhancing the dehydriding properties of perovskite-type $NaMgH_3$ by introducing potassium as dopant. Int. J. Hydrogen Energ. 2017, 42, 3716-3722.

[35] Z. Wang, S. Tao, J. Deng, H. Zhou, Q. Yao, Significant improvement in the dehydriding properties of perovskite hydrides, $NaMgH_3$, by doping with K_2TiF_6. Int. J. Hydrogen Energ. 2017, 42, 8554-8559.

[36] D. He, Y. Wang, C. Wu, Q. Li, W. Ding, C. Sun, Enhanced hydrogen desorption properties of magnesium hydride by coupling non-metal doping and nano-confinement. Appl. Phys. Lett. 2015, 107, 243907.

[37] H. Wang, H. J. Lin, W. T. Cai, L. Z. Ouyang, M. Zhu, Tuning kinetics and thermodynamics of hydrogen storage in light metal element based systems - a review of recent progress. J. Alloy Compd. 2016, 658, 280-300.

[38] T. Sadhasivam, H. T. Kim, S. Jung, S. H. Roh, J. H. Park, H. Y. Jung, Dimensional effects of nanostructured Mg/MgH_2 for hydrogen storage applications: a review. Renew. Sust. Energ. Rev. 2017, 72, 523-534.

[39] S. Bouaricha, J. P. Dodelet, D. Guay, J. Huot, R. Schulz, Study of the activation process of Mg-based hydrogen storage materials modified by graphite and other carbonaceous compounds. J. Mater. Res. 2001, 16, 2893-2905.

[40] J. Huot, G. Liang, R. Schulz, Mechanically alloyed metal hydride systems. Appl. Phys. A 2001, 72, 187-195.

[41] B. Bogdanović, M. Schwickardi, Ti-doped alkali metal aluminium hydrides as potential novel reversible hydrogen storage materials. J. Alloy Compd. 1997, 253, 1-9.

[42] A. H. Reshak, MgH_2 and LiH metal hydrides crystals as novel hydrogen storage material: Electronic structure and optical properties. Int. J. Hydrogen Energ. 2013, 38, 11946-11954.

[43] N. Kunkel, H. Kohlmann, Ionic mixed hydride fluoride compounds: stabilities predicted by DFT, synthesis, and luminescence of divalent europium. J. Phys. Chem. C 2016, 120, 10506-10511.

[44] G. Kresse, J. Furthmüller, Efficiency of ab-initio total energy calculations for metals and semiconductors using a plane-wave basis set. Comp. Mater. Sci. 1996, 6, 15-50.

[45] G. Kresse, J. Furthmüller, Efficient iterative schemes for ab initio total-energy calculations using a plane-wave basis set. Phys. Rev. B 1996, 54, 11169.

[46] P. E. Blöchl, Projector augmented-wave method. Phys. Rev. B 1994, 50, 17953-17979.

[47] J. P. Perdew, K. Burke, Ernzerhof, M. Generalized gradient approximation made simple. Phys. Rev. B 1996, 77, 3865.

[48] S. Grimme, J. Antony, S. Ehrlich, H. Krieg, A consistent and accurate ab initio parametrization of density functional dispersion correction (DFT-D) for the 94 elements H-Pu. J. Chem. Phys. 2010, 132, 154104.

[49] H. J. Monkhorst, J. D. Pack, Special points for Brillouin-zone integrations. Phys. Rev. B 1976, 13, 5188-5192.

[50] S. V. Alapati, J. K. Johnson, D. S. Sholl, Identification of destabilized metal hydrides for hydrogen storage using first principles calculations. J. Phys. Chem. B 2006, 110, 8769-8776.

[51] J. P. Bastide, Crystal structure of lithium beryllium hydrides $LiBeH_3$, Li_2BeH_4. Solid State Commun. 1990, 74, 355-358.

[52] A. Bouamrane, J. P. Laval, J. P. Soulie, J. P. Bastide, Structural characterization of $NaMgH_2F$ and $NaMgH_3$. Mater. Res. Bull. 2000, 35, 545-549.

[53] H. H. Park, M. Pezat, B. Darriet, P. Hagenmuller, The KH-MgH_2 system. Revue de chimie minérale 1987, 24, 525-530.

[54] H. H. Park, M. Pezat, B. C. R. Darriet, Deux nouveaux hydrures: $RbCaH_3$ et Rb2CaH_4. Acad. Sci. II 1988, 306, 963.

[55] N. Kunkel, A. Meijerink, H. Kohlmann, Bright yellow and green Eu [II] luminescence and vibronic fine structures in $LiSrH_3$, $LiBaH_3$ and their corresponding deuterides. Phys. Chem. Chem. Phys. 2014, 16, 4807-4813.

[56] D. Li, T. Zhang, S. Yang, Z. Tao, J. Chen, Ab initio investigation of structures, electronic and thermodynamic properties for Li-Mg-H ternary system. J. Alloy Compd. 2011, 509, 8228-8234.

[57] A. Klaveness, O. Swang, H. Fjellvåg, Formation enthalpies of $NaMgH_3$ and $KMgH_3$: A computational study. Europhys. Lett. 2006, 76, 285-290.

[58] H. Wu, W. Zhou, T. J. Udovic, J. J. Rush, T. Yildirim, Crystal chemistry of perovskite-type hydride $NaMgH_3$: implications for hydrogen storage. Chem. Mater. 2008, 20, 2335-2342.

[59] N. Kunkel, A. Meijerink, M. Springborg, H. Kohlmann, Eu [ii] luminescence in the perovskite host lattices $KMgH_3$, $NaMgH_3$ and mixed crystals $LiBa_xSr_{1-x}H_3$. J. Mater. Chem. C 2014, 2, 4799-4804.

[60] A. Andrada-Chacón, J. A. Alonso, V. Pomjakushin, J. Sánchez-Benítez, High-pressure synthesis and structural characterization of $Na_{1-x}K_xMgH_3$ perovskite hydrides. J. Alloy Compd. 2017, 729, 914-920.

[61] Y. Li, L. Zhang, Q. Zhang, F. Fang, D. Sun, K. Li, H. Wang, L. Z. Ouyang, M. Zhu, In situ embedding of Mg_2NiH_4 and YH_3 nanoparticles into bimetallic hydride $NaMgH_3$ to inhibit phase segregation for enhanced hydrogen storage. J. Phys. Chem. C 2014, 118, 23635-23644.

[62] H. Wang, J. Zhang, J. W. Liu, L. Z. Ouyang, M. Zhu, Catalysis and hydrolysis properties of perovskite hydride $NaMgH_3$. J. Alloy Compd. 2013, 580, S197-S201.

[63] W. Grochala, P. P. Edwards, Thermal decomposition of the non-interstitial hydrides for the storage and production of hydrogen. Chem. Rev. 2004, 104, 1283-1316.

[64] Y. Li, Y. Mi, J. S. Chung, S. G. Kang, First-principles studies of $K_{1-x}M_xMgH_3$ (M = Li, Na, Rb, or Cs) perovskite hydrides for hydrogen storage. Int. J. Hydrogen Energ. 2018, 43, 2232-2236.

[65] X. Mo, W. Jiang, Dehydrogenation properties of $LiBH_4$ modified by Mg from first-principles calculations. J. Alloy Compd. 2018, 735, 668-676.

[66] X. B. Xiao, B. Y. Tang, S. Q. Liao, L. M. Peng, W. J. Ding, Thermodynamic and electronic properties of quaternary hydrides $Li_xNa_{1-x}MgH_3$. J. Alloy Compd. 2009, 474, 522-526.

[67] R. F. Bader, A quantum theory of molecular structure and its applications. Chem. Rev. 1991, 91, 893-928.

[68] T. A. Manz, N. G. Limas, Introducing DDEC6 atomic population analysis: part 1. Charge partitioning theory and methodology. RSC Adv. 2016, 6, 47771-47801.

[69] T. A. Manz, Introducing DDEC6 atomic population analysis: part 3. Comprehensive method to compute bond orders. RSC Adv. 2017, 7, 45552-45581.

CHAPTER 4. Perovskite hydride $KMgH_3$ with pressure and dopants M (M = Li, Na, Rb or Cs) for dehydrogenation

4.1. Introduction

Hydrogen is considered an alternative energy source owing to its abundant reserves, highest energy density (per unit mass), and environmental friendliness, particularly for transportation applications [1]. On the other hand, the most difficult hurdle for these applications is associated with hydrogen storage. Hydrogen can be stored safely and effectively using metal hydrides as hydrogen storage materials [2, 3]. Mg-based hydrides have attracted considerable attention due to the lightweight, relatively low cost, and good quality functional properties for hydrogen storage [4-7]. Among them, perovskite-type hydride materials, $AMgH_3$ (A-alkali elements), have attracted considerable interest [8-10]. Komiya et al. [11] examined the decomposition of $NaMgH_3$, $KMgH_3$, and $RbMgH_3$ by ball-milling and heat-treatment methods and found that $KMgH_3$ decomposed in a single-step reaction. They also found that $NaMgH_3$ is the most unstable among the three hydrides examined [11]. Using DFT calculations, Bouhadda and Ghebouli et al. [12, 13] examined the thermal properties of $KMgH_3$ and found that $KMgH_3$ was an insulator. Reshak et al. [14] conducted first-principles studies, and reported that the stability of $KMgH_3$ depends on the hydrogen positions.

The main disadvantages of using Mg-based hydrides are their poor thermodynamic properties and slow desorption kinetics [15]. To develop high-performance hydrogen storage materials, it is essential to tune the thermodynamic and kinetic properties of these hydrides [16, 17]. In recent experimental work, the approach of combining both hydrogen production and storage in one step can reduce energy consumption significantly for hydride [18, 19]. Some

other efforts have been made to overcome these disadvantages, such as alloying with another element, ball milling, adding catalysts and composite effects [20-26]. Modifying the hydrides by doping other elements is beneficial for improving the properties of hydrogen storage [27, 28]. For example, considerable enhancements in the kinetics and cycling stability were observed in the $NaMgH_3$ sample with Mg_2NiH_4 and YH_3 nanoparticles embedded [29]. Alkali metals appear to have a great influence on them due to their active chemical properties and low densities [30, 31]. Liu et al. [32] examined how Li, Na, or K affect the reaction enthalpies and the kinetics of hydrogenation/decomposition of Mg nanoparticles by reduction and heat treatment methods. They suggested that these alkali metals can be used to enhance the properties of Mg nanoparticles for hydrogen storage. Xiao et al. [33] reported that the reaction enthalpy of the dehydrogenation reactions was decreased by the substitution of Li at the Na site of $NaMgH_3$ by DFT calculations. Using a high-energy ball milling method, Tao et al. [34] prepared $NaMgH_3$ and $Na_{0.9}K_{0.1}MgH_3$ hydrides and reported that this addition of K in $NaMgH_3$ improved the dehydriding kinetic properties and increased the amount of the hydrogen desorbed.

In addition, pressure can induce the decomposition of hydrides [35, 36]. Yan et al. [37] examined how pressure affects the desorption kinetics of hydrogen in $Mg(NH_2)_2$-2LiH-0.07KOH compacts. They suggested that pressure is an important factor for hydrides to release hydrogen. Besides, interface is another factor responsible for hydrogen storage of Mg-based hydrides [38].

A first-principle approach is a valuable and powerful tool in the design of alloy systems [39]. This study examined the effects of different alkali metal dopants M (M = Li, Na, Rb, or

Cs) and pressures (0, 0.5, 1.0, 1.5, and 2 GPa) on the hydrogen release in $KMgH_3$ hydride using the first-principles DFT calculations.

4.2. Computational details

All DFT calculations were conducted with the projector augmented plane wave (PAW) [40] on the Vienna *ab initio* simulation package (VASP) [41]. The generalized-gradient approximation (GGA) functional of Perdew-Burke-Ernzerhof (PBE) was used [42]. The three phases of $KMgH_3$ having different space groups (P$m\overline{3}m$, P*nma*, and R3*c*) were taken into consideration. The same number of atoms (12 K, 12 Mg, and 36 H atoms) was used in all phases for a consistent comparison. All structures were relaxed completely. The Brillouin zones were sampled with the Monkhorst-Pack scheme [43] by 3×5×5, 3×5×7, and 4×7×3 **k**-points for P$m\overline{3}m$, P*nma* and R3*c* phases, respectively. A kinetic energy cutoff of 550 eV was employed. The total energy difference of all self-consistent iterative loops was less than 10^{-6} eV. Relaxation processes were conducted using conjugate gradient algorithms until the force was smaller than 10^{-2} eVÅ^{-1}.

4.3. Results and discussion

4.3.1. Structure and optimization

$KMgH_3$ was reported to have a P$m\overline{3}m$ perovskite-type structure as the ground state structure [44]. Table 4.1 lists the DFT results of the lattice parameters. The computational lattice values were comparable to the available lattice parameters in the experiments [45, 46] and other calculations [14, 47, 48] (Table 4.1). Alkali dopants M (M = Li, Na, Rb or Cs) were then introduced at the K-sites of optimized $KMgH_3$. The various configurations for the

different positions of dopants were considered to obtain the most stable structure in all doped systems.

The first aim of these calculations was to identify the most likely dehydrogenation reaction pathway. Four different reaction pathways for hydrogen release were considered. These reactions do not include MgH_2 as products [33] because of the lower stability of MgH_2 than alkali hydrides, such as LiH, NaH, KH, RbH, and CsH. The four possible reactions can be described as follows:

$$K_{1-x}M_xM_gH_3 \rightarrow xM + (1-x)K + M_g + \frac{3}{2}H_2 \quad (1)$$

$$K_{1-x}M_xM_gH_3 \rightarrow xMH + (1-x)K + M_g + \frac{3-x}{2}H_2 \quad (2)$$

$$K_{1-x}M_xM_gH_3 \rightarrow xM + (1-x)KH + M_g + (1+\frac{x}{2})H_2 \quad (3)$$

$$K_{1-x}M_xM_gH_3 \rightarrow xMH + (1-x)KH + M_g + H_2 \quad (4)$$

The reaction enthalpies affect the heat of hydrogenation and dehydrogenation reactions [49]. Therefore, the reaction enthalpies (ΔH) were calculated to study the hydrogen release properties of $KMgH_3$. For all possible dehydrogenation reactions, the reaction enthalpies (ΔH) at 0 K were calculated as follows [50]:

$$\Delta H = \sum_{products} E - \sum_{reactants} E. \quad (5)$$

Here $\sum_{products} E$ and $\sum_{reactants} E$ represent the sum of the reactants' DFT total energies and the sum of the products' DFT total energies, respectively. The effects of the zero-point energy (ZPE) are significant for hydrogen [51]. Therefore, the ZPE of the $KMgH_3$ structure with the $Pm\overline{3}m$ phase was checked at the ground state. The calculated ZPE of a hydrogen molecule was

Table 4.1. Lattice constants and bond lengths *d* of the $KMgH_3$ ($Pm\overline{3}m$) structure.

	Calc. (Å)	Expt. (Å)	Other Calc. (Å)
Lattice constants	a = 4.018	a = 4.023[a], a = 4.018[b]	a = 4.0295[c], a = 4.035[d], a = 4.01[e]
d (K-H)	2.841	-	2.85[c], 2.853[d]
d (K-Mg)	3.480	-	3.49[c], 3.495[d]
d (Mg-H)	2.009	-	2.018[d]
d (H-H)	2.841	-	2.853[d]

[a] Reference [45] [b] Reference [46] [c] Reference [47] [d] Reference [14] [e] Reference [48].

Table 4.2. Reaction enthalpies, ΔH (eV) with and without ZPE corrections of $KMgH_3$ in each reaction pathway.

Reaction enthalpy (ΔH)	Eq.(6)	Eq.(7)
With ZPE	0.763	0.324
Without ZPE	0.400	0

Table 4.3. Relative ground state energies (eV) of $KMgH_3$ and $K_{1-x}M_xMgH_3$ (x = 0, 0.0833 and 0.1667) structures with three phases.

Structures	$Pm\bar{3}m$	P*nma*	R3*c*
$KMgH_3$	0	0.065	0.220
$K_{0.9167}Li_{0.0833}MgH_3$	-0.044	-0.278	-0.290
$K_{0.8333}Li_{0.1667}MgH_3$	-0.374	-0.678	-0.696
$K_{0.9167}Na_{0.0833}MgH_3$	0.150	0.184	0.171
$K_{0.8333}Na_{0.1667}MgH_3$	0.266	0.278	0.285
$K_{0.9167}Rb_{0.0833}MgH_3$	0.377	0.417	0.595
$K_{0.8333}Rb_{0.1667}MgH_3$	0.730	0.769	0.955
$K_{0.9167}Cs_{0.0833}MgH_3$	0.728	0.776	0.967
$K_{0.8333}Cs_{0.1667}MgH_3$	1.358	1.377	1.404

0.273 eV/f.u. Velikokhatnyi et al. [49] reported the DFT calculated ZPE of a hydrogen molecule as 0.279 eV/f.u. which was similar to the present ZPE value. The ZPE of $KMgH_3$, KH, and H_2 were included to obtain ΔH with the ZPE corrections. Table 4.2 lists these reaction enthalpies with the ZPE corrections. To understand the effects of ZPE on the reaction enthalpies, the ΔH with ZPE corrections and the enthalpies without ZPE corrections in each reaction pathway were compared. The reaction enthalpy (ΔH) of $KMgH_3$ without ZPE corrections in the reaction that has the lowest reaction enthalpy was set to zero as a reference.

$$\mathrm{KM_gH_3} \rightarrow \mathrm{K} + \mathrm{M_g} + \frac{3}{2}\mathrm{H_2} \tag{6}$$

$$\mathrm{KM_gH_3} \rightarrow \mathrm{KH} + \mathrm{M_g} + \mathrm{H_2} \tag{7}$$

A similar difference between the reaction enthalpies (ΔH) with ZPE and ΔH without ZPE was observed in reactions (6) and (7) (Table 4.2), indicating that the ZPE correction has a slight effect in determining the most favorable reaction pathway. Therefore, the ZPE corrections were excluded from later calculations with the aim of finding the most favorable reaction pathway. This approach is consistent with others in that the ZPE corrections for the reaction enthalpy were neglected [52-54].

To find the ground state structure of each compound, the DFT total energies of the different phases were compared, as shown in Table 4.3. Here, the total energy of the most stable phase of $KMgH_3$ was set to zero as a reference. This is consistent with the experimental structure of $KMgH_3$ as a P$m\bar{3}m$ structure [55, 56]. The ground state structure of $K_{1-x}M_xMgH_3$ varied with the dopants (M). For example, the R3*c* phase was the most stable phase among the other phases investigated in $K_{1-x}Li_xMgH_3$ (x = 0.0833 and 0.1667). On the other hand, the Na,

Rb or Cs-doped structures showed the P$m\overline{3}m$ phase as their ground state structures. The optimized lattice constants of all doped structures are shown in Table 4.4.

4.3.2. Favorable reaction pathway and dopant

Using the most stable phase of $K_{1-x}M_xMgH_3$ (x = 0, 0.0833 and 0.1667), the reaction enthalpies (ΔH) of the doped systems were calculated to obtain the most plausible reaction pathway with the most promising dopant. The calculated reaction enthalpies (ΔH) of all the doped systems showed similar curves in each reaction pathway. Fig. 4.1 presents the results of $K_{1-x}Li_xMgH_3$ with the most stable phase of the reactants and the most stable phase of products. The reaction enthalpies (ΔH) of pathways (1) and (2) were higher than ΔH of pathways (3) and (4), showing that pathways (1) and (2) were unfavorable for hydrogen release. On the other hand, the reaction enthalpies (ΔH) of pathway (4) decreased with increasing Li concentrations in $K_{1-x}M_xMgH_3$. The lowest reaction enthalpies can be found in pathway (4), indicating that the reaction pathway (4) was the most favorable for the dehydrogenation reaction of $K_{1-x}Li_xMgH_3$. Other systems with Na, Rb, and Cs dopants also showed similar results.

Each doped structure with different dopants showed the same favorable reaction pathway as pathway (4). The reaction enthalpies of each doped material in this dehydrogenation reaction (4) were calculated to find the useful dopant for hydrogen release. All reaction enthalpies (ΔH) of doped structures were lower than ΔH of dopant-free $KMgH_3$, as shown in Fig. 4.2. In particular, $K_{1-x}Li_xMgH_3$ (x = 0.0833 and 0.1667) showed the lowest reaction enthalpies among the other doped systems (Fig. 4.2), indicating that among the four dopants examined, Li was the most useful dopant for the $KMgH_3$ hydride to release hydrogen. Moreover, the reaction enthalpies (ΔH) of $K_{0.9167}Li_{0.0833}MgH_3$, and $K_{0.8333}Li_{0.1667}MgH_3$ were

Table 4.4. DFT calculated lattice constants (Å) and volume (Å^3) of all the materials studied.

Structures	Space group	a	b	c	Volume
Li	I$m\bar{3}m$	3.491	3.491	3.491	42.545
Na	I$m\bar{3}m$	4.235	4.235	4.235	75.956
K	I$m\bar{3}m$	5.225	5.225	5.225	142.646
Rb	I$m\bar{3}m$	5.585	5.585	5.585	174.209
Cs	I$m\bar{3}m$	6.045	6.045	6.045	220.897
Mg	P$6_3/mmc$	3.208	3.208	5.133	45.745
KH	F$m\bar{3}m$	5.701	5.701	5.701	185.279
LiH	F$m\bar{3}m$	3.998	3.998	3.998	63.907
NaH	F$m\bar{3}m$	4.787	4.787	4.787	109.678
RbH	F$m\bar{3}m$	6.075	6.075	6.075	224.197
CsH	F$m\bar{3}m$	6.439	6.439	6.439	267.027
$KMgH_3$	P$m\bar{3}m$	12.052	8.034	8.034	777.945
	Pnma	17.017	8.020	5.667	773.401
	R3c	11.308	5.654	13.873	768.165
$K_{0.9167}Li_{0.0833}MgH_3$	P$m\bar{3}m$	11.996	7.998	7.998	767.271
	Pnma	16.977	7.990	5.666	768.482
	R3c	11.309	5.664	13.859	769.042
$K_{0.8333}Li_{0.1667}MgH_3$	P$m\bar{3}m$	11.996	7.961	7.961	760.305
	Pnma	16.892	7.965	5.655	760.842
	R3c	11.291	5.649	13.828	762.784
$K_{0.9167}Na_{0.0833}MgH_3$	P$m\bar{3}m$	12.015	8.010	8.010	770.899
	Pnma	16.970	7.998	5.654	767.425
	R3c	11.318	5.660	13.859	768.812
$K_{0.8333}Na_{0.1667}MgH_3$	P$m\bar{3}m$	11.977	7.989	7.984	763.909
	Pnma	16.920	7.979	5.642	761.649
	R3c	11.279	5.641	13.808	760.765
$K_{0.9167}Rb_{0.0833}MgH_3$	P$m\bar{3}m$	12.079	8.053	8.053	783.285
	Pnma	17.065	8.045	5.686	780.570
	R3c	11.333	5.667	13.912	773.796
$K_{0.8333}Rb_{0.1667}MgH_3$	P$m\bar{3}m$	12.105	8.071	8.071	788.519
	Pnma	17.105	8.064	5.700	786.238

Structures	Space group	a	b	c	Volume
$K_{0.9167}Cs_{0.0833}MgH_3$	R3*c*	11.357	5.680	13.949	779.210
	P*m*$\bar{3}$*m*	12.112	8.075	8.075	789.790
	P*nma*	17.117	8.067	5.706	787.853
$K_{0.8333}Cs_{0.1667}MgH_3$	R3*c*	11.364	5.684	13.956	780.581
	P*m*$\bar{3}$*m*	12.180	8.103	8.117	801.131
	P*nma*	17.207	8.115	5.740	801.410
	R3*c*	11.469	5.737	14.056	800.870

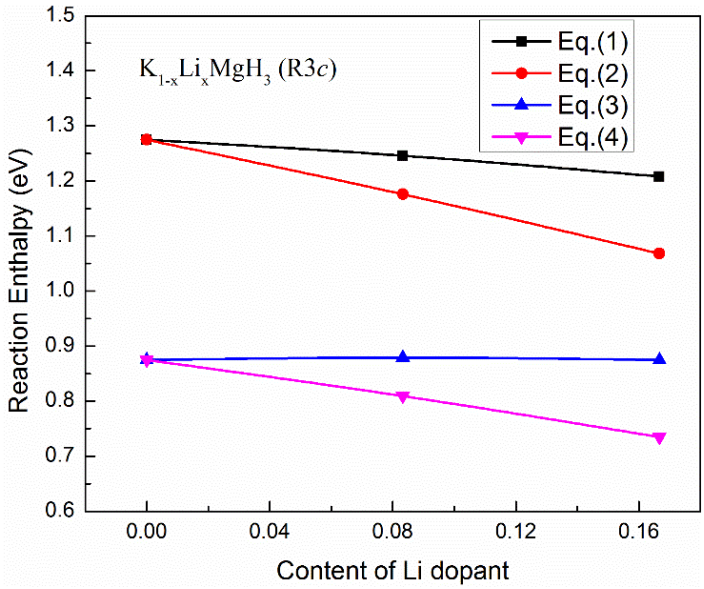

Figure 4.1. Reaction enthalpies (ΔH) of $K_{1-x}Li_xMgH_3$ (x = 0, 0.0833 and 0.1667) hydrides.

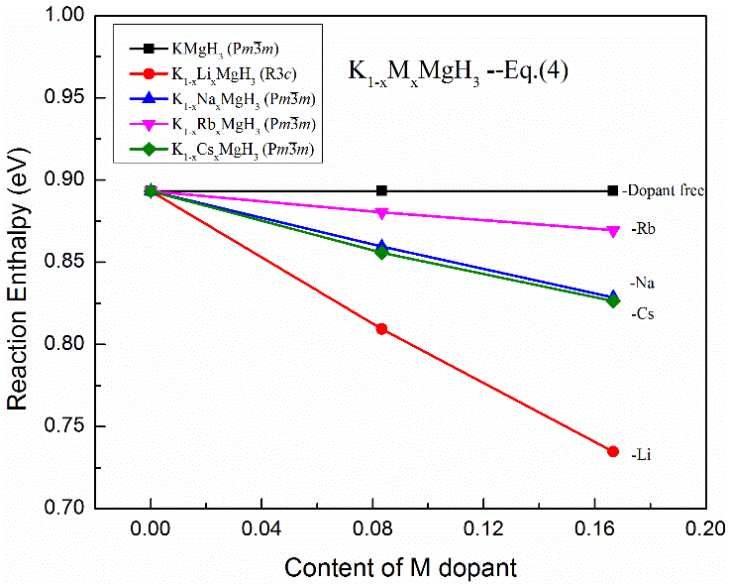

Figure 4.2. Calculated reaction enthalpies (ΔH) of $KMgH_3$ and $K_{1-x}M_xMgH_3$ (x = 0.0833 and 0.1667) by reaction (4).

0.085 eV and 0.160 eV lower, respectively, than that of the $KMgH_3$ structure. Therefore, Li doping was effective in reducing the reaction enthalpy of the dehydrogenation reactions.

4.3.3. Pressure effects and the partial density of states

Pressures of 0, 0.5, 1.0, 1.5 and 2 GPa were applied to dopant-free and doped $KMgH_3$. The reaction enthalpies (ΔH) decreased with increasing applied pressures (Fig. 4.3). In $KMgH_3$, H was reduced by 0.79 eV when 2 GPa was applied to the dopant-free hydride. Similar trends of decreasing reaction enthalpies by pressure were observed in M-doped $KMgH_3$, showing that pressure can be used to enhance the dehydriding properties of dopant-free and doped $KMgH_3$ hydride.

To further understand the effects of the Li dopant and pressure on the hydrogen release of $KMgH_3$, the partial density of states (PDOS) of $KMgH_3$ and $K_{0.9167}Li_{0.0833}MgH_3$ structures were calculated, as shown in Fig. 4.4 (a-c). All structures exhibited wide band gaps (approximately 2.38 ~ 2.47 eV) possessing non-metal features (Fig. 4.4). The band gap of 2.38 eV for $KMgH_3$ was in good agreement with other computational values (2.32 eV) [47]. The *s* and *p* states of K and Mg made the main contributions to the conduction band of $KMgH_3$ at P = 0 GPa (Fig. 4.4 (a)). The contribution of the Li dopant-*s* state to the conduction band was observed in Li-doped $KMgH_3$ (Fig. 4.4 (b)). After 2 GPa pressure was applied, the band gap of $KMgH_3$ was increased by approximately 0.25 eV and the electronic states of K and Mg were clearly enhanced (Fig. 4.4 (c)). This indicates that the change in electronic states may make the structures unstable after the dopant or pressure was introduced. In summary, both dopant and pressure can facilitate the release of hydrogen from $KMgH_3$ hydride, decreasing the reaction enthalpies.

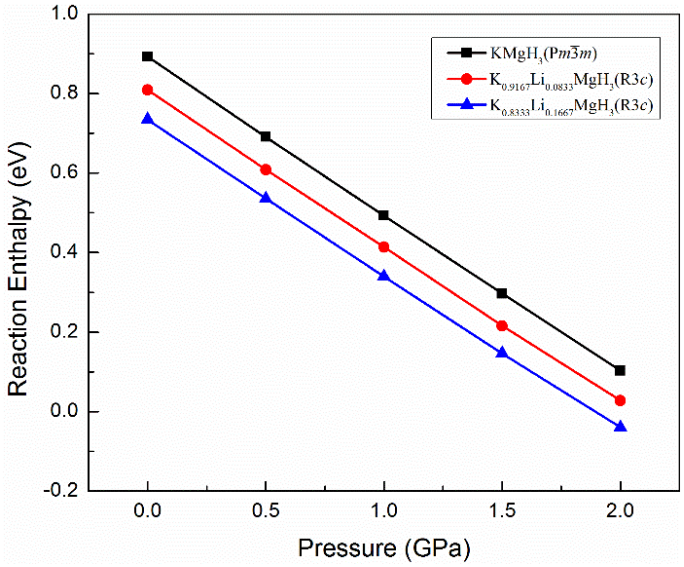

Figure 4.3. Reaction enthalpies (ΔH) of $KMgH_3$ and $K_{1-x}Li_xMgH_3$ (x = 0.0833 and 0.1667) structures with the applied pressure.

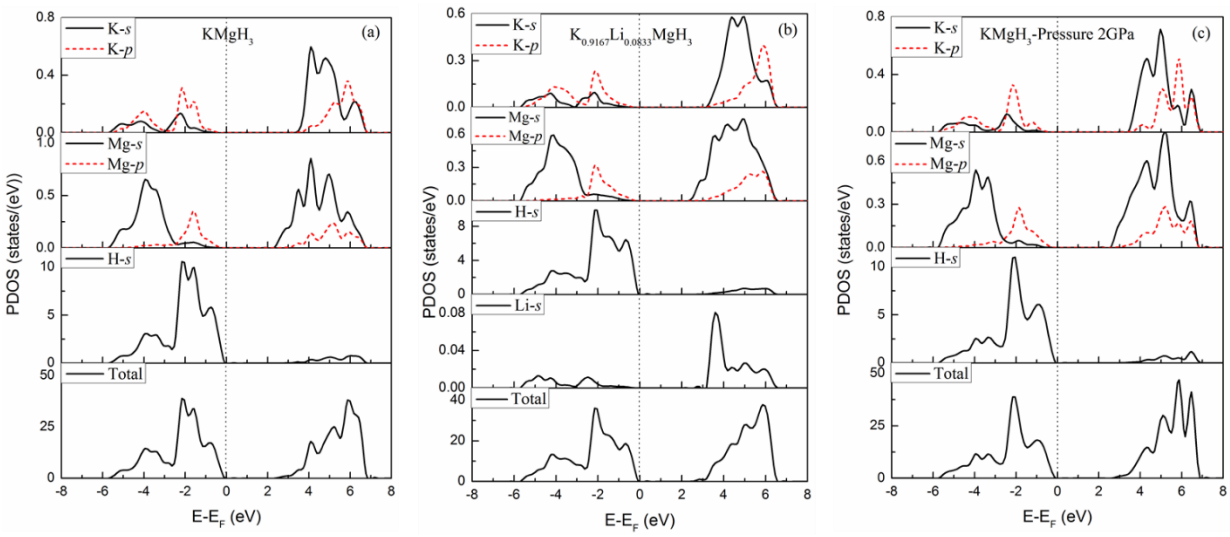

Figure 4.4. Partial density of states (PDOS) of (a) $KMgH_3$, (b) $K_{0.9167}Li_{0.0833}MgH_3$ and (c) $KMgH_3$ at 2 GPa.

4.4. Conclusions

Using first-principles modeling, this study examined the hydrogen release properties of $KMgH_3$ and $K_{1-x}M_xMgH_3$ (x = 0.0833 and 0.1667). Alkali dopants M (M = Li, Na, Rb or Cs) were introduced at the K-sites of $KMgH_3$ and four possible reaction pathways for hydrogen release were considered. Reaction pathway (4) was found to be the most favorable pathway among the other reaction pathways examined. Li was also found to be the most useful dopant for releasing hydrogen. The effects of pressure (0, 0.5, 1.0, 1.5, and 2 GPa) on $KMgH_3$ and $K_{1-x}M_xMgH_3$ structures were also examined. The results showed that the reaction enthalpies (ΔH) decreased with increasing applied pressure. The calculated electronic states showed that the Li dopant and pressure may reduce the stability of $KMgH_3$, inducing a decrease in the reaction enthalpy.

Reference

[1] L. Schlapbach, A. Züttel, Hydrogen-storage materials for mobile applications. Nature 2001,414, 353-358.

[2] I.A. Richardson, J.T. Fisher, P.E. Frome, B.O. Smith, S. Guo, S. Chanda, M.S. McFeely, A.M. Miller, J.W. Leachman, Low-cost, transportable hydrogen fueling station for early market adoption of fuel cell electric vehicles. Int. J. Hydrogen Energ. 2015, 40, 8122-8127.

[3] D. Wu, L. Ouyang, C. Wu, H. Wang, J. Liu, L. Sun, M. Zhu, Phase transition and hydrogen storage properties of Mg–Ga alloy. J. Alloy Compd. 2015, 642, 180-184.

[4] P. Jena, Materials for hydrogen storage: past, present, and future. J. Phys. Chem. Lett. 2011, 2, 206-211.

[5] I.P. Jain, C. Lal, A. Jain, Hydrogen storage in Mg: a most promising material. Int. J. Hydrogen Energ. 2010, 35, 5133-5144.

[6] M. Ma, R. Duan, L. Ouyang, X. Zhu, C. Peng, M. Zhu, Hydrogen generation via hydrolysis of H-$CaMg_2$ and H-$CaMg_{1.9}Ni_{0.1}$. Int. J. Hydrogen Energ. 2017, 42, 22312-22317.

[7] M. Huang, L. Ouyang, Z. Chen, C. Peng, X. Zhu, M. Zhu, Hydrogen production via hydrolysis of Mg-oxide composites. Int. J. Hydrogen Energ. 2017, 42, 22305-22311.

[8] H. Wang, J. Zhang, J.W. Liu, L.Z. Ouyang, M. Zhu, Catalysis and hydrolysis properties of perovskite hydride $NaMgH_3$. J. Alloy Compd. 2013, 580, S197-S201.

[9] A.H. Reshak, $NaMgH_3$ a perovskite-type hydride as advanced hydrogen storage systems: Electronic structure features. Int. J. Hydrogen Energ. 2015, 40, 16383-16390.

[10] M. Fornari, A. Subedi, D.J. Singh, Structure and dynamics of perovskite hydrides $AMgH_3$ (A = Na, K, Rb) in relation to the corresponding fluorides: A first-principles study. Phys. Rev. B 2007, 76, 214118.

[11] K. Komiya, N. Morisaku, R. Rong, Y. Takahashi, Y. Shinzato, H. Yukawa, M. Morinaga, Synthesis and decomposition of perovskite-type hydrides, $MMgH_3$ (M = Na, K, Rb). J. Alloy Compd. 2008, 453, 157-160.

[12] Y. Bouhadda, N. Kheloufi, A. Bentabet, Y. Boudouma, N. Fenineche, K. Benyalloul, Thermodynamic functions from lattice dynamic of $KMgH_3$ for hydrogen storage applications. J. Alloy Compd. 2011, 509, 8994-8998.

[13] M.A. Ghebouli, B. Ghebouli, A. Bouhemadou, M. Fatmi, S. Bin-Omran, Structural, elastic, electronic, optical and thermodynamic properties of $KMgH_3$. Solid State Sci. 2011, 13, 647-652.

[14] A.H. Reshak, M.Y. Shalaginov, Y. Saeed, I.V. Kityk, First-Principles Calculations of Structural, Elastic, Electronic, and Optical Properties of Perovskite-type $KMgH_3$ Crystals: Novel Hydrogen Storage Material. J. Phys. Chem. B 2011, 115, 2836-2841.

[15] D.-L. Zhao, Y.-H. Zhang, Research progress in Mg-based hydrogen storage alloys. Rare Met. 2014, 33, 499-510.

[16] L. Ouyang, Z. Cao, H. Wang, R. Hu, M. Zhu, Application of dielectric barrier discharge plasma-assisted milling in energy storage materials–a review. J. Alloy Compd. 2017, 691, 422-435.

[17] L.Z. Ouyang, Z.J. Cao, H. Wang, J.W. Liu, D.L. Sun, Q.A. Zhang, M. Zhu, Enhanced dehydriding thermodynamics and kinetics in Mg (In)–MgF_2 composite directly synthesized by plasma milling. J. Alloy Compd. 2014, 586, 113-117.

[18] H. Zhong, L.-Z. Ouyang, J.-S. Ye, J.-W. Liu, H. Wang, X.-D. Yao, M. Zhu, An one-step approach towards hydrogen production and storage through regeneration of $NaBH_4$. Energ. Storage Mater. 2017, 7, 222-228.

[19] W. Chen, L.Z. Ouyang, J.W. Liu, X.D. Yao, H. Wang, Z.W. Liu, M. Zhu, Hydrolysis and regeneration of sodium borohydride ($NaBH_4$)–a combination of hydrogen production and storage. J. Power Sources 2017, 359, 400-407.

[20] X.-D. Kang, J.-H. Luo, P. Wang, Efficient and highly rapid hydrogen release from ball-milled $3NH_3BH_3/MMgH_3$ (M = Na, K, Rb) mixtures at low temperatures. Int. J. Hydrogen Energ. 2012, 37, 4259-4266.

[21] A.-L. Chaudhary, M. Paskevicius, D.A. Sheppard, C.E. Buckley, Thermodynamic destabilization of MgH_2 and $NaMgH_3$ using Group IV elements Si, Ge or Sn. J. Alloy Compd. 2015, 623, 109-116.

[22] R. Martínez-Coronado, J. Sánchez-Benítez, M. Retuerto, M.T. Fernández-Díaz, J.A. Alonso, High-pressure synthesis of $Na_{1-x}Li_xMgH_3$ perovskite hydrides. J. Alloy Compd. 2012, 522, 101-105.

[23] H. Shao, K. Asano, H. Enoki, E. Akiba, Preparation and hydrogen storage properties of nanostructured Mg–Ni BCC alloys. J. Alloy Compd. 2009, 477, 301-306.

[24] L.Z. Ouyang, Z.J. Cao, H. Wang, J.W. Liu, D.L. Sun, Q.A. Zhang, M. Zhu, Dual-tuning effect of in on the thermodynamic and kinetic properties of Mg_2Ni dehydrogenation. Int. J. Hydrogen Energ. 2013, 38, 8881-8887.

[25] M. Zhu, H. Wang, L.Z. Ouyang, M.Q. Zeng, Composite structure and hydrogen storage properties in Mg-base alloys. Int. J. Hydrogen Energ. 2006, 31, 251-257.

[26] L.-Z. Ouyang, X.-S. Yang, M. Zhu, J.-W. Liu, H.-W. Dong, D.-L. Sun, J. Zou, X.-D. Yao, Enhanced hydrogen storage kinetics and stability by synergistic effects of in situ formed $CeH_{2.73}$ and Ni in $CeH_{2.73}$-MgH_2-Ni nanocomposites. J. Phys. Chem. C 2014, 118, 7808-7820.

[27] N. Kunkel, A. Meijerink, M. Springborg, H. Kohlmann, Eu (ii) luminescence in the perovskite host lattices $KMgH_3$, $NaMgH_3$ and mixed crystals $LiBa_xSr_{1-x}H_3$. J. Mater. Chem. C 2014, 2, 4799.

[28] Y. Li, X. Ding, F. Wu, D. Sun, Q. Zhang, F. Fang, Enhancement of hydrogen storage in destabilized $LiNH_2$ with $KMgH_3$ by quick conveyance of N-containing species. J. Phys. Chem. C 2016, 120, 1415-1420.

[29] Y. Li, L. Zhang, Q. Zhang, F. Fang, D. Sun, K. Li, H. Wang, L. Ouyang, M. Zhu, In situ embedding of Mg_2NiH_4 and YH_3 nanoparticles into bimetallic hydride $NaMgH_3$ to inhibit phase segregation for enhanced hydrogen storage. J. Phys. Chem. C 2014, 118, 23635-23644.

[30] Z.-m. Wang, J.-j. Li, S. Tao, J.-q. Deng, H. Zhou, Q. Yao, Structure, thermal analysis and dehydriding kinetic properties of $Na_{1-x}Li_xMgH_3$ hydrides. J. Alloy Compd. 2016, 660, 402-406.

[31] J.A. Teprovich, D.A. Knight, B. Peters, R. Zidan, Comparative study of reversible hydrogen storage in alkali-doped fulleranes. J. Alloy Compd. 2013, 58, S364-S367.

[32] W. Liu, K.-F. Aguey-Zinsou, Hydrogen storage properties of in-situ stabilised magnesium nanoparticles generated by electroless reduction with alkali metals. Int. J. Hydrogen Energ. 2015, 40, 16948-16960.

[33] X.-B. Xiao, B.-Y. Tang, S.-Q. Liao, L.-M. Peng, W.-j. Ding, Thermodynamic and electronic properties of quaternary hydrides $Li_xNa_{1-x}MgH_3$. J. Alloy Compd. 2009, 474, 522-526.

[34] S. Tao, Z.-m. Wang, Z.-z. Wan, J.-q. Deng, H. Zhou, Q. Yao, Enhancing the dehydriding properties of perovskite-type $NaMgH_3$ by introducing potassium as dopant. Int. J. Hydrogen Energ. 2017, 42, 3716-3722.

[35] D. Duan, X. Huang, F. Tian, D. Li, H. Yu, Y. Liu, Y. Ma, B. Liu, T. Cui, Pressure-induced decomposition of solid hydrogen sulfide. Phys. Rev. B 2015, 91, 180502(R).

[36] A. Shamp, T. Terpstra, T. Bi, Z. Falls, P. Avery, E. Zurek, Decomposition products of phosphine under pressure: PH_2 stable and superconducting? J. Am. Chem. Soc. 2016, 138, 1884-1892.

[37] M.-y. Yan, F. Sun, X.-p. Liu, J.-h. Ye, Effects of compaction pressure and graphite content on hydrogen storage properties of Mg $(NH_2)_2$–2LiH hydride. Int. J. Hydrogen Energ. 2014, 39, 19656-19661.

[38] L.-Z. Ouyang, S.-Y. Ye, H.-W. Dong, M. Zhu, Effect of interfacial free energy on hydriding reaction of Mg–Ni thin films. Appl. Phys. Lett. 2007, 90, 021917.

[39] C. Wolverton, V. Ozoliņš, First-principles aluminum database: Energetics of binary Al alloys and compounds. Phys. Rev. B 2006, 73, 144104.

[40] P.E. Blöchl, Projector augmented-wave method. Phys. Rev. B 1994, 50, 17953.

[41] G. Kresse, J. Furthmüller, Efficiency of ab-initio total energy calculations for metals and semiconductors using a plane-wave basis set. Comp. Mater. Sci. 1996, 6, 15-50.

[42] J.P. Perdew, K. Burke, M. Ernzerhof, Generalized gradient approximation made simple. Phys. Rev. Lett. 1996, 77, 3865.

[43] H. Mokhorst, J. Pack, Special points for Brillouin-zone integrations. Phys. Rev. B 13 1976, 13, 5188-5192.

[44] H.-H. PARK, M. Pezat, B. Darriet, P. Hagenmuller, The KH-MgH_2 system. Revue de chimie minérale 1987, 24, 525-530.

[45] M.P. H.-H. Park, B. Darriet, P. Hagenmuller, J. Less Common Metals 1987, 136, 1.

[46] T. Sato, D. Noréus, H. Takeshita, U. Häussermann, Hydrides with the perovskite structure: General bonding and stability considerations and the new representative $CaNiH_3$. J. Solid State Chem. 2005, 178, 3381-3388.

[47] P. Vajeeston, P. Ravindran, A. Kjekshus, H. Fjellvåg, First-principles investigations of the $MMgH_3$ (M = Li, Na, K, Rb, Cs) series. J. Alloy Compd. 2008, 450, 327-337.

[48] A. Klaveness, O. Swang, H. Fjellvåg, Formation enthalpies of $NaMgH_3$ and $KMgH_3$: A computational study. EPL 2006, 76, 285.

[49] O.I. Velikokhatnyi, P.N. Kumta, Energetics of the lithium-magnesium imide–magnesium amide and lithium hydride reaction for hydrogen storage: An ab initio study. Mat. Sci. Eng. B 2007, 140, 114-122.

[50] S.V. Alapati, J.K. Johnson, D.S. Sholl, Identification of destabilized metal hydrides for hydrogen storage using first principles calculations. J. Phys. Chem. B 2006, 110, 8769-8776.

[51] L. Hector Jr, J. Herbst, W. Wolf, P. Saxe, G. Kresse, Ab Initio thermodynamic and elastic properties of alkaline-earth metals and their hydrides. Phys. Rev. B 2007, 76, 014121.

[52] X. Ke, I. Tanaka, Decomposition reactions for $NaAlH_4$, Na_3AlH_6, and NaH: First-principles study. Phys. Rev. B 2005, 71, 024117.

[53] G. Wu, J. Zhang, Q. Li, Y. Wu, K. Chou, X. Bao, Dehydrogenation kinetics of magnesium hydride investigated by DFT and experiment. Comp. Mater. Sci. 2010, 49, S144-S149.

[54] J. Liang, Theoretical insight on tailoring energetics of Mg hydrogen absorption/desorption through nano-engineering. Appl. Phys. A 2005, 80, 173-178.

[55] J. Bastide, A. Bouamrane, P. Claudy, Elaboration d'hydrures doubles de magnesium et de potassium par réaction entre solides. J. Less Common Metals 1987, 136, L1-L4.

[56] R. Schumacher, A. Weiss, $KMgH_3$ single crystals by synthesis from the elements. J. Less Common Metals 1990, 163, 179-183.

CHAPTER 5. Hydrogen release of $LiBH_4$(010) surface with strain and dopants (M = Na, K, Al, F, or Cl)

5.1. Introduction

With the increasing energy crisis and environmental issues, exploiting alternative clean energy is becoming increasingly urgent. In recent years, hydrogen energy has been a key research subject for replacing fossil fuels owing to its high energy density, rich reserves, and virtually no pollution [1]. On the other hand, despite hydrogen being an ideal renewable energy source, effective hydrogen storage is still a problem that limits its practical applications [2]. Compared to conventional storage methods, metals and complex hydrides can store hydrogen effectively and safely under moderate conditions [3]. The complex metal hydrides are attractive hydrogen storage media [4]. For example, lithium borohydride ($LiBH_4$) has excellent properties for hydrogen storage because it is lightweight (21.78 g/mol) and the gravimetric/volumetric hydrogen densities are high [5-8]. Nevertheless, high temperatures (> 400 ℃) are needed for hydrogen desorption due to its stable structure [9, 10]. For $LiBH_4$, the combination of ionic and covalent bonding results in high thermodynamic stability [11]. Therefore, weakening the B-H bond strength can be a key idea to promoting hydrogen release.

Several physical and chemical means have been explored to overcome the deficiency of thermodynamics and improve the dehydrogenation of $LiBH_4$. Among various physical methods, the strain and pressure can be used to facilitate hydrogen release for metal hydrides [12-14]. Using first-principles calculations, Hussain et al. observed that dehydrogenation energies of the system were reduced due to destabilization of the MgH_2(001) surface by strain and introducing dopants, such as Al, Si, and Ti to the system [15]. In the authors' previous

work, pressure was used to enhance the hydrogen release in $KMgH_3$ [16]. Hao et al. [17] found that the strain produced by TiH_2 (111) substrates on MgH_2 in the interface of MgH_2/TiH_2 lowers the enthalpy of dehydrogenation reactions.

In addition, chemical methods, including catalyst modification [18-20], destabilization using various reactive additives [21-24], and nano-confinement with mesoporous scaffolds or other nanomaterials [25-27] have been proven to be significant for promoting the desorption of a hydrogen molecule. The destabilization approaches have been employed widely for hydrides due to the significant improvement in hydrogen desorption. Specifically, metals, hydrides, oxides, and metal halides have been used as efficient additives for destabilization [28-30]. In earlier research, MgH_2, as a representative destabilizing additive, was practically employed to reduce the enthalpy of hydrogenation and dehydrogenation of $LiBH_4$ by 25 kJ/mol H_2 [31]. Zhou et al. [32] found the destabilization of $LiBH_4$ with respect to de/hydrogenation by the mechanochemical reactions of MgH_2 and LaH_3. A composite of $LiBH_4$-0.083La_2Mg_{17} exhibited high hydrogen desorption amounts of ~6.8 wt. % and a reversible operating temperature of below 400 ℃. In addition, the dehydrogenation of $LiBH_4$ was enhanced by doping synthesized mesoporous Ni and Co-based oxide nanorods [33]. They suggested that $LiBH_4$-$NiCo_2O_4$ composites have a lower hydrogen desorption temperature and higher dehydrogenation kinetics than those of pure $LiBH_4$ [33]. In previous theoretical calculations, Al doping of $LiBH_4$ was found to destabilize the structure and decrease the energy for dehydrogenation owing to the weaker B-H covalent bonding interactions [34]. All these studies show that the destabilization of metal hydrides is a practical approach for tuning the hydrogen release of $LiBH_4$. Nevertheless, further studies will be needed to fulfill the requirements for the practical applications of $LiBH_4$ to hydrogen storage.

For most hydrides, the surface properties are very significant for dehydrogenation processes [35-37]. For $LiBH_4$ with an orthorhombic structure, the (010) surface was found to be the most stable among the other low-index surfaces according to previous density functional theory (DFT) calculations [38].

Taking all the above into consideration, the changes in hydrogen release of the $LiBH_4$(010) surface with biaxial strain (-3% − +3%) and five dopants were investigated theoretically. Here, the $LiBH_4$(010) surface was chosen because it has the lowest surface energy of 0.110 J/m^2 compared to the other low-index surfaces [38]. Na, K, Al, F, or Cl were employed as modification additives to improve structural/electronic properties of the materials. The dehydrogenation performance of $NaMgH_3$ hydrides was improved by the K dopant [39]. For the MgH_2(110) surface, Al weakens the Mg-H interactions to improve the dehydrogenation properties [40]. In addition, doping with F or Cl atoms also can be helpful for the hydrogen desorption of Mg_2NiH_4 hydride [41]. Therefore, Na, K, Al, F, or Cl were introduced to the $LiBH_4$(010) surface as dopants for improving the hydrogen release in this work. Furthermore, the electronic properties, such as the density of states (DOS) were analyzed further to determine the influences of the dopants on hydrogen release.

5.2. Computational details

The DFT calculations were conducted using the Vienna ab initio simulation package (VASP) [42,43] implementing projector augmented wave (PAW) methods with the generalized gradient approximation (GGA) functional of Perdew-Burke-Ernzerhof (PBE) [44, 45]. A dipole correction was employed [46]. The Grimme's dispersion corrections (D3) method [47] was also incorporated into the DFT calculations. The $LiBH_4$(010) surface with 6

layers was constructed based on the optimized $LiBH_4$ bulk system. A 15 Å vacuum space was included. The top four (bottom two) layers were relaxed (fixed) out of total layers. The 6 × 8 × 6 and 6 × 6 × 1 Monkhorst-Pack k-points [48] were employed for the $LiBH_4$ bulk and (010) surface systems, respectively. The kinetic energy cutoff was 600 eV. The difference in the total energy in all iterative loops was $<10^{-5}$ eV. Using conjugate gradient algorithms, the relaxation processes were conducted until the forces were below 10^{-2} eVÅ^{-1}.

5.3. Results and discussion

5.3.1. Structure and optimization

The lattice parameters obtained by DFT calculations in the P*nma* phase of $LiBH_4$ were a = 7.299 Å, b = 4.382 Å, and c = 6.584 Å, which are similar to the other experimental and theoretical results [7, 33, 49, 50] (Table 5.1). The top four layers of $LiBH_4$(010) surface were relaxed (Fig. 5.1 (a)). The average distance of the B-H bonds was 1.225 Å, which is similar to the range of 1.04 − 1.28 Å and 1.21 − 1.24 Å found in the experiment [49] and calculations [51], respectively. In addition, the surface energy of the $LiBH_4$(010) surface of 0.120 J m^{-2} is comparable to the results found in the literature: 0.119 J m^{-2} [52] and 0.112 J m^{-2} [53]. Dopants (M) including Na, K, Al, F, or Cl were introduced to the top layer of the $LiBH_4$(010) surface. Na or K was doped at the Li site of the top layer, Al was doped at the B-site, and F or Cl were introduced to the hydrogen site of the top layer of the $LiBH_4$(010) surface. The structural stabilities were then investigated based on these doped $LiBH_4$ surfaces. Fig. 5.1 (b) - (f) present the relaxed (010) surfaces of the Na, K, F, Cl, and Al-doped $LiBH_4$, respectively. Table 5.2 lists the mean B-H bond lengths of each system. The average distances of B-H bonds of the doped structures were relatively unchanged except for the Al-doped $LiBH_4$

Table 5.1. Lattice parameters (Å) of the optimized $LiBH_4$ bulk system.

Lattice constants	Calc.	Expt.[49]	Expt. [7]	Other Calc.[33]	Other Calc.[50]
A	7.299	7.179	7.173	7.256	7.248
B	4.382	4.437	4.434	4.398	4.391
C	6.584	6.803	6.798	6.727	6.606

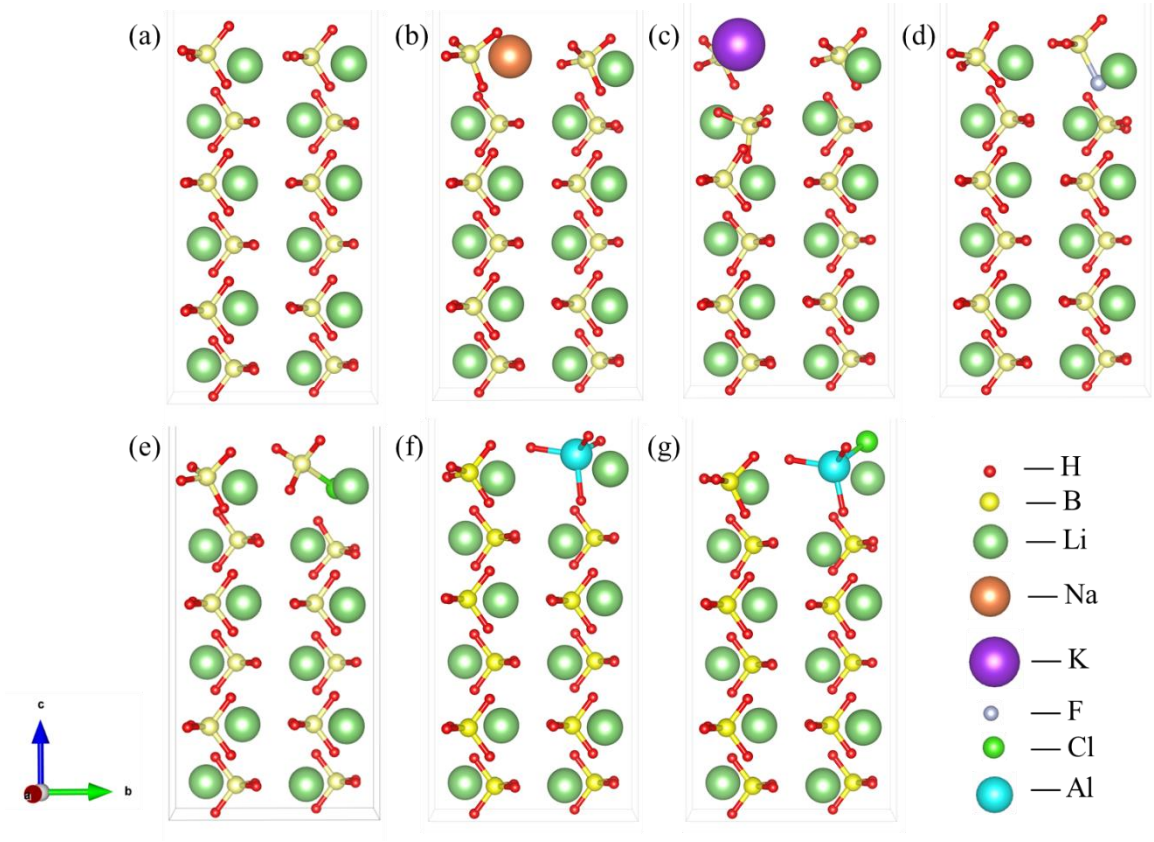

Figure 5.1. Relaxed (010) surfaces of (a) $LiBH_4$, (b) - (g) Na, K, F, Cl, Al-doped, and (Al, Cl)-codoped $LiBH_4$, respectively.

Table 5.2. Average bond lengths (Å) of B-H[a] and relative formation energies (eV) of introducing dopants M (M = Na, K, Al, F, or Cl) to the $LiBH_4$(010) surface.

Systems	Average bond lengths (Å)	Formation energies (eV)
$LiBH_4$	1.225	0
Na-doped $LiBH_4$	1.228	0.696
K-doped $LiBH_4$	1.230	0.428
Al-doped $LiBH_4$	1.428	4.185
F-doped $LiBH_4$	1.225	-2.653
Cl-doped $LiBH_4$	1.223	-0.823

[a]Here, for Al-doped $LiBH_4$, Al-H bond lengths are also included.

system. To assess the stability of the optimized structures, the formation energies (E_f) of each system were calculated using the following equation [54]:

$$E_f = E_{doped} - (E_{undoped} + E_M - E_{replaced}) \quad (1)$$

where E_{doped} and $E_{undoped}$ represent the total energies of doped and undoped systems, respectively. E_M and $E_{replaced}$ are the DFT total energies per atom of the corresponding dopants M (M = Na, K, Al, F, or Cl) and the replaced atoms (Li, B, or H), respectively. Table 5.2 lists the relative formation energies for introducing dopants. This shows that the Na, K, or Al (F or Cl)-doped $LiBH_4$(010) surface systems have higher (lower) formation energies than the $LiBH_4$ system without dopants. Among these systems, the Al-doped $LiBH_4$ system shows the highest formation energy, suggesting that introducing the Al dopant to $LiBH_4$ requires the highest energy. Similar calculated positive formation energies were observed in Ca-Doped $LiBH_4$ [55]. Although Ca-doped $LiBH_4$ shows positive formation energies, this material can be prepared with pressure and temperature [56]. The high formation energy also represents the low stability of the structure [57]. For the Al-doped $LiBH_4$ system, the average distance of the B-H bonds (1.428 Å) was larger than that of the pure structure. This destabilization may weaken the B-H bonds and be helpful in releasing a hydrogen molecule from $LiBH_4$ hydrides.

5.3.2. Hydrogen desorption

To make further investigations of the dehydrogenation performance of dopant-free and M-doped systems, the desorption energy of a hydrogen molecule was calculated using the following equation [53]:

$$E_D = E_{final} + E_{H_2} - E_{initial} \quad (2)$$

where E_{final} and $E_{initial}$ refer to the total energies of optimized structures after releasing a hydrogen molecule and the energies of optimized structures without hydrogen release, respectively. For $LiBH_4$ and $NaAlH_4$, the release of hydrogen molecules tends to occur in surface layers [37, 58]. This shows that the surface properties of a top layer play vital roles on the dehydrogenation process of $LiBH_4$ hydride. Therefore, this study examined all possible cases that release a hydrogen molecule from $[BH_4]^-$ clusters on the top layers of all doped $LiBH_4$(010) surfaces. A hydrogen molecule can be released in two ways. First, two H atoms can be removed from a single $[BH_4]^-$ complex in the top layer (Fig. 5.2 (a)). Second, two hydrogen atoms from two nearest $[BH_4]^-$ complexes in the top layer can be released (Fig. 5.2 (b)). The energy required to remove a H_2 molecule from two nearest $[BH_4]^-$ groups in the top layer of $LiBH_4$(010) surface was found to be 2.225 eV lower than that from the same $[BH_4]^-$ group, indicating that the two hydrogen atoms tend to be released from different $[BH_4]^-$ groups in the top layer. Therefore, this study focused on this second approach to release a hydrogen molecule.

5.3.3. Strain effect on hydrogen desorption

To determine how strain affects hydrogen release from the $LiBH_4$(010) surface, mechanical strains (ε) ranging from -3% to +3% were applied to the optimized structure along the biaxial direction. The strain was calculated using equation (3) [59]:

$$\varepsilon(\%) = \frac{a - a_0}{a_0} \times 100\% \quad (3)$$

where a and a_0 represent the lattice constants of strain-applied $LiBH_4$(010) surface and the surface without strain, respectively. Fig. 5.3 shows the desorption energies of a hydrogen molecule from the strain-applied $LiBH_4$(010) surface. The desorption energies decreased with increasing applied strain. This trend is similar to the hydrogen desorption energies calculated from the MgH_2(001) surface with applied strain [15]. Under a tensile strain (1% − 3%), the reduced hydrogen desorption energies were observed, indicating that tensile strain can be utilized practically to promote the hydrogen release of $LiBH_4$. After the application of 3% tensile strain, the average B-H bond length in the top layer was elongated by approximately 0.002 Å compared to the system without strain. This suggests that the applied tensile strain increases the bond lengths of boron and hydrogen, resulting in weak B-H bond energies. Therefore, tensile strain can be used to promote the dehydrogenation of $LiBH_4$.

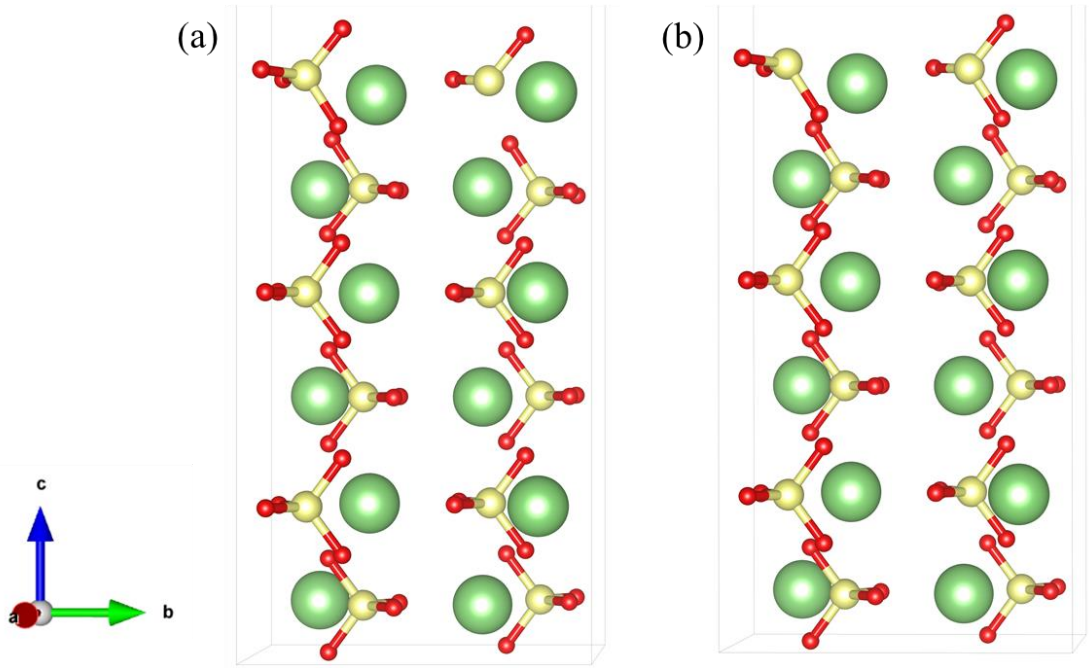

Figure 5.2. Examples of a hydrogen molecule released from: (a) a single $[BH_4]^-$ complex and (b) two nearest $[BH_4]^-$ complexes in the top layer of $LiBH_4(010)$ surface.

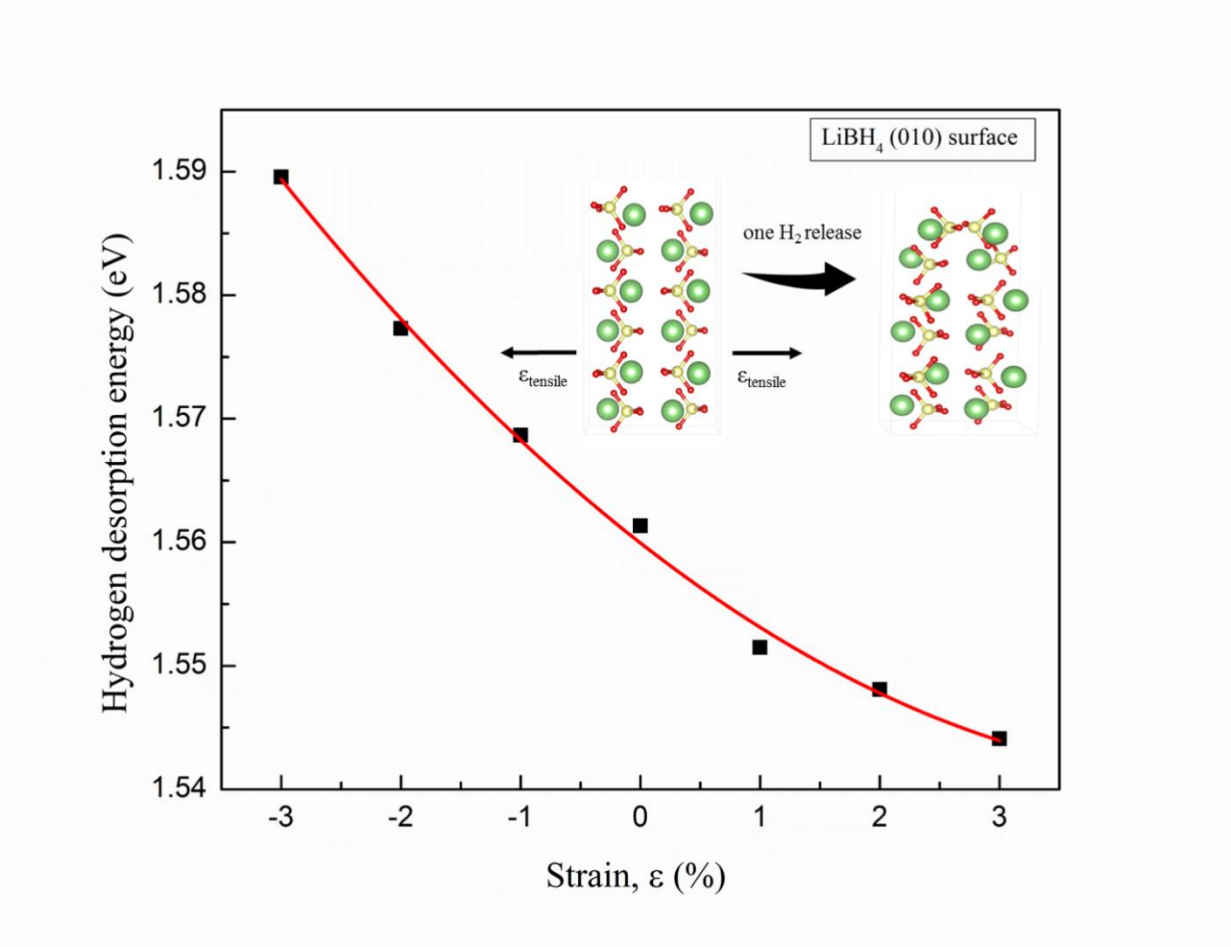

Figure 5.3. Changes in hydrogen desorption energy by the biaxial strain on the $LiBH_4$(010) surface.

To further explore how strain affects hydrogen release from the $LiBH_4$(010) surface, the partial density of states (PDOS) of this system without and with 3% strain were compared, as shown in Fig. 5.4. The electron states (-2.83 − 0 eV) of $LiBH_4$(010) surface without strain are affected mostly by the B-*p* state and H-*s* state (Fig. 5.4 (a)). The hybridization of the *p* orbital of B and *s* orbital of H demonstrates the strong covalent interactions of B with H atoms. This may explain the difficult hydrogen desorption from $LiBH_4$ hydrides. The electron states of B-*p* and H-*s* become smaller after the tensile strain was applied, showing reduced interactions of boron with hydrogen atoms as depicted in Fig. 5.4 (b). Therefore, the application of strain facilitates hydrogen desorption from $LiBH_4$ hydrides by reducing the B-H bond energies.

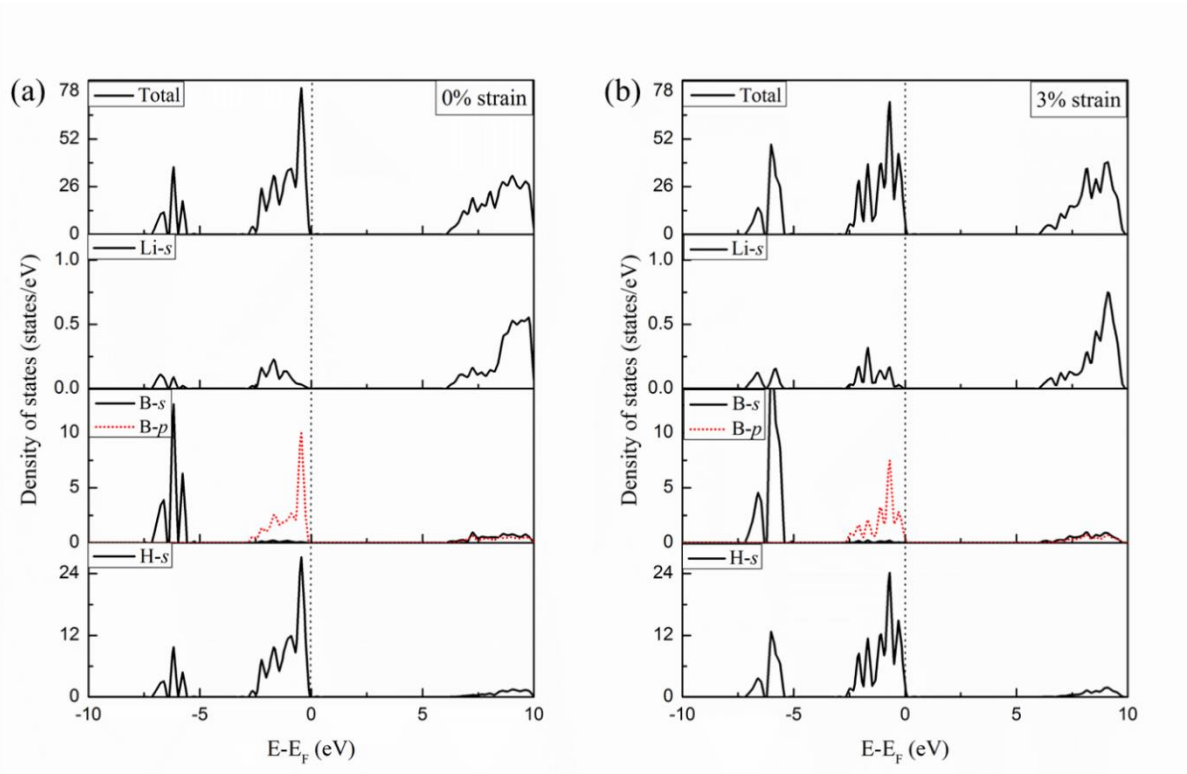

Figure 5.4. Density of states (DOS) of $LiBH_4$(010) surface with (a) 0% strain and (b) 3% strain.

5.3.4. Destabilization for hydrogen desorption

The destabilization of $LiBH_4$ using five dopants, M (M = Na, K, Al, F or Cl), was made to explore the hydrogen release performance of doped systems. The calculated hydrogen desorption energies with and without DFT-D3 methods were compared (Fig. 5.5). All hydrogen desorption energies with DFT-D3 methods were higher (0.067 ~ 0.232 eV) than the results without D3 corrections. For a dopant-free $LiBH_4$(010) surface, all configurations showed similar desorption energies. The lowest hydrogen desorption energy using DFT-D3 methods was found in $LiBH_4$(010) surface to be 1.561 eV, which is higher than the 1.29 eV reported in the literature [53]. After removing a hydrogen molecule from the $LiBH_4$(010) surface, a B_2H_6 cluster is formed. The formation of a B_2H_6 cluster has been reported [60]. For doped systems, with the exception of K-doped $LiBH_4$, all hydrogen desorption energies were lower than those of the dopant-free $LiBH_4$(010) surface, indicating that Na, Al, F, or Cl can be helpful dopants for releasing a hydrogen molecule from $LiBH_4$ hydride. Among the various doped systems, Al-doped $LiBH_4$ showed the lowest desorption energy of the hydrogen molecule as 1.151 eV. On the other hand, the incorporation of Al is energetically unfavorable due to the high formation energy. For practical applications of Al-doped $LiBH_4$, the energy cost needs to be reduced. The ranking of dopants for hydrogen desorption of $LiBH_4$ was Al > Cl > F > Na > K.

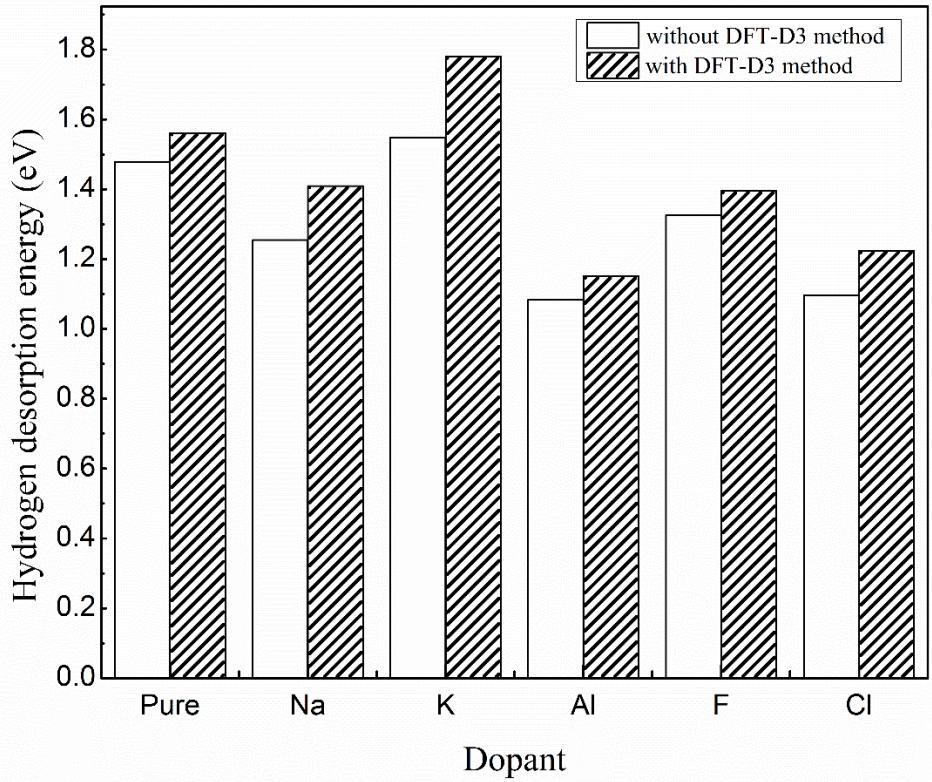

Figure 5.5. Hydrogen desorption energies in a dopant-free and doped $LiBH_4$(010) surface with and without the DFT-D3 method.

Interestingly, the hydrogen desorption energy of the Cl-doped $LiBH_4$ system was only 0.07 eV higher than that of Al-doped $LiBH_4$. This shows that excellent hydrogen desorption performance can be achieved using both Al-doped and Cl-doped systems. Wu et al. [61] enhanced the dehydrogenation of $Mg(BH_4)_2$ *via* Ni and N partial codoping methods. In the present work, as each Al and Cl dopant plays a good role in promoting the dehydrogenation process from the $LiBH_4$(010) surface, these two dopants were codoped on the surface to explore the changes in the hydrogen release properties. All possible cases of (Al, Cl)-codoped structures were considered. Fig. 5.1 (g) shows the optimized (Al, Cl)-codoped $LiBH_4$. Here, the average bond length of B-H is 1.495 Å, which is 0.067 Å larger than that of Al-doped $LiBH_4$. This means the (Al, Cl)-codoping has a better effect of destabilization compared to Al single doping. In addition, the formation energy of (Al, Cl)-codoped was calculated to be 2.256 eV using equation (1). This co-doped system showed a lower formation energy than Al-doped $LiBH_4$ by 1.929 eV, indicating that this co-doped system is easier to form than introducing an Al or Cl single dopant to the system. To understand how codoping of Al and Cl affects the dehydrogenation process of $LiBH_4$(010) surface, the desorption energy of a hydrogen molecule from (Al, Cl)-codoped $LiBH_4$ was calculated using equation (2). The lowest energy for hydrogen desorption obtained in this (Al, Cl)-codoped system was 1.003 eV, indicating that (Al, Cl)-codoping is most favorable for the dehydrogenation of $LiBH_4$(010) surface. After releasing a hydrogen molecule, a complex BH_3-AlH_2Cl exists in the optimized system. This also proves that the two H atoms constituting a H_2 molecule are released from two clusters of $[BH_4]^-$. Similar results were found in the Fe_2O_3 cluster-doped $LiBH_4$(001) surface for hydrogen release [37].

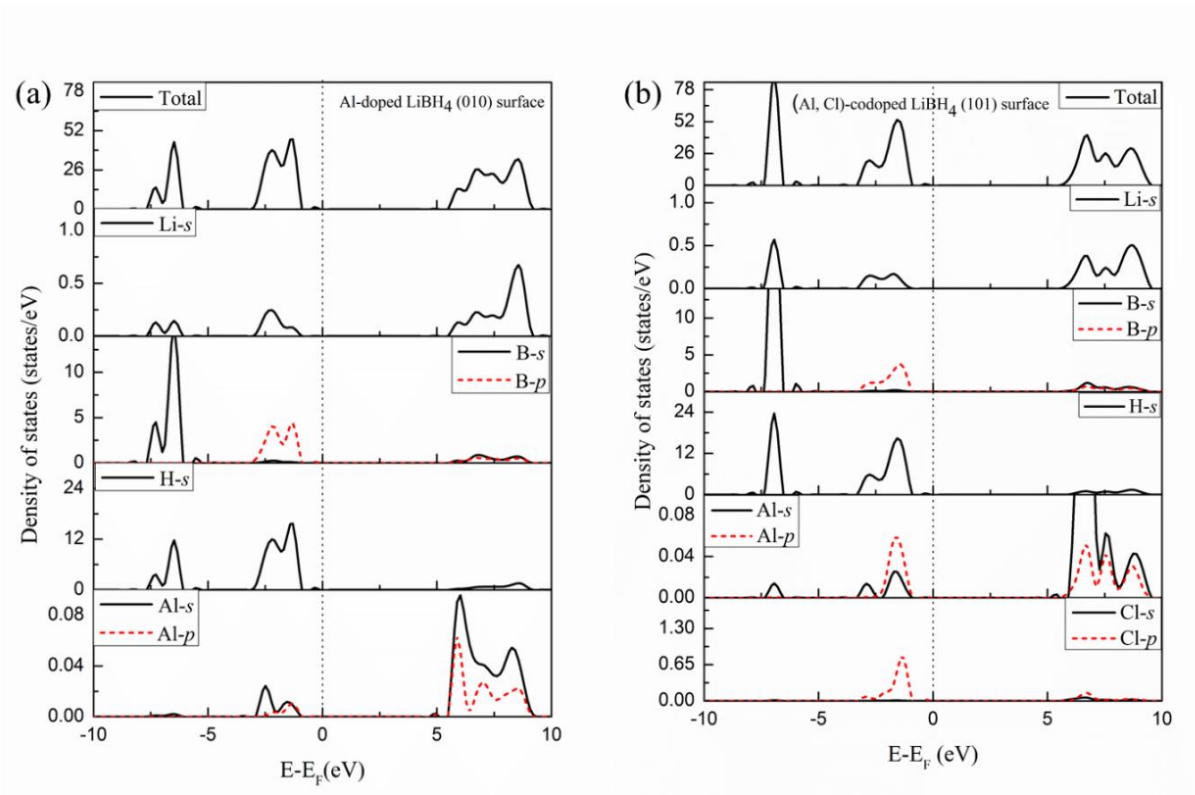

Figure 5.6. Density of states (DOS) of (a) Al-doped and (b) (Al, Cl)-codoped $LiBH_4$(010) surfaces.

To determine the influence of (Al, Cl)-codoping on hydrogen release from the $LiBH_4$(010) surface, the density of states (DOS) of Al-doped and (Al, Cl)-codoped systems were compared, as shown in Fig. 5.6. An analysis of the atomic charge was also conducted using Bader charge methods [62]. Fig. 5.7 (a) - (c) shows the calculated atomic charges on the top layer of the dopant-free, Al-doped and (Al, Cl)-codoped systems, respectively. Moreover, the relevant bond orders [63, 64] are obtained from the Density Derived Electrostatic and Chemical (DDEC) approach, shown in Table 5.3. For Al-doped $LiBH_4$, there are clear orbital hybridizations of B-*p*, H-*s*, and Al-*s* states below the Fermi level (-3.1 − 0 eV), as depicted in Fig. 5.6 (a). Compared to the PDOS of the dopant-free $LiBH_4$(010) surface (Fig. 5.4 (a)), the orbital overlaps (-3.1 − -0.9 eV) of B-*p* and H-*s* clearly decrease after the introduction of Al, showing that the bond strength of B-H is reduced by introducing an Al atom. According to Bader charge analysis, the hydrogen atoms around boron lose electrons by 0.01*e* after introducing Al to the $LiBH_4$(010) surface (Fig. 7 (b)). By bond orders analysis, the average bond order of H atoms and B in Al-doped system is lower 0.009 than that in dopant-free system. It demonstrates that the bond strength of boron and hydrogen becomes weaker in Al-doped system. Therefore, it is beneficial for facilitating the release of a hydrogen molecule from $LiBH_4$ with Al dopant. Fig. 5.6 (b) shows that the overlaps (-3.3 − -0.8 eV) of B-*p* and H-*s* states in the (Al, Cl)-codoped $LiBH_4$ become slightly smaller than that of the Al-doped $LiBH_4$ structure. This shows weaker B-H bond strengths in the (Al, Cl)-codoped system. Compared to Al-doped $LiBH_4$, the Al-*p* state was enhanced clearly after introducing Cl. The (Al, Cl)-codoped structure showed a smaller peak value of the total DOS (-3.4 − -0.8 eV) than the Al-doped $LiBH_4$ system, indicating weak interactions among these atoms of Li, B, and H. The average charge of H atoms around B in the Al-doped ((Al, Cl)-codoped) system is -0.618*e*

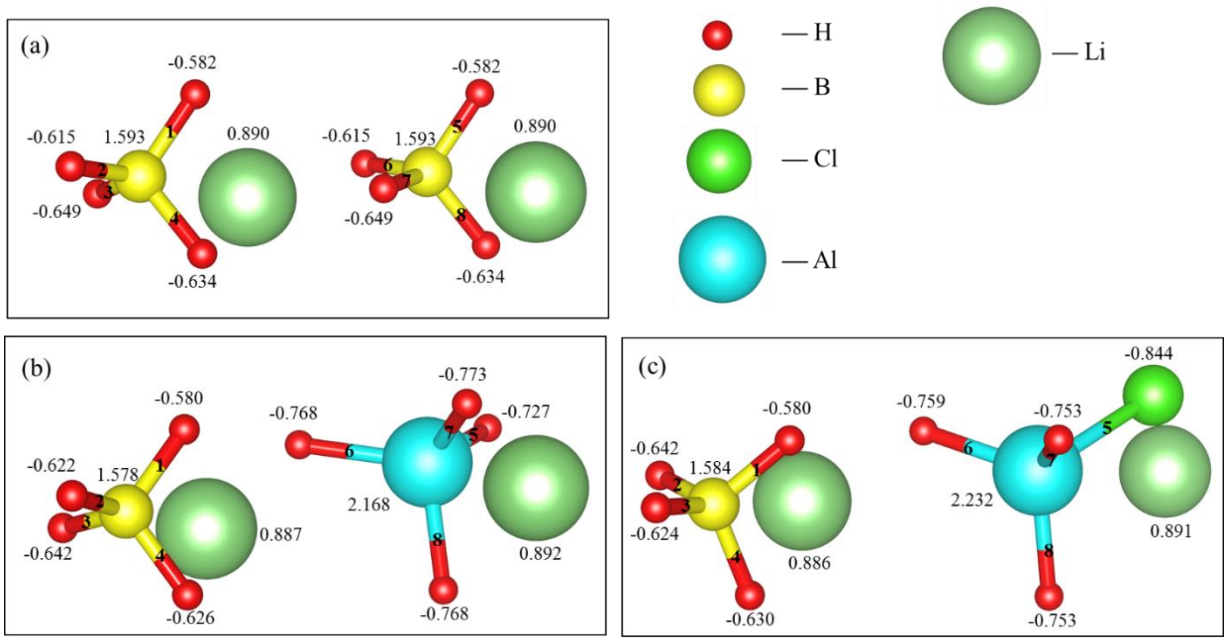

Figure 5.7. Calculated Bader atomic charges (l*e*l) on the top layer of (a) dopant-free, (b) Al-doped and (c) (Al, Cl)-codoped systems [a].

[a] Here, the numbers (1-8) annotated on the bonds are used for the analysis of bond orders.

Table 5.3. Bond orders on the top layer of dopant-free, Al-doped and (Al, Cl)-codoped systems. Here, the numbers (1-8) are corresponding to the annotation in Fig. 5.7.

(-0.619*e*) (Fig. 5.7 (b)-(c)), indicating that the effect of Cl dopant on the charges of hydrogen atoms around boron is not significant. However, after introducing Cl to the Al-doped $LiBH_4$(010) surface, both Al dopant and the H atoms around Al dopant lose electrons by 0.064*e* and 0.004*e*, respectively. These charges can weaken the interactions of aluminum and hydrogen atoms. Furthermore, the average bond order of Al and H atoms in the (Al, Cl)-codoped system (0.721) is obviously lower than that of in the Al-doped system (0.757). It also proves that the bond strength of Al and H atoms is weaker in the (Al, Cl)-codoped system. Similar results can be found in the Mg-doped $LiBH_4$ system [65]. Therefore, Al and Cl are practical dopants for promoting the dehydrogenation processes of $LiBH_4$ hydrides.

5.4. Conclusions

Several ways to enhance the release of a hydrogen molecule from the $LiBH_4$(010) surface were investigated by DFT modeling through the introduction of a wide range of strains and various dopants. The release of two hydrogen atoms from different $[BH_4]^-$ groups in the top layer were preferred over that from a single $[BH_4]^-$ group. Hydrogen desorption was facilitated by tensile strain, which weakens the interactions of B with H atoms. On the other hand, dopants, M (M = Na, K, Al, F, or Cl) were introduced at the topmost layer of the $LiBH_4$(010) system. The Al dopant showed the highest performance for releasing a hydrogen molecule with the lowest energy required for hydrogen desorption of 1.151 eV. The dopant ranking of promoting hydrogen desorption from $LiBH_4$ was Al > Cl > F > Na > K. Moreover, (Al, Cl)-codoped $LiBH_4$ showed the lower formation energy than Al-doped $LiBH_4$ and the lowest hydrogen desorption energy among the other doped systems. This shows that the destabilization of (Al, Cl)-codoping method can effectively facilitate dehydrogenation

processes from $LiBH_4$ hydrides. Overall, strain and dopants can be utilized as efficient means for the design of highly promising hydride-based hydrogen storage materials.

Reference

[1] S. Niaz, T. Manzoor, A.H. Pandith, Hydrogen storage: Materials, methods and perspectives. Renew. Sust. Energ. Rev. 2015, 50, 457-469.

[2] L. Schlapbach, A. Züttel, Hydrogen-storage materials for mobile applications, Materials for sustainable energy: a collection of peer-reviewed research and review articles from nature publishing group. World Scientific, U.K. 2011, 265-270.

[3] A. Züttel, Materials for hydrogen storage. Mater. Today 2003, 6, 24-33.

[4] J. Ren, N.M. Musyoka, H.W. Langmi, M. Mathe, S. Liao, Current research trends and perspectives on materials-based hydrogen storage solutions: a critical review. Int. J. Hydrogen Energ. 2017, 42, 289-311.

[5] M.B. Ley, L.H. Jepsen, Y.-S. Lee, Y.W. Cho, J.M.B. Von Colbe, M. Dornheim, M. Rokni, J.O. Jensen, M. Sloth, Y. Filinchuk, Complex hydrides for hydrogen storage–new perspectives. Mater. Today 2014, 17, 122-128.

[6] S.-i. Orimo, Y. Nakamori, J.R. Eliseo, A. Züttel, C.M. Jensen, Complex hydrides for hydrogen storage. Chem. Rev. 2007, 107, 4111-4132.

[7] A. Züttel, S. Rentsch, P. Fischer, P. Wenger, P. Sudan, P. Mauron, C. Emmenegger, Hydrogen storage properties of $LiBH_4$. J. Alloy Compd. 2003, 356, 515-520.

[8] S. Kumar, U. Jain, A. Jain, H. Miyaoka, T. Ichikawa, Y. Kojima, G. Dey, Development of Mg-Li-B based advanced material for onboard hydrogen storage solution. Int. J. Hydrogen Energ. 2017, 42, 3963-3970.

[9] A. Züttel, P. Wenger, S. Rentsch, P. Sudan, P. Mauron, C. Emmenegger, $LiBH_4$ a new hydrogen storage material. J. Power Sources 2003, 118, 1-7.

[10] C. Li, P. Peng, D. Zhou, L. Wan, Research progress in $LiBH_4$ for hydrogen storage: a review. Int. J. Hydrogen Energ. 2011, 36, 14512-14526.

[11] J.K. Kang, S.Y. Kim, Y.S. Han, R.P. Muller, W.A. Goddard III, A candidate $LiBH_4$ for hydrogen storage: Crystal structures and reaction mechanisms of intermediate phases. Appl. Phys. Lett. 2005, 87, 111904.

[12] J. Zhang, S. Yan, H. Qu, Stress/strain effects on thermodynamic properties of magnesium hydride: A brief review. Int. J. Hydrogen Energ. 2017, 42, 16603-16610.

[13] H. Benzidi, M. Lakhal, A. Benyoussef, M. Hamedoun, M. Loulidi, O. Mounkachi, First principle study of strain effect on structural and dehydrogenation properties of complex hydride $LiBH_4$. Int. J. Hydrogen Energ. 2017, 42, 19481-19486.

[14] J. Zhang, Y. Zhou, Z. Ma, L. Sun, P. Peng, Strain effect on structural and dehydrogenation properties of MgH_2 hydride from first-principles calculations. Int. J. Hydrogen Energ. 2013, 38, 3661-3669.

[15] T. Hussain, A. De Sarkar, T.A. Maark, W. Sun, R. Ahuja, Strain and doping effects on the energetics of hydrogen desorption from the MgH_2 (001) surface. EPL (Europhysics Letters) 2013, 101, 27006.

[16] Y. Li, Y. Mi, J.S. Chung, S.G. Kang, First-principles studies of $K_{1-x}M_xMgH_3$ (M= Li, Na, Rb, or Cs) perovskite hydrides for hydrogen storage. Int. J. Hydrogen Energ. 2018, 43, 2232-2236.

[17] S. Hao, D.S. Sholl, Effect of TiH_2–induced strain on thermodynamics of hydrogen release from MgH_2. J. Phys. Chem. C 2012, 116, 2045-2050.

[18] M.S. Wellons, P.A. Berseth, R. Zidan, Novel catalytic effects of fullerene for $LiBH_4$ hydrogen uptake and release. Nanotechnology 2009, 20, 204022.

[19] W. Cai, H. Wang, J. Liu, L. Jiao, Y. Wang, L. Ouyang, T. Sun, D. Sun, H. Wang, X. Yao, Towards easy reversible dehydrogenation of $LiBH_4$ by catalyzing hierarchic nanostructured CoB. Nano Energy 2014, 10, 235-244.

[20] C. Paduani, A.M. Rappe, A DFT study on the hydrogen desorption from the lithium borohydride and aluminohydride upon the addition of nanostructured carbon catalyzing agent. Int. J. Hydrogen Energ. 2017, 42, 3019-3026.

[21] X.-D. Kang, P. Wang, L.-P. Ma, H.-M. Cheng, Reversible hydrogen storage in $LiBH_4$ destabilized by milling with Al. Appl. Phys. A 2007, 89, 963-966.

[22] H. Kou, G. Sang, Y. Zhou, X. Wang, Z. Huang, W. Luo, L. Chen, X. Xiao, G. Yang, C. Hu, Enhanced hydrogen storage properties of $LiBH_4$ modified by NbF_5. Int. J. Hydrogen Energ. 2014, 39, 11675-11682.

[23] D. Liu, Q. Tan, C. Gao, T. Sun, Y. Li, Reversible hydrogen storage properties of $LiBH_4$ combined with hydrogenated $Mg_{11}CeNi$ alloy. Int. J. Hydrogen Energ. 2015, 40, 6600-6605.

[24] R.N. Muthu, S. Rajashabala, R. Kannan, Hydrogen storage performance of lithium borohydride decorated activated hexagonal boron nitride nanocomposite for fuel cell applications. Int. J. Hydrogen Energ. 2017, 42, 15586-15596.

[25] A. Gasnier, F. Gennari, Graphene entanglement in a mesoporous resorcinol–formaldehyde matrix applied to the nanoconfinement of $LiBH_4$ for hydrogen storage. RSC Adv. 2017, 7, 27905-27912.

[26] X. Meng, C. Wan, Y. Wang, X. Ju, Porous Ni@ C derived from bimetallic Metal–Organic Frameworks and its application for improving $LiBH_4$ dehydrogenation. J. Alloy Compd. 2018, 735, 1637-1647.

[27] P. Plerdsranoy, D. Kaewsuwan, N. Chanlek, R. Utke, Effects of specific surface area and pore volume of activated carbon nanofibers on nanoconfinement and dehydrogenation of $LiBH_4$. Int. J. Hydrogen Energ. 2017, 42, 6189-6201.

[28] J. Yang, A. Sudik, C. Wolverton, Destabilizing $LiBH_4$ with a metal (M= Mg, Al, Ti, V, Cr, or Sc) or metal hydride (MH_2= MgH_2, TiH_2, or CaH_2). J. Phys. Chem. C 2007, 111, 19134-19140.

[29] J.J. Vajo, G.L. Olson, Hydrogen storage in destabilized chemical systems. Scripta Mater. 2007, 56, 829-834.

[30] M. Ismail, Effect of $LaCl_3$ addition on the hydrogen storage properties of MgH_2. Energy 2015, 79, 177-182.

[31] J.J. Vajo, S.L. Skeith, F. Mertens, Reversible storage of hydrogen in destabilized $LiBH_4$. J. Phys. Chem. B 2005, 109, 3719-3722.

[32] Y. Zhou, Y. Liu, W. Wu, Y. Zhang, M. Gao, H. Pan, Improved hydrogen storage properties of $LiBH_4$ destabilized by in situ formation of MgH_2 and LaH_3. J. Phys. Chem. C 2011, 116, 1588-1595.

[33] L. Zang, Q. Zhang, L. Li, Y. Huang, X. Chang, L. Jiao, H. Yuan, Y. Wang, Improved dehydrogenation properties of $LiBH_4$ using catalytic Nickel- and Cobal- based mesoporous oxide nanorods. Chem-Asian J. 2018, 13, 99-105.

[34] J. Weiqing, C. Shilong, Effect of Al on the dehydrogenation of $LiBH_4$ from first-principles calculations. Int. J. Hydrogen Energ. 2017, 42, 6181-6188.

[35] S. Kurko, I. Milanović, J. Grbović Novaković, N. Ivanović, N. Novaković, Investigation of surface and near-surface effects on hydrogen desorption kinetics of MgH_2. Int. J. Hydrogen Energ. 2014, 39, 862-867.

[36] S. Kumar, A. Jain, S. Yamaguchi, H. Miyaoka, T. Ichikawa, A. Mukherjee, G.K. Dey, Y. Kojima, Surface modification of MgH_2 by $ZrCl_4$ to tailor the reversible hydrogen storage performance. Int. J. Hydrogen Energ. 2017, 42, 6152-6159.

[37] C. Liu, S. Huang, A first-principles study of the tuning effect of a Fe_2O_3 cluster on the dehydrogenation properties of a $LiBH_4$ (001) surface. Dalton T. 2016, 45, 10954-10959.

[38] P. Vajeeston, P. Ravindran, H. Fjellvag, Nanostructures of $LiBH_4$: a density-functional study. Nanotechnology 2009, 20, 275704.

[39] L. Wang, X. Chen, H. Du, Y. Yuan, H. Qu, M. Zou, First-principles investigation on hydrogen storage performance of Li, Na and K decorated borophene. Appl. Surf. Sci. 2018, 427, 1030-1037.

[40] F.-H. Wang, C.-L. Chang, Effect of substrate temperature on transparent conducting Al and F co-doped ZnO thin films prepared by rf magnetron sputtering. Appl. Surf. Sci. 2016, 370, 83-91.

[41] L.M. Arnbjerg, D.B. Ravnsbæk, Y. Filinchuk, R.T. Vang, Y. Cerenius, F. Besenbacher, J.-E. Jørgensen, H.J. Jakobsen, T.R. Jensen, Structure and dynamics for $LiBH_4$–LiCl solid solutions. Chem. Mater. 2009, 21, 5772-5782.

[42] G. Kresse, J. Furthmüller, Efficiency of ab-initio total energy calculations for metals and semiconductors using a plane-wave basis set. J. Comput. Mater. Sci. 1996, 6, 5-50.

[43] G. Kresse, J. Furthmüller, Efficient iterative schemes for ab initio total-energy calculations using a plane-wave basis set. Phy. Rev. *B* 1996, 54, 11169.

[44] P.E. Blöchl, Projector augmented-wave method. Phy. Rev. B 1994, 50, 17953-17979.

[45] J.P. Perdew, K. Burke, M. Ernzerhof, Generalized gradient approximation made simple. Phys. Rev. Lett. 1996, 77, 3865.

[46] G. Makov, M.C. Payne, Periodic boundary conditions in ab initio calculations. Phy. Rev. B 1995, 51, 4014-4022.

[47] S. Grimme, J. Antony, S. Ehrlich, H. Krieg, A consistent and accurate ab initio parametrization of density functional dispersion correction (DFT-D) for the 94 elements H-Pu. J. Chem. Phys. 2010, 132, 154104.

[48] H.J. Monkhorst, J.D. Pack, Special points for Brillouin-zone integrations. Phy. Rev. B 1976, 13, 5188-5192.

[49] J.P. Soulié, G. Renaudin, R. Černý, K. Yvon, Lithium boro-hydride $LiBH_4$: I. Crystal structure. J. Alloy Compd. 2002, 346, 200-205.

[50] K. Hoang, C.G. Van de Walle, Hydrogen-related defects and the role of metal additives in the kinetics of complex hydrides: A first-principles study. Phy. Rev. B 2009, 80, 214109.

[51] S. Yu, X. Ju, C. Wan, S. Li, Nb-doped $LiBH_4$(010) surface for hydrogen desorption: First-principles calculations. Int. J. Hydrogen Energ. 2015, 40, 6365-6372.

[52] Q. Ge, Structure and energetics of $LiBH_4$ and its surfaces: A first-principles study. J. Phys. Chem. A 2004, 108, 8682-8690.

[53] H.-C. Wang, X.-J. Yao, Y. Yang, B.-Y. Tang, Synergic effects of V_{Li} and Ti doping on hydrogen desorption on $LiBH_4$(010) surface: A first-principles investigation. Int. J. Hydrogen Energ. 2017, 42, 18442-18451.

[54] E. Germán, V. Verdinelli, C.R. Luna, A. Juan, D. Sholl, A Theoretical study of the effect of Zr-, Nb-doped and vacancy-like defects on H desorption on MgH_2 (110) surface. J. Phys. Chem. C 2014, 118, 4231-4237.

[55] S.H. Lee, V.R. Manga, Z.K. Liu, Effect of Mg, Ca, and Zn on stability of $LiBH_4$ through computational thermodynamics. Int. J. Hydrogen Energ. 2010, 35, 6812-6821.

[56] T. Mezaki, Y. Kuronuma, I. Oikawa, A. Kamegawa, H. Takamura, Li-Ion conductivity and phase stability of Ca-Doped $LiBH_4$ under high pressure. Inorg. Chem. 2016, 55, 10484-10489.

[57] S. Kirklin, J.E. Saal, B. Meredig, A. Thompson, J.W. Doak, M. Aykol, S. Rühl, C. Wolverton, The open quantum materials database (OQMD): assessing the accuracy of DFT formation energies. Npj Comput. Mater. 2015, 1, 15010.

[58] J. Iniguez, T. Yildirim, Hydrogen-related catalytic effects of Ti and other light transition metals on $NaAlH_4$ surfaces. J. Phys. Condens. Matter 2007, 19, 176007.

[59] J.-L. Tang, J. Zhu, W.-F. Qin, J. Xiong, Y.-R. Li, Structure and dielectric characteristics of epitaxially strained $BaTiO_3$ thin films. J. Mater. Sci-Mater. El. 2008, 19, 466-470.

[60] A.J. Du, S.C. Smith, X.D. Yao, G.Q. Lu, Role of lithium vacancies in accelerating the dehydrogenation kinetics on a $LiBH_4$(010) surface: An ab initio study. J. Phys. Chem. C 2007, 111, 12124-12128.

[61] Z. Wu, L.Y. Zhu, Z.X. Zhang, F.S. Yang, Y.Q. Wang, DFT insights into the interactive effect of Ni + N cosubstitution on enhanced dehydrogenation properties of $Mg(BH_4)(NH_2)$-like complex hydride for hydrogen energy storage. J. Phys. Chem. C 2018, 122, 5956-5966.

[62] R.F.W. Bader, A quantum theory of molecular structure and its applications. Chem. Rev. 1991, 91, 893-928.

[63] T.A. Manz, N. Gabaldon Limas, Introducing DDEC6 atomic population analysis: part 1. Charge partitioning theory and methodology. RSC Adv. 2016, 6, 47771-47801.

[64] T.A. Manz. Introducing DDEC6 atomic population analysis: part 3. Comprehensive method to compute bond orders. RSC Adv. 2017, 7, 45552-45581.

[65] X. Mo, W. Jiang, Dehydrogenation properties of $LiBH_4$ modified by Mg from first-principles calculations. J. Alloy Compd. 2018,735, 668-676.

CHAPTER 6. Conclusions

In this dissertation work, the structural and thermodynamic properties of light metal hydrides have been investigated using density functional theory (DFT) calculations. The ground state structures of 25 perovskite-type hydrides ABH_3 (alkali metals A = Li, Na, K, Rb, or Cs, alkaline-earth metals B = Be, Mg, Ca, Sr, or Ba) were obtained. The lattice parameters of all optimized structures are in agreement with the available experimental and theoretical data. Then, we investigated the most favorable dehydrogenation pathway for each ABH_3 system. By analyzing the calculated formation and reaction enthalpies, $NaCaH_3$ was found to be the most attractive ABH_3 system for hydrogen storage. To facilitate the dehydrogenation process of $NaCaH_3$, alkali dopants (Li, K, Rb, or Cs) and alkaline-earth dopants (Be, Mg, Sr, or Ba) were introduced to replace the Na and Ca sites, respectively. It is more useful doping an alkali metal at the Na site for hydrogen release than doping an alkaline-earth metal at the Ca site in $NaCaH_3$ system. For dehydrogenation processes of all doped $NaCaH_3$ systems, Cs was found to be the most beneficial dopant due to the lowest reaction enthalpy. To explore the influence of a Cs-doping at the Na site on hydrogen release, the electronic structures including atomic charges and bond order were analyzed. The bond strengths of both the Na−H and Ca−H bonds became weak after doping Cs at the Na site. Then, the reaction enthalpy for hydrogen release was reduced by the low stability of the structure with Cs doping.

$KMgH_3$, as an interesting cubic perovskite structure, the structural stability and hydrogen release properties with dopants M (M = Li, Na, Rb, or Cs) were examined using DFT calculations. The alkali dopants M were introduced at the K-sites of $KMgH_3$ and the most stable structures with different dopants were obtained. The R3*c* phase was the most stable phase among the other phases investigated in $K_{1-x}Li_xMgH_3$ (x = 0.0833 and 0.1667). On the

other hand, the Na, Rb or Cs-doped structures showed the P$m\bar{3}m$ phase as their ground state structures. Then, four possible reaction pathways to release hydrogen from M-doped $KMgH_3$ systems were considered. Among the other reaction pathways examined, the pathway (4) was found to be the most favorable one for each M-doped structure. To find the useful dopants, the reaction enthalpies of each doped system were calculated. We found that all reaction enthalpies of doped structures were lower than that of dopant-free $KMgH_3$. In particular, the $K_{1-x}Li_xMgH_3$ (x = 0.0833 and 0.1667) showed the lowest reaction enthalpies among the other doped systems. It indicates that all dopants are effective in enhancing the hydrogen release of $KMgH_3$ and Li was the most useful dopant. Moreover, the effects of pressure (0, 0.5, 1.0, 1.5, and 2 GPa) on $KMgH_3$ and $K_{1-x}Li_xMgH_3$ (x = 0.0833 and 0.1667) were also investigated. The results showed that the reaction enthalpies of $KMgH_3$ and $K_{1-x}Li_xMgH_3$ decreased with increasing applied pressure. By the analysis of the electronic structures, the Li dopant and pressure may reduce the stability of $KMgH_3$, inducing a decrease in the reaction enthalpies. Thus, suitable dopants and pressure can be used to enhance the dehydrogenation properties of $KMgH_3$.

The surface performance of hydrogen release from lithium borohydride has been made further investigation by DFT modeling. To enhance the release of a hydrogen molecule from the $LiBH_4$(010) surface, a wide range of strains (-3% - +3%) and various dopants (Na, K, Al, F, or Cl) were applied. The ground state structures of all build models were obtained. All possible cases that release a hydrogen molecule from the $LiBH_4$(010) surface were examined. The results show that the release of two hydrogen atoms from different $[BH_4]^-$ groups in the top layer were preferred over that from a single $[BH_4]^-$ group. The desorption energies of a hydrogen molecule decreased with increasing tensile strain on the $LiBH_4$(010) surface. The

tensile strain can facilitate the dehydrogenation process by weakening the interactions of boron with hydrogen atoms. On the other hand, the dopants Na, K, Al, F, or Cl were introduced at the topmost layer of the $LiBH_4$(010) system. Among all dopants examined, Al shows the highest performance to release a hydrogen molecule with the lowest energy required for hydrogen desorption of 1.151 eV. The dopant ranking of promoting hydrogen desorption from $LiBH_4$(010) system was Al > Cl > F > Na > K. Besides, co-doping system with Al and Cl shows the lower formation energy than Al-doped $LiBH_4$ and the lowest hydrogen desorption energy among the other doped systems. It means that the destabilization method with (Al, Cl)-codoping can effectively facilitate dehydrogenation processes from $LiBH_4$ hydrides.

Overall, dopants and pressure or strain can be utilized as efficient means for the design of highly promising hydride-based hydrogen storage materials.

LIST OF PUBLICATIONS

1. **Yuanyuan Li**, Jin Suk Chung, Sung Gu Kang, Role of hydrogen-related defects in the kinetics of complex hydrides. Under Preparation (2020).

2. **Yuanyuan Li**, Jin Suk Chung, Sung Gu Kang, First-principles computational screening of perovskite hydrides for hydrogen release. ACS Comb. Sci. 2019, 21, 736-742.

3. **Yuanyuan Li**, Jin Suk Chung, Sung Gu Kang, First-principles rational design of M-doped $LiBH_4$(010) surface for hydrogen release: Role of strain and dopants (M = Na, K, Al, F, or Cl). Int. J. Hydrogen Energ. 2019, 44, 6065-6073.

4. Aniruddha Molla, **Yuanyuan Li**, Bikash Mandal, Sung Gu Kang, Seung Hyun Hur, Jin Suk Chung, Selective adsorption of organic dyes on graphene oxide: Theoretical and experimental analysis. Appl. Surf. Sci. 2019, 464, 170-177.

5. **Yuanyuan Li**, Yiming Mi, Jin Suk Chung, Sung Gu Kang, First-principles studies of $K_{1-x}M_xMgH_3$ (M= Li, Na, Rb, or Cs) perovskite hydrides for hydrogen storage. Int. J. Hydrogen Energ. 2018, 43, 2232-2236.

6. Aniruddha Molla, **Yuanyuan Li**, Mahima Khandelwal, Seung Hyun Hur, Jin Suk Chung, Anion-controlled sulfidation for decoration of graphene oxide with iron cobalt sulfide for rapid sonochemical dyes removal in the absence of light. Appl. Catal. A-Gen. 2018, 561, 49-58.

7. Aniruddha Molla, **Yuanyuan Li**, Mahima Khandelwal, Bikash Mandal, Sung Gu Kang, Seung Hyun Hur, Jin Suk Chung, Facile synthesis and structural analysis of graphene oxide decorated with iron-cerium carbonate for visible-light driven rapid degradation of organic dyes. J. Environ. Chem. Eng. 2018, 6, 2616-2626.

8. Mahima Khandelwal, **Yuanyuan Li**, Seung Hyun Hur, Jin Suk Chung, Surface modification of co-doped reduced graphene oxide through alkanolamine functionalization for enhanced electrochemical performance. New J. Chem. 2018, 42, 1105-1114.

9. Mahima Khandelwal, **Yuanyuan Li**, Aniruddha Molla, Seung Hyun Hur, Jin Suk Chung, Single precursor mediated one-step synthesis of ternary-doped and functionalized reduced graphene oxide by pH tuning for energy storage applications. Chem. Eng. J. 2017, 330, 965-978.